BARRIER PROPERTIES OF ETHYLENE VINYL ALCOHOL FILMS

IN THERMAL PROCESSING

By

KEREILEMANG KHANAH MOKWENA

A dissertation submitted in partial fulfillment of
the requirements for the degree of

DOCTOR OF PHILOSOPHY

WASHINGTON STATE UNIVERSITY
Department of Biological Systems Engineering

MAY 2010

To the Faculty of Washington State University:

The members of the Committee appointed to examine the dissertation of KEREILEMANG KHANAH MOKWENA find it satisfactory and recommend that it be accepted.

_____

Juming Tang, PhD., Chair

_____

Marvin Pitts, PhD.

_____

Carolyn F. Ross, PhD.

_____

Marie-Pierre Laborie, PhD.

ACKNOWLEDGEMENT

I would like to thank my advisor, Dr. Juming Tang, for his great support throughout the years I spent here at Washington State University. I acknowledge his tireless efforts in providing technical and scientific direction for me to carry out my research. The financial support afforded for both research and personal living cannot be overemphasized. Through him I was able to stay and work with EVAL Company of America where I learned a great deal about the materials used in this study, and gained appreciation of industry work.

I also thank my committee members Dr. Marvin Pitts, Dr. Carolyn Ross and Dr. Marie-Pierre Laborie for all their constructive critique which helped to shape my research work and contributed positively to my research experience. My colleagues and fellow students are not to be forgotten for their everyday assistance. Galina Mikhaylenko has all the patience and determination to attend to each and every small and big issue around the laboratory. Gopal Tiwari helped a lot with some of the issues I went through in executing experiments and analyzing my data. Dr. Frank Liu assisted with the initial pilot plant experiments that shaped up the whole research. Wayne Dewitt often helped me with fixing my test cell whenever something went wrong. I thank them and other unnamed colleagues for their often overlooked support.

I owe much to EVAL Company of America for giving me an opportunity to do a major part of my experimental work in their facilities with their technical support. Their financial support allowed me to stay two summers in Houston, TX, to carry out this work. The staff at Kuraray Research and Technical Center in Pasadena, TX, were all great to

work with: Edgard, Robert, Al, Julie, Tammie and others. I also thank Dr Nindo and Binying Ye of the University of Idaho in Moscow, ID, for letting me use their equipment for some of my experiments. I thank Dr Shyam Sablani and the students in his laboratory, particularly Roopesh Syamaladevi, for assistance in some of my work.

My heartfelt appreciation goes to my family who provided the much needed moral support. My husband Patrick was a great inspiration and his daily encouragement kept me motivated everyday even though we were miles apart. My little Lara-Mmei had to live with the daily paperwork from the day she was born. I thank all the friends I made in Pullman since I came here.

Finally, I acknowledge the financial support and the opportunity I was given by my employer, Botswana College of Agriculture, to come and have the experience here at Washington State University.

BARRIER PROPERTIES OF ETHYLENE VINYL ALCOHOL FILMS IN THERMAL PROCESSING

ABSTRACT

by Kereilemang Khanah Mokwena, PhD

Washington State University

May 2010

Chair: Juming Tang

Ethylene vinyl alcohol (EVOH) copolymers are widely used in food packaging for shelf stable foods because of their good oxygen barrier. However, EVOH is very sensitive to moisture which adversely affects its oxygen barrier. The overall objective of this research was to understand the influences of thermal processing on oxygen barrier properties of multilayer EVOH films, with emphasis on influence of water absorption by packaging films when exposed to conditions of high moisture and high temperature during processing. The research focused on two multilayer films containing EVOH as the oxygen barrier which were used as lidstock for rigid trays. Film A was a laminated structure of oriented polyethylene terephthalate (PET), EVOH and polypropylene (PP). Film B consisted of PET laminated to a co-extruded structure of PP/tie/Nylon 6/EVOH/Nylon 6/tie/PP. Oxygen transmission rates were measured on films after retort

and combined microwave-hot water heating under conditions necessary to produce shelf-stable low acid foods. For both films, the retort treatments resulted in more deterioration of the oxygen barrier than microwave treatments. This was attributed to the amount of moisture absorbed during retort treatment, which was thought to be directly related to duration of direct exposure of films to high temperature humid environment during processing. Storage of packages for 2 months under ambient conditions resulted in recovery of more than 50% of the oxygen barrier. Further studies were carried out to investigate the relationship between the amount of water absorbed during retort processing and oxygen transmission through the films. Results confirmed dramatic increases in oxygen transmission at high film water contents which was attributed to plasticization and stresses created by high moisture and temperature conditions. Water absorption behavior of multilayer films was also studied at different temperatures and compared to monolayer films representing the individual components of the multilayer films. A preliminary study on use of split post dielectric resonator (SPDR) technique as a method for measuring amount of water in polymers was carried out. The measured dielectric property data correlated well with water absorption data, indicating that the method can be used to rapidly and non-destructively measure water absorption in these films.

Table of Contents

LIST OF TABLES

LIST OF FIGURES

DEDICATION

This dissertation is dedicated to my late father, Tale Mokwena,

who taught me and inspired into me the value of education.

CHAPTER 1 INTRODUCTION

1.1 Background

The critical factors in maintaining quality and shelf life of foods include the ingredients/raw materials, the processing method, packaging and storage conditions. Food processing methods subject food to conditions that are meant to inhibit microorganisms and other undesirable reactions and at the same time promote desirable physical and chemical changes that give the food its final attributes. Once the food leaves the processing stage, its quality and the extent to which it retains its attributes depends on the packaging and storage conditions. The interrelationship between the processing method and packaging and storage conditions is the basis of the current research.

Shelf stable, low acid foods (pH>4.6) are commonly produced using thermal processing methods. The aim of every thermal sterilization process is to supply sufficient heat to inactivate pathogenic spore forming microorganisms and food spoilage microorganisms in order to comply with public health standards (Holdsworth, 1997). Thermal sterilization using retorts is one of the most widely used industrial methods. In conventional retort sterilization pre-packaged food is heated in pressurized vessels (retorts) at specified temperatures for prescribed lengths of time using saturated steam, steam-air mixtures or superheated water as heating medium (May, 2000).

One of the functions of food packages is to protect against oxygen entry. Availability of oxygen in food packages can result in lipid oxidation of foods, affecting

nutritional and sensory quality of the foods. For example, maximum oxygen ingress of 1 to 5ppm is enough to limit the shelf life of canned meats, vegetables, soups and spaghetti in storage at 25°C for 1 year (Koros, 1990). Various forms and types of package materials are available for packaging heat processed shelf stable foods. The attractiveness of plastics lies in their versatility and ability to offer a broad variety of properties, and yet are cheap and readily processed and conformed into a multitude of shapes and sizes. While metal cans, glass jars and aluminum foil all offer absolute barrier and exclude oxygen from reaching the food product, plastic containers are permeable to oxygen and other gases at a rate characteristic of the plastic material used. Oxidative deterioration would continue during storage of foods packaged in plastic packages due to the continuous permeation of oxygen into the package. Protection against oxidation in plastic packages is possible by use of polymers that have low oxygen permeability (i.e. high barrier polymers). Not many polymers are available which can offer the high oxygen barrier required to maintain shelf life of heat processed foods. Ethylene vinyl alcohol (EVOH) copolymers are widely used in food packaging applications because of their very good barrier against oxygen. At 23°C and 0% relative humidity (RH) the oxygen permeability of EVOH with 27 mol % ethylene is 0.006 cm^3 mil/100 in^2 day atm (EVAL Americas). EVOH is hydrophilic, absorbing substantial amounts of moisture when placed in RH environments. The presence of even small amounts of moisture in EVOH is known to negatively affect the oxygen barrier properties (Zhang et al., 2001; Muramatsu et al., 2003). In food packages, EVOH layer is usually protected from contact with moisture by layers of polyolefins such as polypropylene (PP) and polyethylene (PE), polyesters such as polyethylene terephthalate (PET), polycarbonate, polystyrene, etc., at the surfaces.

Therefore, plastic based packages are essentially multilayer structures that combine different polymer materials each contributing a specific requirement or function.

1.2 Rationale

The synergistic effects of high moisture, high temperatures and the stresses created during thermal processing reduce the oxygen barrier of food packages containing EVOH. In particular, the long exposure to water at retort temperatures may cause severe losses to the oxygen barrier of EVOH layers in flexible pouches or thin films used as lidstock for rigid trays, bowls and cups. Quite a few studies were conducted on the effect of retorting on the oxygen barrier of multilayer films and containers with EVOH as the oxygen barrier resin, and the findings revealed severe effects on oxygen barrier after retort. Because of the wide range of possible multilayer structures that result from combining different polymers, thicknesses, polymer processing methods, positioning and arrangement of different layers, etc., it is difficult to get definitive information from the studies. In addition the various studies found in literature use empirical time-temperature conditions to mimic retort sterilization. This makes it difficult to compare and draw reliable quantitative conclusions from reported data. Tsai and Jenkins (1988) reported 100 times increase in oxygen permeability immediately after retorting at 121.1°C for 120 min for containers made of EVOH and an unspecified polyolefin. Lopez-Rubio et al. (2005) reported an increase of over 450 times for PP/EVOH/PP films immediately after retorting at 121°C for 20 min. Data from Hernandez and Giacin (1998) showed 60 times

increase in oxygen transmission rates for PET/EVOH/PP films immediately after retort at 125°C for 20 min.

In this research, the multilayer films studied were designed to represent typical production processes for multilayer flexible films for lid films and pouches, and rigid sheets which are thermoformed into trays, bowls, cups, etc. A preliminary study was carried out to establish the effect of thermal processing on oxygen barrier properties of multilayer EVOH films. Representative food processing conditions were designed to mimic closely the methods used in the industry for production of shelf stable, low acid food products (i.e. pH > 4.6). That is, the minimum process equivalent to $F_0 = 3\ min$ for low acid foods and a more severe process equivalent to $F_0 = 6\ min$ usually applied to control spoilage microorganisms were used (Holdsworth, 1997).

1.3 Research Hypothesis and Objectives

During thermal processing using retorts, pressurized water at high temperatures easily penetrates the outer protective layers of thin multilayer films and saturates the EVOH layer. This causes plasticization of the EVOH matrix and possible reductions in crystallinity, resulting in increased oxygen permeability of films immediately following processing and during storage. Increased oxygen permeation into food packages may cause oxidative degradation reactions in foods resulting in quality losses. The overall goal of this research is to correlate the amount of water absorbed during thermal processing with the changes within the polymer matrix and their effect on oxygen barrier properties of multilayer films (figure 1.1).

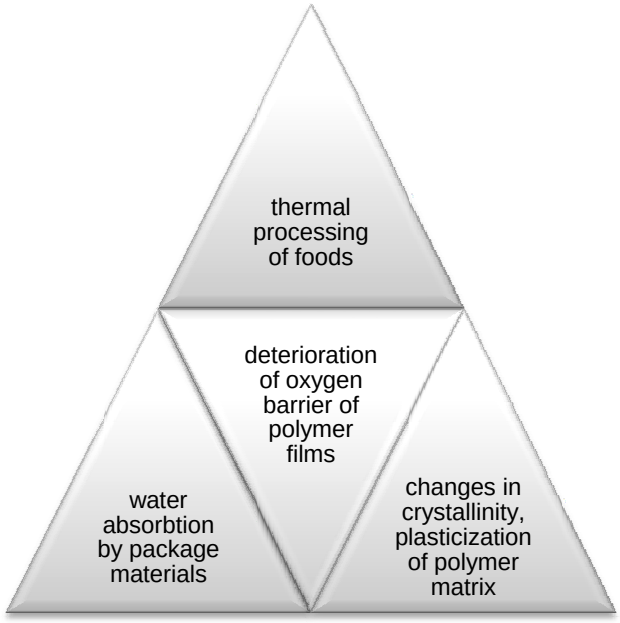

Figure 1.1. Interrelationships between thermal processing, water absorption, polymer structure and deterioration of oxygen barrier

The specific objectives were considered for this research:

1. **To determine the effect of thermal treatments on oxygen transmission rates of multilayer EVOH films during processing and storage**

In retort processing the time needed to raise product temperature to the required level is relatively long. Microwave heating, on the other hand, generates thermal energy within the food which makes higher heat fluxes possible and consequently reducing heating up time and overall processing times. It is therefore presumed that less water will be absorbed during microwave processing, resulting in less plasticization of polymer matrix and consequently less deterioration of oxygen barrier as compared to retort processing. Two different multilayer EVOH films which have similar oxygen barrier properties when

dry were used as lidstocks for rigid trays containing mashed potato processed by retort and microwave sterilization. The effect of the thermal processes on oxygen transmission rates of the films was evaluated immediately after processing and during storage over a period of 12 months. The findings from this study are the basis for the subsequent objectives.

2. To evaluate the correlation between water absorption at retort conditions and oxygen transmission rates in multilayer EVOH films.

Due to the conditions of high moisture and temperatures, combined with long processing times during retort sterilization, significant amount of water penetrates are absorbed by thin films. The total amount of water absorbed is directly related to the duration of thermal processing. Higher amount of water absorption is likely to result in more plasticization of the EVOH matrix and reduction in the polymer crystallinity, resulting in increased oxygen permeability immediately following processing. Simulated retort experiments were used to correlate the amount of water absorbed at retort conditions with oxygen transmission rates of multilayer EVOH films. The changes in polymer crystalline morphology as a result of water absorption were also evaluated. The absorbed water was quantified according to the different states of water existing in the films (i.e., whether bound or free) in order to explain the manner in which water interacts with the polymer.

3. To determine water transport characteristics of packaging films over a range of temperatures.

The total amount of water accessible to the EVOH layer is limited by the types, thickness and water transport characteristics of the outer layers. Due to the thin protective layers used in lid films and flexible pouches, the EVOH layer becomes saturated with water within very short times when exposed to high moisture and high temperature environments. A better understanding of the water transport characteristics in the different polymer materials that make up multilayer films is necessary. Thermodynamic and kinetic data of water in each component of a multilayer structure is required to identify the optimum conditions for use of packaging structures.

4. To evaluate the potential of using dielectric characterization as a means for measuring water absorption in films.

Because of the important role of water in polymer properties, it is necessary to have an efficient method to determine the amount of water absorbed in polymers. The widely used gravimetric technique is time consuming and destructive. Therefore, more rapid and non-destructive methods are needed. Dielectric property measurements have shown the potential in this regard since water has a great influence on dielectric properties of materials. The dielectric properties were measured and the unknown water content of the material was determined on the basis of these measurements. The split post dielectric resonator method was used to measure dielectric properties of polymer films.

1.4 Research Layout

The dissertation was organized into seven chapters. The first chapter gives background information on the role of EVOH as an oxygen barrier polymer and presents the motivation and objectives of the research. Chapter 2 is a review of the structure-property relationship of EVOH copolymers. Chapters 3 through 6 present and discuss experimental findings from the studies to address the research objectives outlined above. Specifically, in chapter 3 the effect of retort and microwave sterilization on oxygen transmission rates immediately following thermal processing and during storage are evaluated. In chapter 4 oxygen transmission rates of the films are studied in relation to the amount of water absorbed at retort conditions simulated using oil bath experiments. Chapter 5 investigates the water transport characteristics of multilayer and monolayer films at different temperatures. In chapter 6 a novel method for rapid detection of moisture update in EVOH laminated films was developed using a dielectric characterization technique. Chapter 7 is a compilation of the major conclusions from the dissertation and suggestions for future work. The following manuscripts have been prepared (or are being prepared) for publication in relevant journals:

(i). Mokwena, K.K., J. Tang, C.P. Dunne, T.C.S. Yang, and E. Chow. 2009. Oxygen transmission of multilayer EVOH films after microwave sterilization. Journal of Food Engineering 92, 291-296.

(ii). Mokwena, K. and J. Tang. Ethylene vinyl alcohol copolymers: a review of structure and properties. Prepared for submission to Critical Reviews in Food Science and Nutrition (in review).

(iii). Mokwena, K. J. Tang, and Marie-Pierre Laborie. Water sorption characteristics and oxygen barrier of multilayer EVOH films at retort conditions. Prepared for submission to Journal of Food Engineering (in review).

(iv). Dielectric study of water absorption in multilayer films using split post dielectric resonator (in preparation).

References

EVAL Americas. Technical Bulletin No. 110. Gas barrier properties of EVAL™ Resins. Downloaded from http://www.eval.be/upl/1/default/doc/EA%20-%20Technical%20Bulletin%20No%20110.PDF

Hernandez, R.J. and Giacin, J.R. 1998. Factors affecting permeation, sorption and migration processes in package-product systems. In Taub, I.A. and Singh, R.P. (Eds.), Food Storage Stability. CRC Press. Boca Raton, FL. pp. 269-330.

Holdsworth, S.D. 1997. Thermal Processing of Packaged Foods. Blackie Academic & Professional. New York, USA.

Koros, W.J. 1990. Barrier polymers and structures: overview. In Koros, W.J. (Ed.). Barrier Polymers and Structures. ACS Symposium Series 423, American Chemical Society. Washington, DC. pp 1-21.

Lopez-Rubio, A., Hernandez-Munoz, P., Catala, R., Gavara, R., and Lagaron, J.M. 2005. Improving packaged food quality and safety. Part 1: Synchrotron X-ray analysis. Food Additives and Contaminants 22, 988-993.

May, N. 2000. Developments in packaging format for retort processing. In Richardson, P.S. (Ed). Improving the Thermal Processing of Foods. Woodhead Publishing. Cambridge, England. 138-151.

Muramatsu, M., Okura, M., Kuboyama, K., Ougizawa, T., Yamamoto, T., Nishihara, Y., Saito, Y., Ito, K., Hirata, K., and Kobayashi, Y. 2003. Oxygen permeability and free volume hole size in ethylene vinyl alcohol copolymer film: temperature and humidity dependence. Radiation Physics and Chemistry 68, 561-564.

Tsai, B.C. and Jenkins, B.J. 1988. Effect of retorting on the barrier properties of EVOH. Journal of Plastic Film & Sheeting 4, 63-71.

Zhang Z., Britt, I.J. and Tung, M.A. 2001. Permeation of oxygen and water vapor through EVOH films as influenced by relative humidity. Journal of Applied Polymer Science 82, 1866-1872.

CHAPTER 2 REVIEW OF ETHYLENE VINYL ALCOHOL

2.1 Introduction

The traditional barrier material in flexible packages has been aluminum in the form of sheets of a few micrometers thick and more recently as a vacuum deposited coating or metallization (Lange and Wyser, 2003). Aluminum foil provides the ultimate gas and moisture barrier in flexible packages when it is used at thickness greater than 25.4μm (Robertson, 2006). However, when used in smaller thicknesses it is susceptible to pinholes and other stress induced fractures such as flex crack. Incorporation of foil into the multilayer structure requires multiple lamination steps which is expensive compared to coextrusion which reduces the process to a single step. Additionally, foil-based packaging results in non-recyclable material, generating excess waste. Other limitations of aluminum foil include lack of transparency (product visibility), and microwavability. Therefore eliminating the foil layer in packages has become an important factor in package design.

Apart from EVOH, the other important high barrier polymer for food packaging applications is polyvinylidene chloride (PVDC). The oxygen permeability of high barrier PVDC is about 0.08 cc mil/100 in^2 day atm at 23°C (Brown, 1986). Unlike EVOH, the gas barrier properties of PVDC are not affected by moisture, and PVDC itself has relatively low water vapor transmission rate. Saran XU-32024 PVDC has water vapor transmission rate of 0.06 g mil/100in^2 day as opposed to 8.0 g mil/100in^2 day for EVOH resin with 27 mol % ethylene (EVAL Americas). Use of PVDC is challenged by several

issues that include cost, processing difficulties and environmental concerns. First, PVDC has a fairly narrow range of feasible processing temperatures (i.e. 10-15°C), which makes its coextrusion with other polymers that require high processing temperatures such as nylons, PET, polycarbonate, etc. difficult (Massey, 2003). The limited extrusion conditions also make recovery of mixed waste that contains polymers with high processing temperatures particularly difficult. The use of PVDC has also been seriously questioned in terms of recycling. Among the approaches currently taken in packaging design is selection of materials that do not produce harmful by-products during disposal (Katsura and Sasaki, 2001). PVDC, a copolymer of vinylidene chloride and vinyl chloride, contains chlorine which gives rise to hazardous by-products such as hydrogen chloride during incineration (Hui, 2006). While PVDC is still being produced and used for packaging its demand has shown a decline while that for other (non-PVDC) barrier materials has increased. For example, in Japan demand for PVDC coated films declined markedly during the period between 1995 and 1999 (Katsura and Sasaki, 2001).

The most significant issue concerning use of EVOH as barrier material is its moisture sensitivity. EVOH is very hydrophilic, absorbing significant amount of moisture when exposed to humid conditions, leading to an increase in its oxygen permeability. The importance of this in food packaging is dependent upon the food processing method used and storage conditions. The most severe conditions are encountered during retort processing of packaged foods due to the high moisture and high temperature conditions involved. Despite the problems of moisture sensitivity EVOH is still a preferred barrier material for various packaging applications, accounting for about 70-75% of barrier resin used for retortable containers, according to Burke (1990). In recent years, there has been

significant research on the mechanisms and effects of water absorption by EVOH containing films which has led to a better understanding of its performance in various food processing environments. Innovations in food processing and polymer film technologies present end users with opportunities to reinvent EVOH barrier packaging to drive new business. For example, advanced food processing technologies such as microwave sterilization and high pressure processing provide processing conditions that are less stringent than those encountered during conventional retort heating. These factors plus the compatibility of EVOH in coextrusion with a wide range of other polymers, ease of recycling, etc. make EVOH an important barrier polymer.

The main objective of this review was to develop an overview of research on oxygen barrier properties of EVOH copolymers in relation to its use in food packaging applications. The review will provide a general discussion on EVOH synthesis and morphological/structural characteristics that determine its inherent high gas barrier property. The influence of high relative humidity conditions such as those in retort processing on oxygen barrier of EVOH will be evaluated.

2.2 Overview of Oxygen Barrier Properties of EVOH

As already indicated, EVOH has one of the lowest reported oxygen permeability among existing barrier polymers when dry. Figure 2.1 compares oxygen permeability of EVOH with that of other common polymers. From the figure, it is clear that the oxygen permeability of polyvinyl alcohol (PVOH) is lower than that of EVOH. However, PVOH is soluble in water and difficult to melt extrude, and therefore has limited use in food

packaging. PVDC, nylon 6, and PET all have oxygen permeability that is 1-2 orders of magnitude higher than that of EVOH. Nonpolar polymers such as PP, PE, polystyrene, exhibit oxygen permeabilities over 4 orders of magnitude higher than that of EVOH. The differences in oxygen barrier properties depend in most part on the chemical composition and molecular structure of the polymers. However, there exists a complex interdependence of polymer factors with environmental conditions. Oxygen permeability in EVOH is controlled by morphological characteristics such as crystallinity, chain structure, cohesive energy density, free volume as well as by external factors such as temperature and moisture (Koros, 1990; Lopez-Rubio et al., 2003).

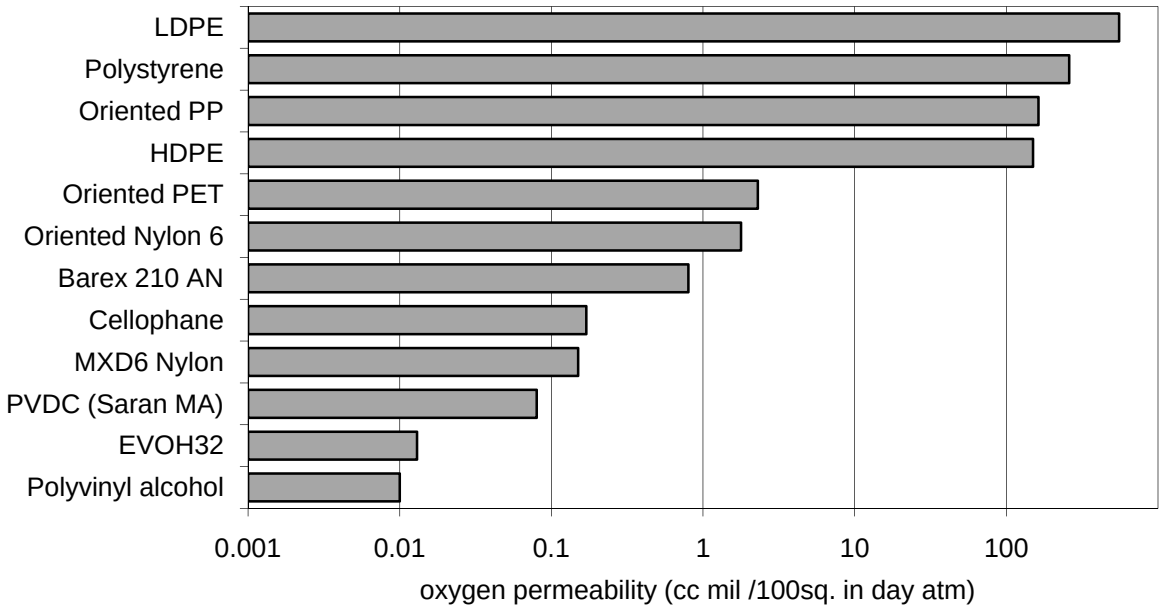

Figure 2.1. Oxygen permeability of selected polymers at 23°C and 0% RH. LDPE is low density polyethylene; HDPE is high density polyethylene; EVOH32 is EVOH with 32 mol % ethylene; MXD6 is a copolymer of meta-xylylene diamine and adipic acid; Barex 210 is acrylonitrile-methyl acrylate copolymer. (Data from EVAL Americas).

2.3 EVOH Synthesis

EVOH is a semi-crystalline copolymer of ethylene and vinyl alcohol monomer units (Iwanami and Hirai, 1983). The repeating unit of EVOH has the following chemical structure:

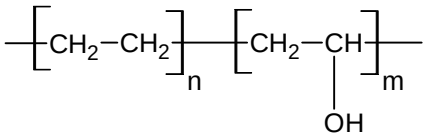

Copolymerization is widely used to provide an opportunity to adjust properties of the resulting resins to meet specific needs in utility of polymers that would otherwise be of limited use. As mentioned earlier, PVOH, one of the monomer units in EVOH, has exceptional gas barrier properties, but it is water soluble and its melting point is close to its heat degradation temperature, which makes it difficult to process. PE, the other parent monomer, has good water resistance, but also has one of the poorest gas barrier properties. Therefore copolymerization of monomer units based on PVOH and PE results in EVOH copolymers which have improved properties in terms of gas barrier, processability, and sensitivity to moisture (Robertson, 2006).

Commercial production of EVOH is generally a two step process involving free radical polymerization followed by saponification (Iwanami and Hirai, 1983). Vinyl alcohol is unstable and cannot be isolated into a free state, hence the polymerization process utilizes ethylene and vinyl acetate instead (Blackwell, 1986). The acetate functional groups in polyvinyl acetate copolymer are converted into alcohol (hydroxyl) groups during a saponification process according to the reaction scheme shown below.

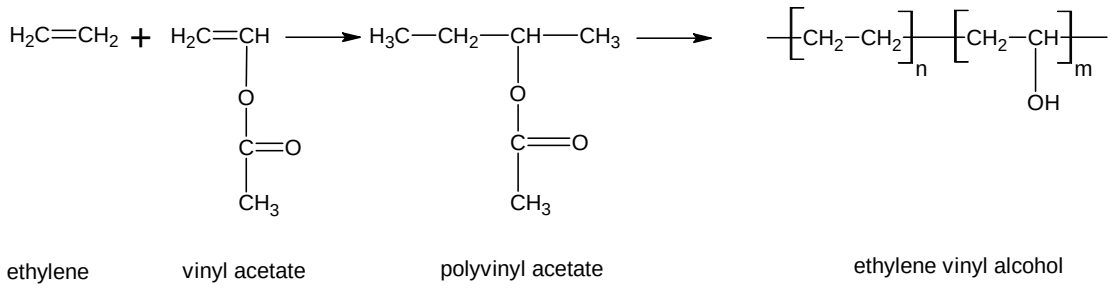

The EVOH copolymer composition (i.e., relative amounts of ethylene and vinyl alcohol) affects almost all properties of EVOH copolymers, hence influences EVOH processing and end-use applications. EVOH resins are commercially available in a range of compositions, most commonly encompassing vinyl alcohol contents of about 52–76 mol %. Generally, copolymers of higher vinyl alcohol content have properties resembling those of PVOH. Similarly, those with higher ethylene contents resemble properties of PE. EVOH copolymers with lower ethylene contents have better gas barrier properties. Data from EVAL Company of America (EVALCA) show that EVOH of 27 mol % ethylene offers ten times more oxygen barrier than one of 44 mol % ethylene (see Figure 2.2). Zhang et al. (2001) reported oxygen transmission rates 4 to 6 times higher for an EVOH copolymer with 44 mol % when compared to a film containing 32 mol % ethylene. Copolymer composition also affects water absorption and transmission by EVOH copolymers. Copolymers with low ethylene contents absorb more water than those with higher ethylene (Zhang et al., 1999, Cava et al., 2006). Since water absorption takes place by water molecules hydrogen bonding to hydroxyl groups in vinyl alcohol, an increase in vinyl alcohol leads to an increase in the number of water molecules sorbed to the polymer (Lagaron et al., 2003).

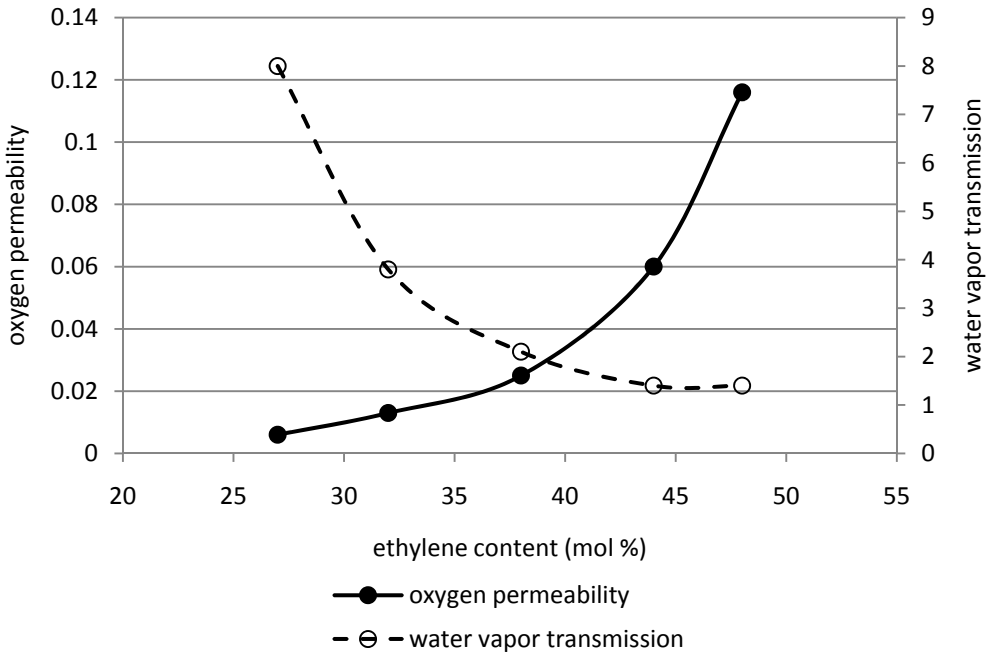

Figure 2.2. Oxygen permeability (cc mil/100 in^2 day atm) and water vapor transmission (g mil/100 in^2 day) as a function of ethylene content for EVOH copolymers. (Data from EVAL Americas).

2.4 Degree of Crystallinity

At a microscopic scale, semi-crystalline polymers are heterogeneous materials typically represented as crystalline domains dispersed in an amorphous matrix (Ezquerra, et al., 2002). The crystalline phase contains segments that are organized into three-dimensional arrays characterized by existence of long range order with respect to molecular arrangement, while the amorphous regions consist of disordered chain segments (Gestoso and Brisson, 2001). Properties of semi-crystalline polymers are usually related to degree of crystallinity (which indicates the relative proportions of the crystalline and non-crystalline phases) and to the crystalline features such as size and

perfection of the crystals (Ezquerra, et al., 2002). The exceptional barrier properties of EVOH copolymers are largely attributed to their inherent high degree of crystallinity. EVOH has a degree of crystallinity of about 30% when produced (Armstrong, 2008). The benefits of a higher degree of crystallinity include improved barrier to gases and solutes. Oxygen permeability becomes lower as the degree of crystallinity increases as shown in Table 2.1 for EVOH and other polymers. It is suggested that permeation of most low molecular weight substances such as gases and vapors occurs mainly through the amorphous regions. Hence the presence of large amounts of impermeable crystalline regions in EVOH creates a more tortuous diffusive path for penetrant molecules and hence reduces permeability (Lagaron et al., 2004).

Table 2.1. Effect of crystallinity on oxygen permeability (cc mil/100 in^2.day.atm) of polymers

Polymer	Morphology	Oxygen Permeability	Environmental conditions
EVOH[a]	58% crystallinity (non-oriented)	0.71	at 20°C, 100% RH
	68% crystallinity (uniaxial orientation)	0.25	
	70% crystallinity (biaxial orientation)	0.15	
LDPE[b]	50% crystalline	480	at 23°C, 50% RH
	75% crystalline	110	
PET[b]	10% crystalline	10	at 23°C, 50% RH
	50% crystalline	5	
PP[b]	Atactic (low crystallinity)	250	at 23°C, 50% RH
	Isotactic (higher crystallinity)	150	

[a] Data from Armstrong (2002)

[b] Data from Salame (1986)

2.4.1 Molecular and Crystal Structure of EVOH

Thermoplastic polymers such as EVOH will crystallize to varying extents when the molten polymer is cooled below the melting point of the crystalline phase (Young and Lovell, 1991). During the process of polymer crystallization, polymer chains aggregate to form crystals, which possess a high degree of order. Whether or not crystallization occurs depends on the thermodynamics of the crystallization process. In particular,

crystallization is favored thermodynamically when the system is in thermodynamic equilibrium, i.e. when Gibbs free energy of the system is at the lowest (Young and Lovell, 1991). Many factors affect the rate and extent to which crystallization occurs, including chemical composition, geometrical structure, and processing variables (such as cooling rate and melt temperature).

For crystallization to occur a polymer must possess some degree of chemical, geometrical and spatial regularity. Naturally copolymers are known to lack the necessary chemical regularity along their chains. In addition geometrical regularity in those copolymers produced by free radical polymerization occurs only infrequently (Vaughan and Bassett, 1989). EVOH chains are known to be atactic, having spatially disordered configurations (Takahashi et al., 1999). X-ray diffraction studies have shown that vinyl alcohol and ethylene monomer units in EVOH are distributed randomly along the polymer chains in a planar zigzag conformation. Despite the lack of stereoregularity, it has been established that EVOH copolymers can crystallize at all copolymer compositions (Nakamae, et al., 1979; Takahashi et al., 1999). This has been attributed to the fact that the size of the hydroxyl groups on the polymer chains is small enough relative to the space available in the crystal structure such that the symmetry of the polymer is not significantly affected. Therefore, the atactic nature of EVOH chains plays a diminished role in the ability of EVOH copolymers to crystallize. Significant cohesion between adjacent polymer chains is also necessary for polymer molecules to aggregate together into a crystalline solid. The large number of hydroxyl groups in EVOH copolymers results in high intermolecular and intramolecular forces and hence a high cohesive energy (Lagaron et al. 2004). Both intermolecular and intramolecular hydrogen

bond strength decrease with an increase in ethylene content (Ketels, 1989). Thus, in EVOH with higher content of vinyl alcohol unit, chain mobility in the amorphous region is more restricted by intermolecular hydrogen-bonding interactions (Zhang et al., 2000). A comparison of the cohesive energy of EVOH with that of other common polymers is shown in Table 2.2.

Table 2.2. Cohesive energy (cal/cm^3) and oxygen permeability (cm^3 · mil/100in^2 day atm) of some polymers

Polymer	Repeating unit	Cohesive energy[a]	Oxygen Permeability[b]
LDPE	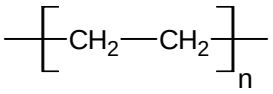	66	554
PP	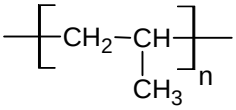	84	160
PET	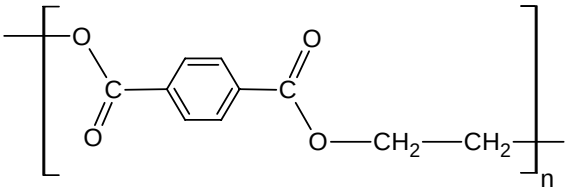	115	2.3
PVDC	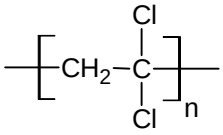	149	0.08
Nylon 6	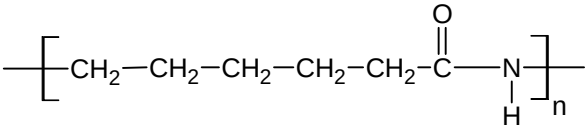	185	1.8
EVOH	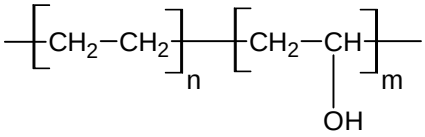	205	0.03
PVOH	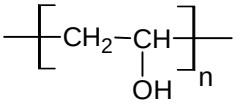	220	<0.01

[a] Data from van Krevelen (1990) and Brandrup and Immergut (1989)

[b] Data from Salame (1986) (oxygen permeability measured at 23°C and 0% RH)

A good amount of work has been done to identify and define the crystal structure of EVOH copolymers. It is generally recognized that the type of structure of EVOH crystals depends on the relative proportions of ethylene and vinyl alcohol in the copolymer. Several researchers proposed three crystal structures for EVOH, depending on the amount of ethylene or vinyl alcohol in the copolymer. An orthorhombic crystal structure similar to that of PE was proposed for copolymers with vinyl alcohol composition range below 20 mol %, a pseudo-hexagonal structure for the range of 20-60 mol %, and a monoclinic structure similar to that of polyvinyl alcohol above 60 mol% (Nakamae et al., 1979). Similarly Cerrada et al. (1998) studied crystal structure of copolymers with 56, 68 and 71 mol % vinyl alcohol. These authors reported monoclinic lattice for the higher vinyl alcohol copolymer (i.e. those with 68 and 71 mol % vinyl alcohol) and an orthorhombic lattice for the copolymer with 56 mol % vinyl alcohol. Takahashi et al. (1999) reported a similar general trend except with different margins of vinyl alcohol content between the different crystal structures. EVOH copolymers with vinyl alcohol contents of 6–14 mol % were reported to resemble the orthorhombic crystal structure of PE, while those between 27–100 mol % resemble the monoclinic structure of polyvinyl alcohol. An intermediate hexagonal structure was observed at vinyl alcohol contents between 14–27 mol %. Cerrada et al. (1998) observed that the existence of different crystalline structures with copolymer composition was influenced not only by the copolymer composition, but also by the crystallization conditions, in particular, the cooling rates. These authors determined that while slowly cooled samples showed varying crystal structure as reported by other authors, fast cooling or quenching (e.g., at 100°C/min) exhibited only the orthorhombic structure for all copolymer compositions.

2.4.2 Orientation

Crystallinity of polymers can be enhanced by orientation, a process in which polymer chains are drawn or stretched in specific directions (Peacock, 2000). If a molten polymer is subjected to external forces (e.g., mechanical drawing) the molecules may align preferentially in the stress direction. This is possible because the intrinsic properties of a polymer chain are strongly directional dependent (Gedde, 1999). The melt is then rapidly cooled to retain the resulting chain orientation. Orientation is usually described as uniaxial or biaxial. Uniaxial orientation results when the material is stretched or drawn in one direction only. Biaxial orientation results when drawing is performed in two orthogonal directions.

In general, EVOH can be oriented uniaxially fairly easily. However biaxial orientation is challenging, requiring optimized conditions to achieve the simultaneous orientation. Due to the strong intermolecular and intramolecular hydrogen bonding interactions in its polymer chains EVOH displays a sheet-like structure (Matsui et al. (2003). Because of this EVOH does not have good stretchability as compared to other general resins such as polyolefins. Seguela et al. (1998) also noted that the planar distribution of the hydrogen bonds in the stable monoclinic crystalline form involves strong mechanical anisotropy that is responsible for a splitting trend that prejudices biaxial drawing. Nonetheless, EVOH copolymers have been successfully oriented into materials with improved oxygen barrier properties. As shown in Table 2.1, uniaxial orientation of EVOH resulted in 68% crystallinity as compared to 58% crystallinity for unoriented material (Armstrong 2002). Biaxial orientation resulted in slightly more crystallinity of 70%. Orientation also affects water uptake by EVOH copolymers. Zhang

et al. (1999) reported 8.4% water absorption for non-oriented film as compared to 6.8% uptake for biaxially oriented film with the same ethylene content (32 mol %).

2.5 Free Volume

Approaches to describe permeability of gases in polymers are commonly based on free volume models. Free volume is a concept used to characterize the amount of space in a polymer matrix that is not occupied by the constituent atoms of the polymer (Freeman and Hill, 1998). This space is therefore available to assist in the molecular transport of gas and other small molecules. The free volume concept embodies inter and intra-molecular interaction as well as the topology of molecular packing in the amorphous phase. The relationship between oxygen permeability and free volume is generally explained using models based on the original work of Cohen and Turnbull (1959). The theory implies that the gas diffusion within the polymers is proportional to both the kinetic velocity and the probability of finding enough space for gas molecules to move (Cohen and Turnbull, 1959). Local free volume holes arise as a consequence of irregular and inefficient packing of disordered chains, implying that the free volume exists mainly in the amorphous regions (Ito et al., 2003). As such polymers with high degree of crystallinity such as EVOH would generally have less free volume and consequently lower gas permeability values. The efficient packing of chains in crystals or in the ordered regions of oriented EVOH copolymers reduces the available free volume to the extent that these regions are considered impermeable. The available free volume therefore presents diffusing gas molecules with a low-resistance path for their movement

through the polymer. Thermally induced chain segment rearrangement can result in transient gaps which also add to the free volume. Thus, the cooperative movement of both gas molecules and polymer chain segments is required for mobility of gas molecules through the polymer matrix (Eyring, 1936).

Limited studies directly measured the free volume in EVOH copolymers in order to elucidate the molecular mechanism of gas permeation in these polymers. Ito et al. (2003) and Muramatsu et al. (2003) studied the relationship between oxygen permeability and free volume hole size in an EVOH copolymers. Correlations were obtained between permeability and free volume hole size for EVOH at different temperatures and humidities, suggesting that the free volume hole size plays a crucial role in the oxygen permeation in EVOH copolymers. In a study by Ito et al. (2001) the authors observed that the free volume size of EVOH copolymers increased significantly with free volume at ethylene contents above 30 mol %. These authors reported free volume size ranging from $0.04nm^3$ for EVOH copolymer with 30 mol % ethylene or less to $0.18nm^3$ for PE. The increase in free volume size was related to reduction of hydrogen bonding interactions at higher ethylene contents, allowing polymer chains greater flexibility.

2.6 Glass Transition

One of the phenomena defining amorphous and semi-crystalline polymers is the glass transition. The glass transition concept describes transitions between the “rubbery” state and the “glassy” state in a polymer as it experiences temperature rise or reduction. Solidification from a rubber to a ‘glass’ (or vitrification) occurs without crystallization.

The temperature at which the polymer undergoes e glass-to-rubber transition is called glass transition temperature (T_g). The glass transition occurs over a narrow temperature range specific for each polymer. Below T_g (i.e. in the glassy state) polymer chain segments are 'frozen' in place; atoms undergo only low amplitude vibratory motions (Ebewele, 2000). In terms of the free volume theory it is suggested that below T_g there is only a small fraction of space in a polymer matrix that is not occupied by the polymer molecules. Therefore movement of polymer chain segments is negligible in the glassy state, and because of the limited free volume there is not enough space for gas molecules to pass through, resulting in low gas permeability. As temperature is increased, there is enough thermal energy to overcome the intramolecular and intermolecular forces holding together molecules and chain segments and the chains undergo viscous flow and experience rotational and translational motion (Bicerano, 1993; Aharoni, 1998). Sufficient free volume is created that allows polymer chains to move relative to one another. Therefore, the glass transition is usually referred to as the onset of large scale cooperative motion of chain segments.

T_g plays an important role in barrier properties of polymers since gas permeation mechanisms are greatly altered depending on whether the permeation process occurs in the rubbery or the glassy state. Increased mobility of polymer chain segments at temperatures above T_g implies that gas molecules and other small penetrant molecules have great deal of freedom to move around. As is with other properties of EVOH copolymers, T_g varies with the copolymer composition. T_g values of EVOH copolymers are much higher that of PE and below that of PVOH. In general, T_g decreases as ethylene

content increases. Product data from EVAL Americas show that T_g values of EVOH copolymers with 27, 32 and 48 mol % ethylene are 60°C, 57°C, and 49°C, respectively.

2.7 Sensitivity of EVOH to Moisture

The major limitation for EVOH is its inherent sensitivity to moisture which poses a negative effect on its oxygen barrier and other properties. EVOH fully exposed to humid conditions absorbs significant amounts of moisture when exposed to high relative humidity conditions. Lagaron et al. (2001) reported equilibrium water uptake of about 9.0% by EVOH films with 32 mol% ethylene in saturated relative humidity conditions at 21°C. Aucejo et al. (1999) reported water absorption of up to 13%, while Zhang et al. (1999) reported equilibrium water sorption values of 8.4% for EVOH films with 32 mol %. The moisture sensitivity of the permeability of EVOH to oxygen has been observed experimentally to be a function of degree of crystallinity (Armstrong, 2002). Zhang et al. (1999) reported 8.4% water absorption for non-oriented film as compared to only 6.8% uptake for biaxially oriented film with the same ethylene content (32 mol %). These authors (and others) offer theories that reduction in free volume as degree of crystallinity increases explains this behavior.

The hydroxyl group that confers EVOH with the good oxygen barrier is also the main cause for its moisture sensitivity. The hydrophilic nature of EVOH polymers is attributed to the specific associations between water molecules and the polar hydroxyl groups in EVOH chains. The hydroxyl groups in EVOH are not totally self associated, but are partly isolated in the hydrophobic matrix (Iwamoto et al., 2001). The fraction of

isolated hydroxyl groups is said to increase with ethylene content. These authors reported that at lower ethylene contents (up to 75 mol % ethylene content) a hydroxyl group has enough hydroxyl groups around its vicinity to be fully hydrogen bonded, but at higher ethylene contents, a hydroxyl group is surrounded by fewer hydroxyl groups. Plasticization takes place with molecular dispersion of water in the structure of the polymer. Plasticization implies intimate mixing in which water is dissolved in a polymer. Due to the small size of the water molecule, water is easily incorporated into the supermolecular structure of the polymer. The first water molecules absorbed form hydrogen bonding networks with the surrounding hydroxyl groups in EVOH chains. It is believed that water molecules in EVOH are hydrogen bonded one-to-one to isolated hydroxyl groups in EVOH (Iwamoto et al., 2006). At molecular level, plasticization leads to an increase in the distance between neighboring chains in the polymer chain (i.e. increase in free volume) due to swelling. This decreases the energy of polymer-polymer interactions and may involve weakening or breaking of polymer-polymer hydrogen bonds (Levine and Slade, 1988; Hodge et al., 1996a). Therefore, the interaction of water with the associated hydroxyl groups in EVOH has a much larger influence on the physicochemical properties of EVOH (Iwamoto et al., 2006). An increase in free volume cavity size during water absorption was demonstrated for polyvinyl alcohol (Hodge et al., 1996a). Large scale rotation about C-C covalent bonds (i.e. macromolecular mobility) at higher water contents concurrent with disruption of the vast majority of hydrogen bonds were observed. These authors concluded that water that engages in hydrogen bonding with the hydroxyl groups is believed to be the most effective plasticizing water for the

polymer. When hydroxyl groups are fully occupied, subsequent water molecules start bonding with each other, forming water clusters.

2.7.1 Effect on Oxygen Permeability

The degree to which moisture affects oxygen permeability of EVOH copolymers depends on the relative humidity of the environment. Zhang et al. (2001) and Muramatsu et al. (2003) carried out studies on the effect of a wide range of RH levels on oxygen permeability of EVOH films. Both authors reported an initial decline in oxygen permeability at low RH (i.e. from 0 and 25-35%). Above 25-35% RH, oxygen permeability increased with RH and a rapid increase was observed above 75-80%. The general trend of change in oxygen permeability with RH as reported by the above authors is shown schematically in Figure 2.3. Muramatsu et al. (2003) also compared the change in free volume hole size with RH with the oxygen permeability data. The authors noted that the free volume hole size similarly decreased in the low RH region below 25% followed by an increase as RH increased. Similar trends for change in oxygen permeability as a function of water activity were reported for other hydrophilic polymer like for nylon 6, cellophanes, edible films, etc. (Hernandez, 1994; Gontard et al., 1996).

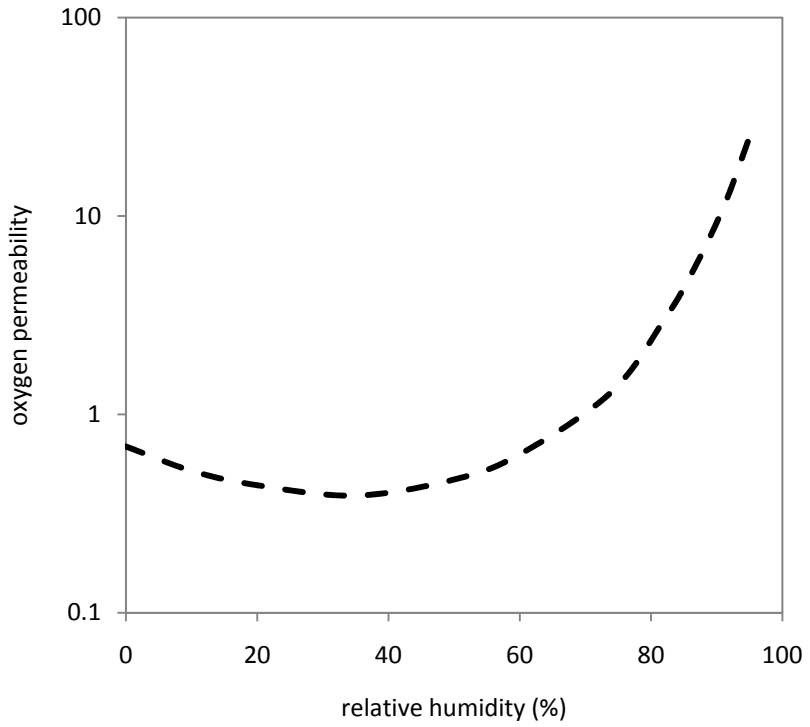

Figure 2.3. Effect of relative humidity on oxygen permeability of EVOH films (figure adapted from Zhang et al. (1999))

2.7.2 Effect on Glass Transition Temperature

It has become well established that plasticization by water affects the glass-to-rubber transition of polymers by depressing the T_g of the polymer matrix. The critical effect of plasticization leads to increased mobility and chain flexibility in the dynamically constrained amorphous component of the polymer brought about by the dilution of the main chain by water (Levine and Slade, 1988). T_g depression can be related simply to an increase of the volume, or in the case of specific polymer-water interactions, to the distribution of hydrogen bonds in the polymer. Indeed, T_g depression is commonly used as a measure of plasticization by water in polymers. Figure 2.4 shows the effect of

relative humidity on T_g of two EVOH copolymers. The data used in the figure (from Soarnol®) indicate that T_g decreased from 60°C to 3°C for EVOH with 32 mol % ethylene, and decreased from 55°C to 8°C for EVOH with 44 mol % ethylene. Zhang et al. (1999) reported a 24°C drop in T_g for similar EVOH films when RH increased from 0 to 43%, and T_g below room temperature when RH was above 75%. Aucejo et al. (1999) reported a T_g drop from 50°C to -60°C for EVOH films (29 mol % ethylene content) containing 13% moisture. Lagaron et al. (2001) reported depression of T_g by about 80°C (from about 62°C to -18°C) for EVOH films (32 mol % ethylene content) with about 9% moisture.

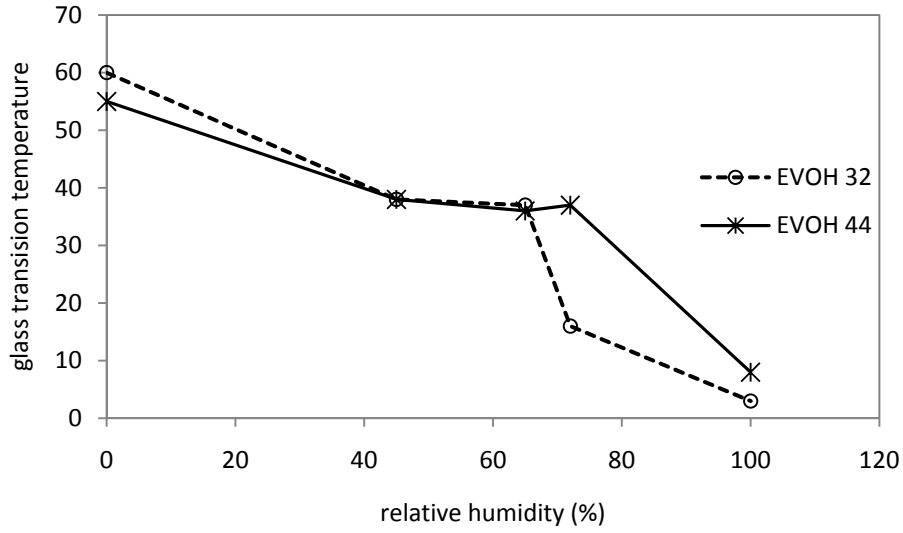

Figure 2.4. Effect of relative humidity on T_g of EVOH copolymers (Data from Soarnol®)

2.8 EVOH Use in Food Packaging

Because of the stringent package requirement of withstanding the rigors of high temperatures and pressures, relatively few polymers are suitable for retort applications. The most common retortable plastic containers are thermoformed from co-extruded or laminated multilayer structures. Structural materials such as polyolefins (e.g., PP, PE), polyesters (e.g., PET), polycarbonate, polystyrene, etc., located at the surfaces are generally used to support an internal oxygen barrier layer. The surface layers generally provide mechanical properties (strength, rigidity, abrasion resistance, etc.) and good water barrier at low cost (Massey, 2003). PP is commonly used as the food contact layer in food packages and provides strong heat seals because it seals very well upon itself (e.g. in pouches). The water vapor transmission rates of oriented PP and low density PE measured at 40°C and 90% RH are 0.38 and 1.14 g mil/100 in^2 day, respectively, compared to 1.4-8.0 g mil/100 in^2 day for EVOH copolymers (EVAL Americas). Nylons are usually incorporated in multilayer structures because of their thermal stability, toughness, and resistance to cracking and puncture (Massey, 2003). Biaxially oriented nylon has improved strength, oxygen barrier properties, impact and pinhole resistances, and films are more flexible. PET is also commonly used as an outer due to its strength, abrasion resistance and good printability.

With the wide range of polymers available, there are many possible combinations of structures that can be fabricated to meet specific needs. Special adhesives (generally polyesters, copolymers of ethylene, polyurethanes or acrylics) known as tie layers may be used to bond adjacent layers to avoid delamination (Osborn and Jenkins, 1992). For example, EVOH can be coextruded with nylon 6 without the use of adhesives but

coextrusion with polymers such as PP, PE, PET, etc., requires use of suitable adhesives (Sidwell, 1992). Rigid and semi-rigid containers such as bottles, tubs, trays, bowls and tubes are formed by thermoforming, vacuum and pressure molding. Examples of commercial packaging using EVOH in retort include all of Campbells soup, Dinty Moore MRE and dinner trays, retort pet food such as Meow Mix and Beneful, etc. Multilayer configurations can be either symmetrical (as shown in Figure 2.5) or asymmetrical to meet the customized needs of a broad variety of applications.

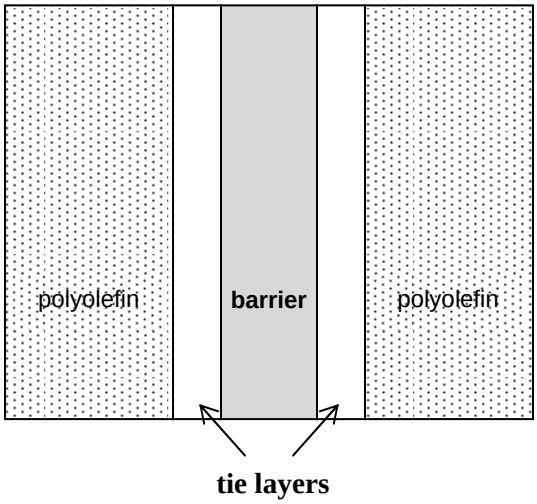

Figure 2.5. Illustration of multilayer structure

Due to the conditions of moisture and temperature used in retort processing, permeability has been reported to increase substantially when packages containing EVOH are subjected to retorting (Tsai and Jenkins, 1988). The effect of thermal processing on EVOH films is addressed in the next chapter. Nevertheless, Table 2.3 shows a comparison of oxygen transmission rates (OTR) before and after retort among EVOH containing films and other barrier materials typically used in food packaging. The

data reveal a severe effect on EVOH containing films than other barrier materials such as PVDC. For example, OTR increased by 30-70 times for EVOH containing films, compared to only 1.4 times for silica deposited laminated film and PVDC films under similar retort conditions.

Table 2.3. OTR (cc/m^2 day) of multilayer films before and after retort process

Structure	Oxygen transmission	
	Before	After
12μ PET/15μ EVOH/60μ cPP	0.3	18.8
12μ PET/15μ PVDC/15μ ONy/60μ cPP	1.8	2.6
12μ PET/25μ PVDC/15μ ONy /60μ cPP	1.0	1.6
12μ PET/GL film/60μ cPP	0.5	0.7
15μ OSM/15μ ONy/60μ cPP	3.8	6.0
25μ ONy/60μ cPP	15.8	21.5

Data from Hernandez and Giacin (1998); retort at 125°C for 20min, OTR measured at 25°C and 70% RH; cPP is cast polypropylene; EVOH are all EVAL resins; PVDC is Saran UB resin; GL film is silica deposited laminated film (Toppan Printing Co. Ltd); Ony is oriented nylon; OSM is metaxylene diamine adipic acid copolymer.

2.9 Conclusions

The good oxygen barrier properties of EVOH are compromised when used in applications that expose packages to high moisture conditions such as retort processing of foods. However, EVOH has been effectively used in rigid retort packages like thermoformed trays and blow molded bottles in combination with polypropylene and other water resistant polymers. It is clear from research results that for thin film structures (< 10 mils) EVOH is still vulnerable to the effects of high moisture and high temperature conditions used in retort processing of shelf stable foods. Some film structures may not provide sufficient water barrier during retort processes in order to prevent unacceptable quantities of oxygen permeation during processing and later in storage. Hence a properly designed package that incorporates both good material selection and their positioning in the multilayer structure are important to obtain the best oxygen barrier.

Efforts to tackle the issue of moisture sensitivity of EVOH in food packaging are being addressed from both the food industry and package industry perspective. Food scientists and engineers are continuously investigating novel thermal sterilization processes which shorten process times to reduce severity on both the food and the package. For example, in 2009, FDA accepted the use of pressure assisted thermal sterilization of mashed potato in a retort pouch (Somerville and Balasubramaniam, 2009), and microwave sterilization of mashed potato in a single serve polytray (Higgins, 2010). On the other hand, packaging scientists also proposed a variety of solutions over the years to address the issue of moisture sensitivity. The use of oxygen scavenging packaging technology, incorporation of dessicants in the layers surrounding EVOH to reduce the amount of moisture reaching the EVOH layer, blending of EVOH with other

materials to improve properties, use of nanocomposites, etc., are just a few examples. A nanocomposite film based on nylon MXD6 (developed by Mitsubishi Gas Chemical and Nanocor) delivers enhanced barrier to gases when used with an inner PET food contact layer for beverage packaging (Brody, 2006). For retort processing applications, a nanocomposite film based on PET or nylon 6 (Kurarister$^{(TM)}$) was been developed by Kuraray Co. (Kuraray Co.). Although the prospect of alternative packaging technologies is promising, much of it is still in the research and development stages.

In recent years there has been increased production capacity by the main EVOH producing companies, which might be taken as demonstration of continued confidence and expectation about future growth of EVOH markets worldwide. According to the 2000 annual report for Nippon Gohsei the world demand for EVOH was at 54,000 tonnes per year and expected to grow at an annual rate of 10% (Nippon Gohsei, 2000). In preparation for this anticipated growth, Nippon Gohsei increased its total production capacity at its US plant to 30,000 tonnes per year in 1999, started production of about 15,000 tonnes per year in the UK in 2003, in addition to the 10,000 tonnes per year produced in Japan. Likewise, Kuraray Co. increased its total production from 43,000 tonnes per year in 2001 to over 80,000 tonnes per year from their facilities in Europe, US and Japan (Kuraray Co., 2006).

References

Aharoni, S.M. 1998. Increased glass transition temperature in motionally constrained semicrystalline polymers. Polymers for Advanced Technologies 9, 169-201.

Armstrong, R.B. 2002. Effect of polymer structure on gas barrier of ethylene vinyl alcohol (EVOH) and considerations for package development. TAPPI PLACE Conference. September 8-12, 2002, Boston, MA.

Armstrong, R.B. 2008. EVOH barrier applications. A paper presented at Coextrusion Topcon 2008, October 21-22, Cincinnati, Ohio.

Aucejo, S., Marco, C., and Gavara, R. 1999. Water effect on morphology of EVOH copolymers. Journal of Applied Polymer Science 74, 1201-1206.

Bicerano, J. 1993. Prediction of Polymer Properties. Marcel Dekker, Inc. New York.

Blackwell, A.L. 1986. Ethylene vinyl alcohol copolymers. In Seymour, R.B. and Kirshenbaum, G.S. (Eds.). High performance polymers: their origin and development. Proceedings of the Symposium on the History of High Performance Polymers at the American Chemical Society Meeting held in New York, April 15-18, 1986. Elsevier. New York. pp 425-435.

Brandrup, J., and Immergut, E.H. 1989. Polymer Handbook. John Wiley and Sons, Inc. New York.

Brody, A.L. 2006. Nano and food packaging converge. Food Technology 60, 92-94.

Brown, W.E. 1986. Vinylidine chloride copolymers. In Baker, M., and Eckroth, D. (Eds). The Wiley Encyclopedia of Packaging Technology. John Wiley & Sons. New York. pp 692-696.

Burke, P. 1990. High barrier polymeric materials for increased shelf life. US Army Natick RD & E Center, Activities report: Research and Development 42, 76-79.

Cava, D., Sammon, C., and Lagaron, J.M. 2006. Water diffusion and sorption induced swelling as a function of temperature and ethylene content in ethylene vinyl

alcohol copolymers as determined by attenuated total reflection Fourier transform infrared spectroscopy. Applied Spectroscopy 60, 1392-1398.

Cerrada, M.L., Perez, E., Perena, J.M., and Benavente, R. 1998. Wide angle X-ray diffraction study of the phase behavior of vinyl alcohol-ethylene copolymers. Macromolecules 31, 2559-2564.

Cohen, M.H, and Turnbull D. 1959. Molecular transport in liquids and glasses. Journal of Chemical Physics 31, 1164-1169.

Ebewele, R.O. 2000. Polymer Science and Technology. Chapman and Hall/CRC Press LLC. Boca Raton, FL.

EVAL Americas. Technical Bulletin No. 110. Gas barrier properties of EVAL™ Resins. Downloaded from http://www.eval.be/upl/1/default/doc/EA%20-%20Technical%20Bulletin%20No%20110.PDF

Eyring, H. 1936. Viscosity, plasticity and diffusion as examples of absolute reaction rates. Journal of Chemical Physics 4, 283-291.

Ezquerra, T.A., Sics, I., Nogales, A,. Denchey, Z., and Balta-Calleja, J. 2002. Simultaneous crystalline-amorphous phase evolution during crystallization of polymer systems. Europhysics Letters 59, 417-422.

Freeman, B.D., and Hill, A.J. 1998. Free volume and transport properties of barrier and membrane polymers. In Tant, M.R., and Hill, A.J. (Eds.). Structure and Properties of Glassy Polymers. American Chemical Society, Washington, D.C. pp 306-325.

Gedde, U.W. 1999. Polymer Physics. Kluwer Academic Publishers. The Netherlands.

Gestoso, P., and Brisson, J. 2001. Effect of hydrogen bonds on the amorphous phase of a polymer as determined by atomistic molecular modeling. Computational and Theoretical Polymer Science 11, 263-271.

Gontard, N., Thibault, R., Cuq, B., and Guilbert, S. 1996. Influence of relative humidity and film composition on oxygen and carbon dioxide permeabilities of edible films. Journal of Agricultural and Food Chemistry 44, 1064-1069.

Hernandez, R.J. 1994. Effect of water vapor on the transport properties of oxygen through polyamide packaging materials. Journal of Food Engineering 22, 495-507.

Hernandez, R.J. and Giacin, J.R. 1998. Factors affecting permeation, sorption and migration processes in package-product systems. In Taub, I.A. and Singh, R.P. (Eds.) Food Storage Stability. Boca Raton, FL. pp 269-330

Higgins, K.T. 2010. Engineering R&D: Move over, retort. Food Engineering Magazine. pp 67-68.

Hodge, R.M., Bastow, T.J., Edward, G.H., Simon, G.P., and Hill, A.J. 1996a. Free volume and mechanism of plasticization in water swollen polyvinyl alcohol. Macromolecules 29, 8137-8143.

Hodge, R.M., Edward, G.H., and Simon, G.P. 1996b. Water absorption and states of water in semi-crystalline poly(vinyl alcohol) films. Polymer 37, 1371-1376.

Hui, Y.H. 2006. Handbook of Food Science, Technology and Engineering, Volume 3. Taylor and Francis Group, LLC. Boca Raton, FL.

Ito, K., Saito, Y., Yamamoto, T., Ujihira, Y., and Nomura, K. 2001. Correlation study between oxygen permeability and free volume of ethylene vinyl alcohol

copolymer through positronium lifetime measurement. Macromolecules 34, 6153-6155.

Ito, K., Li, H.-L., Saito, Y., Yamamoto, T., Nishihara, Y., Ujihira, Y., and Nomura, K. 2003. Free volume study of ethylene vinyl alcohol copolymer evaluated through positronium lifetime measurement. Journal of Radioanalytical and Nuclear Chemistry 255, 437-441.

Iwanami, T. and Hirai, Y. 1983. Ethylene vinyl alcohol resins for gas barrier material. TAPPI Journal 66, 85-90.

Iwamoto, R., Amiya, S., Saito, Y., and Samura, H. 2001. FT-NIR spectroscopic study of OH groups in EVOH copolymer. Applied Spectroscopy 55, 864-870.

Iwamoto, R., Matsuda, T., Amiya, S. and Yamamoto, T. 2006. Interactions of water with OH groups in poly(ethylene-co-vinyl alcohol). Journal of Polymer Science. Part B: Polymer Physics 44, 2425-2437.

Katsura, T., and Sasaki, H. 2001. On-going solutions to environmental issues in plastic packaging. Packaging Technology and Science 14, 87-95.

Ketels, H. 1989. Synthesis, Characterization and Applications of Ethylene vinyl Alcohol Copolymers. PhD Thesis. University of Eindhoven, The Netherlands.

Koros, W.J. 1990. Barrier polymers and structures: overview. In Koros, W.J. (Ed.). Barrier Polymers and Structures. ACS Symposium Series 423, American Chemical Society. Washington, DC. pp 1-21.

Kuraray Co. 2006. Annual Report 2006. Downloaded from http://www.kuraray.co.jp/ir/library/pdf/annual/ar2006.pdf.

Kuraray Co. Kurarister – Transparent High Barrier Retortable Film. Downloaded from http://www.kurarister.com/upl/1/default/doc/Kurarister%20Technical%20Brochure%20AP(1).pdf.

Lagaron J.M., Powell, A.K., and Bonner, G. 2001. Permeation of water, methanol, fuel and alcohol containing fuels in high barrier ethylene vinyl alcohol copolymer. Polymer Testing 20, 569-577.

Lagaron, J.M., Giménez, E., Gavara, R., and Catala, R. 2003. Mechanisms of moisture sorption in barrier polymers used in food packaging: amorphous polyamide vs. high barrier ethylene–vinyl alcohol copolymer studied by vibrational spectroscopy. Macromolecular Chemistry and Physics 204, 704-713.

Lagaron, J.M., Catala, R., and Gavara, R. 2004. Structural characteristics defining high barrier properties in polymeric materials. Materials Science and Technology 20, 1-7.

Lange, J., and Wyser, Y. 2003. Recent innovations in barrier technologies for plastic packaging – a review. Packaging Technology and Science 16, 149-158.

Levine, H., and Slade, L. 1988. Water as a plasticizer: physic-chemical aspects of low moisture polymeric systems. In Franks, F. (Ed.). Water Science Reviews, Vol. 3. Cambridge University Press. Cambridge, England. pp 79-185.

Lopez-Rubio A., Lagaron, J.M., Gimerez, E., Cava, D., Hernandez-Munoz, P., Yamamoto, T. and Gavara, R. 2003. Morphological alterations induced by temperature and humidity in ethylene vinyl alcohol copolymers. Macromolecules 36, 9467-9476.

Massey, L.L. 2003. Permeability Properties of Plastics and Elastomers: A Guide to Packaging and Barrier Materials. PDL Handbook Series. Plastic Design Library/William Andrew Publishing. Norwich, NY.

Matsui, I., Omishi, H. and Yamamoto, T. 2003. Study on orientable EVOH. 9th EUROPLACE Conference. May 12-14, 2003, Roma, Italy.

Muramatsu, M., Okura, M., Kuboyama, K., Ougizawa, T., Yamamoto, T., Nishihara, Y., Saito, Y., Ito, K., Hirata, K., and Kobayashi, Y. 2003. Oxygen permeability and free volume hole size in ethylene vinyl alcohol copolymer film: temperature and humidity dependence. Radiation Physics and Chemistry 68, 561-564.

Nakame, K., Kameyama, M., and Matsumoto, T. 1979. Elastic moduli of the crystalline regions in the direction perpendicular to the chain axis of ethylene vinyl alcohol copolymers. Polymer Engineering and Science 19, 572-578.

Nippon Gohsei. 2000. Annual Report 2000. Downloaded from http://www.nichigo.co.jp/ir/pdf/ar2000.pdf

Osborn, K. R. and Jenkins, W.A. 1992. Plastic Films - Technology and Packaging Applications. Technomic Publishing Company, Inc. Lancaster, PA.

Peacock, A.J. 2000. Handbook of Polyethylene: Structures, Properties and Applications. Marcel Dekker, Inc. New York.

Robertson, G.L. 2006. Food Packaging: Principles and Practice. CRC Taylor and Francis, New York.

Salame, M. 1986. Barrier polymers. In Baker, M., and Eckroth, D. (Eds). The Wiley Encyclopedia of Packaging Technology. John Wiley and Sons. New York. pp 48-54.

Seguela, R., Djezzar, K., Penel, L., Lefebvre, J-M., and Germain, Y. 1998. Tensile drawing of ethylene vinyl alcohol copolymers: 3. Biaxial orientation. Polymer 40, 47-52.

Sidwell, J.A. 1992. Food Contact Polymeric Materials. Vol. 6. No. 1. Report 61. Rapra Technology Ltd. England.

Soarnol®. Relationship Between Relative Humidity and T_g. Downloaded from http://www.soarnol.com/eng/s_data/s_data13.html.

Somerville, J., and Balasubramaniam, V.M. 2009. Pressure assisted thermal sterilization of low acid, shelf stable foods. Resource Magazine 16, 14-17.

Takahashi, M., Tashiro, K., and Amiya, S. 1999. Crystal structure of ethylene vinyl alcohol copolymers. Macromolecules 32, 5860-5871.

Tsai, B.C., and Jenkins, B.J. 1988. Effect of retorting on the barrier properties of EVOH. Journal of Plastic Film & Sheeting 4, 63-71.

van Krevelen, D.W. 1990. Properties of Polymers: Their Correlation with Chemical Structure; Their Numerical Estimation and Prediction from Additive Group Contributions. Elsevier. Amsterdam, The Netherlands.

Vaughan, A.S. and Bassett, D.C. 1989. Crystallization and morphology. In Allen, G. and Bevington, J.C. (Eds.). Comprehensive Polymer Science: The Synthesis, Characterization, Reactions and Applications of Polymers. Volume 2: Polymer Properties. Pergamon Press. Oxford, England. pp 415-457.

Young, R.J., and Lovell, P.A. 1991. Introduction to Polymers. CRC Press. Boca Raton, FL.

Zhang, Q., Lin, W., Chen, Q., and Yang, G. 2000. Phase structure of EVOH copolymers as revealed by variable temperature solid state high resolution ^{13}C NMR spectroscopy. Macromolecules 33, 8904-8906.

Zhang, Z., Britt, I.J., and Tung, M.A. 1999. Water absorption in EVOH films and its influence on glass transition temperature. Journal of Polymer Science. Part B: Polymer Physics 37, 691-699.

Zhang, Z., Britt, I.J., and Tung, M.A. 2001. Permeation of oxygen and water vapor through EVOH films as influenced by relative humidity. Journal of Applied Polymer Science 82, 1866-1872.

CHAPTER 3 THERMAL PROCESSING EFFECTS ON OXYGEN TRANSMISSION RATES OF MULTILAYER EVOH FILMS

3.1 Introduction

Ready-to-eat meals that are aimed at extended shelf life under ambient storage conditions are generally processed by thermal sterilization methods to produce microbiologically safe foods (Ramaswamy and Marcotte, 2006). In thermal processing, the change in temperature is the main processing factor. The aim of every thermal sterilization process is to supply sufficient heat to achieve inactivation of pathogenic and food spoilage microorganisms in food packages to comply with public health standards. The process schedule is minimally defined by the combination of temperature and time to which containers are subjected in order to effect sterilization. The time and temperature required for a heat treatment are established from characterizing the heat resistance of the target microorganism. A criterion against which to judge the effectiveness or severity of thermal processes uses the concept of lethality values, which quantitatively measures the rate of inactivation (i.e., lethal effect) of microorganisms at a given temperature. Lethality is calculated from the following equation (Holdsworth and Simpson, 2008):

$$L = 10^{\frac{T-T_{ref}}{z}} \tag{3.1}$$

where L is the lethal rate; T is the actual temperature of the product (°C) at the cold spot and T_{ref} is reference temperature; z is the temperature increase required to reduce the thermal death time of the target microorganism. In practice, the product temperature varies from the initial temperature to the desired processing temperature, and the

achieved lethal rates are integrated over the processing period. The integrated lethal rate is known as the F value introduced by Ball (1923). This is calculated using data obtained at the point of slowest heating (or cold spot) according to the following equation (Downing, 1996):

$$F = \int_0^t L dt = \int_0^t 10^{\frac{T-T_{ref}}{z}} dt \qquad (3.2)$$

where t is heating time. The F value is additive such that the various stages of heating, holding and cooling in a complete thermal process contribute to the total F value for a complete process cycle. Thus, the F value is used to determine the level of heat treatment that would be required for a particular foodstuff (i.e. time and temperature combinations required to give an "adequate" thermal treatment of the food).

From the public health standpoint the most important microorganism in low acid (pH>4.5) canned foods is *Clostridium botulinum*, a heat resistant spore forming pathogen which can grow and produce the deadly botulin toxin under anaerobic conditions if it survives processing. A minimum process which should decrease the microbial population of *Clostridium botulinum* by 12 logarithmic cycles (12D concept) has been established for production of low acid canned foods which are adequately processed to prevent public health hazard (Holdsworth and Simpson, 2008). The 12D concept suggests that a thermal treatment is sufficient to ensure that the chance of *Clostridium botulinum* surviving is $1/10^{12}$ (i.e., only 1 can in 10^{12} cans may be expected to possess a viable spore). In the case of *Clostridium botulinum*, where the z value is 10°C and when the reference temperature is 121.1°C (250°F), the F value is designated as F_o value (Lewis and Heppell, 2000). Thus, for low acid foods where *Clostridium botulinum* is considered for

public safety, the 12D process relates to a minimum heat treatment of an F_o value of 3 minutes. This level of treatment has been used over decades to give acceptably low risk to public health. However, for most food products, heat treatment greater than this minimum process must be achieved in order to prevent spoilage of the food by more resistant but nonpathogenic microorganisms (Lewis and Heppell, 2000). This also takes into consideration any additional processing requirements, excessively high initial spore loads, variations in product formulation variations and filled weight, etc.

Although the fundamental objective of thermal processing is microbial inactivation, the acceptability of the product depends on the sensory attributes. The heat applied to the food product not only inactivates microorganisms but also facilitates the cooking of the product to give an acceptable texture and destroys active enzymes (Holdsworth and Simpson, 2008). Concurrently, nutrients, color and other quality attributes are destroyed. Therefore, a balance between excessive heating and under-processing is very important. This requires control of time and temperature combinations during processing to avoid either under- or over-processing. In practice, there are limits to suitability of processes, and sterilization temperatures are generally in the range 115-130°C (Holdsworth and Simpson, 2008). The higher the temperature, the shorter the time required.

3.2 Overview of Thermal Processing Methods

Thermal sterilization of canned foods in retorts has been one of the most widely used industrial methods for food preservation during the twentieth century and has

contributed significantly to the nutritional well-being of much of the world's population (Teixeira and Tucker, 1997). Technologies used for thermal processing of foods have evolved with time from the traditional retort heating to dielectric heating (i.e. microwave and radio frequency heating), ohmic heating, inductive heating, etc. Despite the development of these novel methods, retorting is still the food industry's most common commercial sterilization process for prepackaged shelf stable foods low acid foods. In conventional retort sterilization, food packages are heated in pressurized vessels (retorts) at specified temperatures for prescribed lengths of time using saturated steam, steam-air mixture or superheated water as heating medium. The retort temperature is raised to desired temperature as rapidly as possible, held at the temperature until the desired microbial destruction has been achieved, and then cooled rapidly. Retort processing is characterized by slow heat conduction from the heating medium to the slowest heating point in solid or semi-solid foods. This often results in long process times and overheating at the periphery of the food package. Texture of canned foods may become softer than desired, product color may become darker, and heat labile components such as vitamins may be destroyed.

While the traditional heating methods rely essentially on conductive, convective and radiative heating, the newer "novel" methods involve generation of heat directly inside the food. This has direct implications in terms of both energy efficiency, and consequently the quality of the processed food product (Tewari and Juneja, 2007). Microwave (MW) heating is a result of interaction between alternating electromagnetic field and dielectric material. Microwaves interact with polar water molecules and charged ions. The friction resulting from molecules aligning in rapidly alternating electromagnetic

field generates the heat within food. Compared with conventional heating using water or steam as the heating media for packaged foods, microwave energy has the potential to sharply reduce the time to raise product temperature required to achieve thermal lethality to target bacteria (Bengtsson and Ohlsson, 1974).

Microwave heating has drawn much attention of researchers in developing novel pasteurization and sterilization processes for packaged foods. A great deal of scientific and engineering data information has been generated to support regulatory acceptance of microwave sterilization technology for industrial applications. For example, a 915-MHz, single-mode, microwave sterilization system for processing packaged foods was developed at Washington State University (WSU) (Tang et al., 2006). During several studies, some necessary processing parameter, such as microwave power, flow rate and temperature of circulating water, were established for optimum operation of this system. A chemical-marker computer vision technique for determining heating patterns and cold spots inside microwave treated food packages was developed by the WSU microwave research group (Pandit et al., 2007). The system at WSU has been used for studying the influence of microwave sterilization on quality of various foods, including asparagus (Sun et al., 2007), macaroni and cheese (Guan et al., 2002; Guan et al., 2003), salmon, chicken, rice, scrambled eggs, and mashed potatoes. Guan et al. (2002) reported that it took only eight minutes to raise the temperature of a macaroni and cheese product to 127°C in a microwave-circulated water combination heating system, while it took 40 minutes for conventional hot water retort for the same sized trays. Sensory analysis using a trained panel revealed that the short microwave sterilization process resulted in much

better color, texture and flavor for the macaroni and cheese product as compared to conventional retorting (Guan et al., 2002).

The objective of this study was to compare the oxygen transmission rate of two multilayer EVOH films subjected to conventional retort and microwave sterilization processes. Analysis of oxygen transmission rates was performed immediately following processing and at predetermined time periods during 12 months of storage at ambient conditions.

3.3 Materials and Methods

3.3.1 Experimental Design

The experimental plan consisted of two thermal treatment methods (microwave and retort); two process lethality levels ($F_0 = 3\,min$ and $F_0 = 6\,min$); and two film structures (film A and film B). The $F_0 = 3\,min$ process is the minimum process required for low acid foods, while the $F_0 = 6\,min$ process is a more severe process usually applied to control spoilage microorganisms (Holdsworth, 1997). For the retort treatment, only the $F_0 = 3\,min$ process was used. Preliminary tests showed that $F_0 = 6\,min$ retorting caused severe distortion and visible de-lamination in the lidstock films due to water penetration through the PP and PET layers into the EVOH layer. This observation is consistent with the fact that EVOH containing films are currently not used as flexible pouch or lidstock materials for thermally processed foods in the USA because of the severe thermal degradation during commercial industrial retorting practices. Thus conventional (still) retorting for $F_0 = 6\,min$ was not included in the experimental design.

Control samples for both films (i.e., films not exposed to any thermal treatment) were also evaluated in duplicate for comparison. The experimental plan is summarized in Table 3.1.

Table 3.1. Experimental design for oxygen transmission tests after post-processing storage (number in the table shows replicates)

Thermal Treatment	Process Lethality	Film Structure	Storage Time (months)				
			0	1	2	3	12
Microwave	$F_0 = 3\ min$	A	2	2	2	2	2
		B	2	2	2	2	2
	$F_0 = 6\ min$	A	2	2	2	2	2
		B	2	2	2	2	2
Retort	$F_0 = 3\ min$	A	2	2	2	2	2
		B	2	-	2	-	2

3.3.2 Description of Multilayer EVOH Films and Rigid Trays

Two multilayer films containing a thin layer of EVOH (EVAL™) as a barrier material were supplied by EVAL Company of America, Houston, TX. Film A was a laminated structure consisting of a 12μm of EF-XL resin layer sandwiched between a 75μm of cast polypropylene layer on the side to be in direct contact with food and a 12μm of biaxially oriented PET layer on the outer side (denoted PET//EVOH//PP). Film B consisted of PET laminated to a 7-layer co-extruded structure of 15μm L171 resin

between 10μm nylon 6 homopolymer and 50μm PP homopolymer on both sides (denoted PET//PP/tie/Nylon 6/EVOH/Nylon 6/tie/PP). The tie layer between PP and nylon 6 was a maleic anhydride acid modified polypropylene. The EF-XL EVOH resin used in film A was biaxially oriented with 32 mol % ethylene, while L171 EVOH in film B was a non-oriented resin with 27 mol % ethylene. At 20°C and 0% RH, the two EVOH resins have oxygen permeability in the order of $0.002 cm^3.mm/m^2.24hrs.atm$ (EVAL Americas). Description of lamination and co-extrusion processes can be found in literature such as Frey (1986).

Rigid trays used for packing mashed potato were supplied by Rexam Containers, Union, MO, USA. The structure of the trays consisted of PP/regrind/tie/EVOH/tie/regrind/PP with a total wall thickness of about 1.8mm. The proportion of EVOH in the trays was about 1.4% by volume. The trays had a net volume of about $300 cm^3$ and dimensions of 10.0×14.0×2.5cm.

3.3.3 Preparation of Mashed Potato

Mashed potato was prepared by mixing 15.4% instant mashed potato flakes (obtained from Washington Potato Company, Warden, WA, USA) with 84.6% deionized water. About 300 ± 0.2g deaerated mashed potato at a temperature of 75 ± 1°C was filled into the rigid trays described above. The filled trays were vacuum sealed with the lidstocks from film A and B using a custom vacuum tray sealer (Rexam Containers, Union, MO, USA) with a top sealing plate temperature set at 193°C, 305mm Hg vacuum and a seal time of 3 seconds. The complete description of the vacuum sealer can be found

in Guan et al. (2003). For both film A and film B, the PP side of the film was in direct contact with the food while the PET side was on the outside of the package.

3.3.4 Microwave and Retort Heating Procedures

A pilot scale 915-MHz single mode microwave sterilization system developed at Washington State University (WSU, Pullman, WA, U.S.A.) was used for the thermal treatments (Tang et al., 2006). This system consisted of two 5-kW 915-MHz microwave generators (Microdry Model IV-5 Industrial Microwave Generator, Microdry Incorporated, Crestwood, KY., U.S.A.), a pressurized microwave heating vessel connecting two microwave cavities, a water circulation heating and cooling system, and a control and data acquisition system. The pressurized microwave heating vessel allowed batch treatments of four meal trays held in a microwave transparent customized conveyor system. In operation, food trays were conveyed through the two microwave cavities in a thin bed of circulating water. In each cavity, microwave energy was applied from two microwave applicators through a pair of microwave transparent widows that were a part of the top and bottom walls of the heating vessel. One microwave generator provided equal power to the pair of the applicators for each cavity via a T-splitter in the waveguides. A detailed description of waveguide arrangement is provided in Tang et al. (2006).

An over-pressure of 1.8 atm (26 psig) via compressed air was applied to the circulating water during heating and cooling to maintain the integrity of food packages. This system also enables the heating vessel to function as a hot water immersion still

retort when microwave power is not applied. The temperature of the circulating water was controlled via two plate heat exchangers, one for heating, and another for cooling. The exchangers were heated and cooled with steam and tap water, respectively. A Think & Do^{TM} computer program (Entivity, Ann Arbor, Mich., U.S.A.) was used to control the modulating valves of the exchangers. More details of the microwave heating system can also be found in Chen et al. (2007) and Tang et al. (2008).

For temperature measurement during processing, four fiber optic sensor cables (FISO Technologies, Inc., Canada) were fed through pressure tight fittings on one of the pressure vessel walls; each sensor tip was inserted at the cold spot of one tray through polyimide tubing that prevented food from leaking out through the probe. The cold spot was predetermined using a chemical marker method and computer vision system described in Pandit et al. (2006). Meal trays moved through the two microwave cavities on a conveyor belt at a speed that allowed the cold spot in the tray to reach 121°C upon exiting the second microwave cavity. During processing, the circulating water temperature for heating and cooling, as well as the temperature of the mashed potato at the cold spot of the four trays, were displayed and recorded every second. The degrees of sterilization (F_0 values) were also shown on the screen. System over-pressure was monitored using a pressure gauge. Thermal treatment procedures were selected to achieve two levels of sterilization of $F_0 = 3\ min$ and $F_0 = 6\ min$ at the cold spot in the mashed potato. In general, the $F_0 = 3\ min$ process is the minimum for commercial sterility while $F_0 = 6\ min$ is generally used for commercial retail markets.

For microwave sterilization, the output microwave power for each of the two generators was maintained at 2.5 kW by regulating anode current to the magnetron. In the

heating vessel the food product was first preheated to 75°C using circulating hot water at 100°C. The combined heating started when the microwave power was turned on and hot water at 125°C was circulated at a flow rate of 40 liter/min. The holding stage began by maintaining the circulated water at 125°C while the microwave was turned off. After the desired holding period, the trays were cooled using circulating water at 80°C under pressure, then by tap water at 20 °C at ambient pressure. To achieve $F_0 = 3\ min$ thermal lethality at the cold spot, it required a total processing time of 9 min after preheating (excluding cooling) and 12 min to reach $F_0 = 6\ min$ thermal lethality in the prepackaged mashed potato. To simulate conventional still retort processing the system was used without turning on the microwave power generators. The same procedures for filling, preheating, and water heating and cooling were used to achieve $F_0 = 3\ min$ at the cold spot. It took a total heating time of 28 min to achieve $F_0 = 3\ min$ at the cold spot in trays for the still retort treatments. Figure 3.1 shows representative temperature profiles at the cold spot of the trays for both microwave and still retort processes.

The microwave and retort sterilized trays were shipped overnight to the Kuraray Research and Technical Center of EVAL Company of America in Pasadena, TX via FEDEX for analysis of O_2 transmission rates. Due to the limitations in processing capacity of the heating system, trays for the $F_0 = 3\ min$ and $F_0 = 6\ min$ treatments were processed and shipped on different dates. Trays marked for control (no heat treatment) and for 0 month storage were analyzed immediately when they arrived at Kuraray Research and Technical Center. The remaining food trays were stored at ambient conditions (approximately 20°C and 65% RH) until analyses were conducted at specified time intervals over a 12-month period as indicated in Table 3.1.

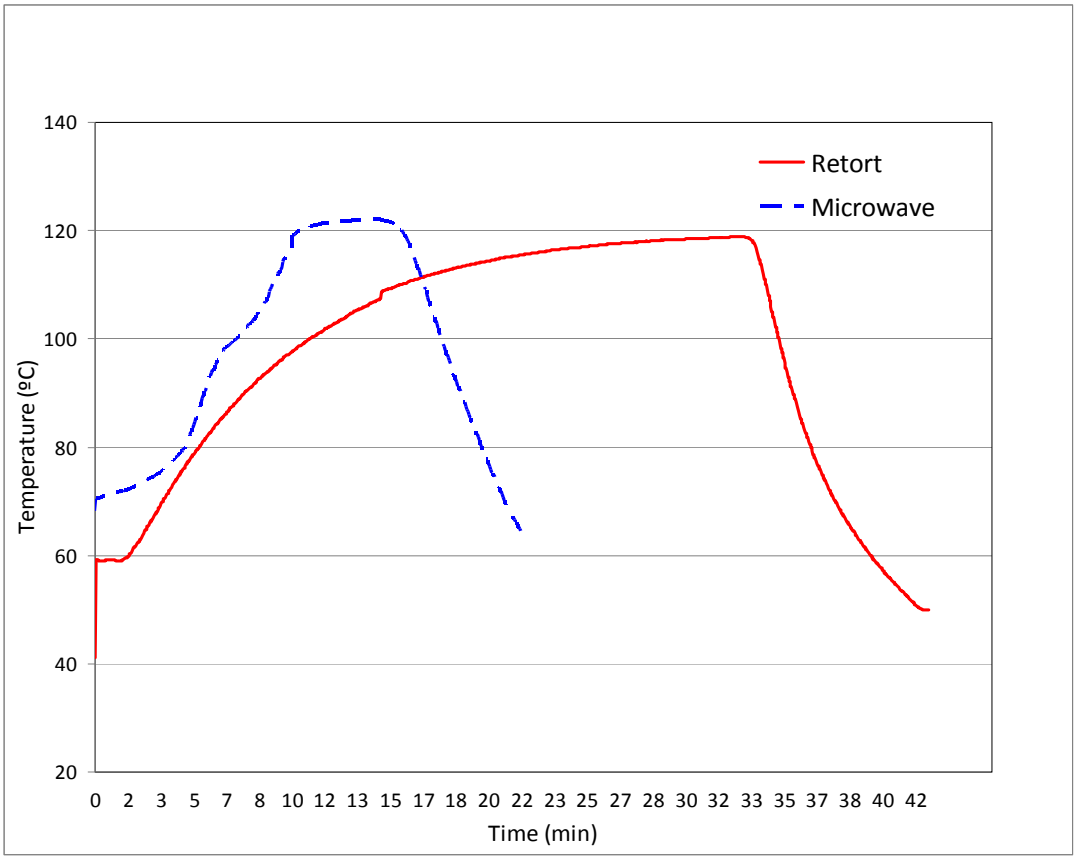

Figure 3.1. Representative temperature-time profiles for the cold spot of mashed potato in trays during microwave and retort treatments ($F_0 = 6\ min$)

3.3.5 Determination of Oxygen Transmission Rates of Films

OTR represents the ease with which oxygen passes the films when submitted to a gradient in the partial pressure of Oxygen across the films. It is expressed as the quantity (Q) of Oxygen molecules passing through a film surface area (A) during time (t) at steady state under a partial pressure difference (Δp) in Oxygen between the two surfaces of the sample (Massey, 2003):

$$OTR = \frac{Q}{At\Delta p} \tag{3.3}$$

Oxygen transmission rates (OTR) were analyzed using MOCON OX-TRAN 2/20 devices (MOCON, Inc., USA). This instrument uses the ASTM D3985 standard method (ASTM, 1995), which covers a procedure for determination of the steady-state rate of transmission of oxygen gas through plastics in the form of film, sheeting, laminates, coextrusions, or plastic-coated papers or fabrics. The specimen is mounted as a sealed semi-barrier between two chambers at ambient atmospheric pressure. 100% oxygen (the test gas) is continuously admitted to the outer half of the test cell and is allowed to exit through an exhaust port. A special mixture of carrier gas (a mixture of 98% nitrogen and 2% hydrogen) is continuously admitted to the inner half of the test cell. Before entering the test cell, the nitrogen/hydrogen passes through a catalyst. The hydrogen reacts with any oxygen that happens to be in the carrier gas to form water vapor. This helps ensure that the carrier gas does not contain any oxygen that might affect transmission rate data (ASTM, 1995). As the test gas (oxygen) permeates the film sample, it is picked up by the carrier gas and carried through the oxygen sensor, a coulometric fuel cell (COULOX®) that produces an electrical current when exposed to oxygen. The current generated is directly proportional to the amount of oxygen passing through the sensor.

The sensor operates on a coulometric process whereby oxygen in the carrier gas is reduced in an electrochemical cell. The carrier gas diffuses through a simple gas diffusion barrier to the cathode of an electrochemical cell which is in contact with an electrolyte of potassium hydroxide. Oxygen is reduced at this electrode to hydroxyl ions. Assisted by the conductivity of the potassium hydroxide electrolyte the ions migrate to the anode, where they are oxidized back to oxygen. The reaction is driven by an external voltage. The reaction produces an electrical current the magnitude of which is proportional to the

oxygen concentration in the carrier gas. The concentration is amplified accurately by solid state circuitry and displayed. The sensor output current should increase gradually, ultimately stabilizing at a constant value. The computer collects data from the Coulox sensor and calculates a final value describing the oxygen transmission rate of the test material. After passing through the sensor, the carrier gas exits through an exhaust port. A picture of MOCON OX/TRAN instruments and schematic of the diffusion cell are shown in Figure 3.2

Trays containing mashed potato were selected at random and the lidstock films were peeled off and food residues were cleaned by rinsing with distilled water and wiping with a paper towel. A single film specimen was cut out from each tray lid to have a measurement area of $50cm^2$. The specimens were mounted onto the diffusion cells the test gas (i.e. oxygen) was routed through the PET side of the film specimens while a the carrier gas passes on the PP side. The amount of oxygen measured in the sensor reached steady state/equilibrium value after 14 to 30 days. Thus, the length of test to obtain one data point of two replications was 14-30 days. The test conditions used in the MOCON OX-TRAN 2/20 system were 20°C and 65% RH. Duplicate film samples were tested after 0, 1, 2, 3 and 12 month storage at 20°C and 65% RH. Analysis of variance was performed on the data to determine statistical significance between treatment effects.

MOCON OX/Tran instruments at Kuraray Research and Technical Center, Pasadena, TX

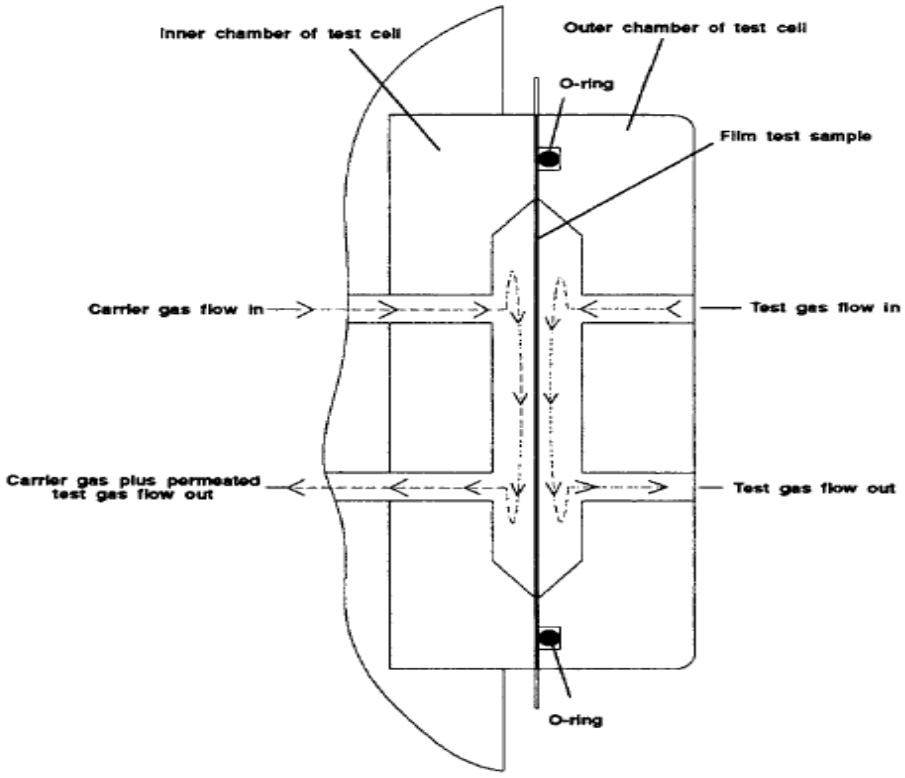

Diffusion cell inside MOCON OX/Tran instrument

Figure 3.2. MOCON OX-TRAN instruments

3.4 Results and Discussion

Table 3.2 summarizes the O_2 transmission rate data for all treatments studied. In general, oxygen transmission in the multilayer EVOH films increased many fold after the thermal processes; it was recovered to a certain degree during the first two months storage, and was stabilized or increased during 12 months in storage.

Table 3.2. Oxygen transmission rates (cc/m^2 day) of EVOH films after microwave and retort treatments and during storage for 12 months at 20°C and 65% RH

Storage Time (months)	Film A			Film B		
	Microwave ($F_0 = 3\ min$)	Microwave ($F_0 = 6\ min$)	Retort ($F_0 = 3\ min$)	Microwave ($F_0 = 3\ min$)	Microwave ($F_0 = 6\ min$)	Retort[a] ($F_0 = 3\ min$)
Control[b]	0.16 ± 0.01[a]			0.096 ± 0.01		
0	0.79 ± 0.01[a]	1.58 ± 0.38 [ab]	1.75 ± 0.04[ab]	1.58 ± 0.22	2.30 ± 0.32	4.57 ± 0.59
1	0.62 ± 0.004[a]	0.72 ± 0.01[a]	1.35 ± 0.16[b]	1.40 ± 0.30	1.19 ± 0.01	-
2	0.44 ± 0.23[a]	0.66 ± 0.03[ab]	0.85 ± 0.03[bc]	1.05 ± 0.04	0.81 ± 0.05	0.83 ± 0.17
3	0.73 ± 0.03[a]	0.77 ± 0.004[a]	0.83 ± 0.01[ab]	0.92 ± 0.02	1.28 ± 0.11	-
12	0.80 ± 0.07[a]	0.79 ± 0.03[a]	2.30 ± 0.21[c]	1.36 ± 0.11	1.09 ± 0.136	1.33 ± 0.34

[a] No data were collected at 1 and 3 months of storage

[b] Control films received no heat treatment

Means with different letters within a row are significantly different at $\alpha < 0.05$

3.4.1 Effect of Thermal Treatments

A comparison of oxygen transmission rates of the two films before and immediately after thermal processing is shown in figure 3.3. Before thermal treatments, the oxygen transmission rates of film A and film B were 0.160 and 0.096 cc/m^2.day, respectively. These values are lower than the oxygen transmission rates of 0.3–2.3cc/m^2.day reported by commercial packaging companies for similar thickness of laminated PVDC (commonly referred to as Saran) barrier film or silicon dioxide (SiOx) coated films currently used as lid films and flexible pouch materials for thermally processed shelf-stable foods in retail markets. Microwave and retort processes had adverse impacts on the oxygen barrier of both films as indicated by the increased oxygen transmission rates observed immediately after processing. The oxygen transmission rate of film A increased 5 fold and 10 fold for the $F_0 = 3\,min$ and $F_0 = 6\,min$ microwave processes, respectively, and increased by about 11 times due to the hot water retort ($F_0 = 3\,min$) treatment. The oxygen transmission rate of film B increased by about 16 and 24 times, respectively, for $F_0 = 3\,min$ and $F_0 = 6\,min$ microwave processes, and about 47 times for the retort treatment. That is, the oxygen transmission rate after the $F_0 = 6\,min$ microwave process was about twice that of the $F_0 = 3\,min$ microwave process for film A and about 1.5 times that of $F_0 = 3\,min$ process for film B. The oxygen transmission rate immediately after retort treatment was twice that of the microwave treatment for film A ($F_0 = 3\,min$) and almost 3 times that of the microwave process for film B. Thus, the short time microwave sterilization process sharply reduced the adverse thermal processing impact to both EVOH films as compared to conventional retorting.

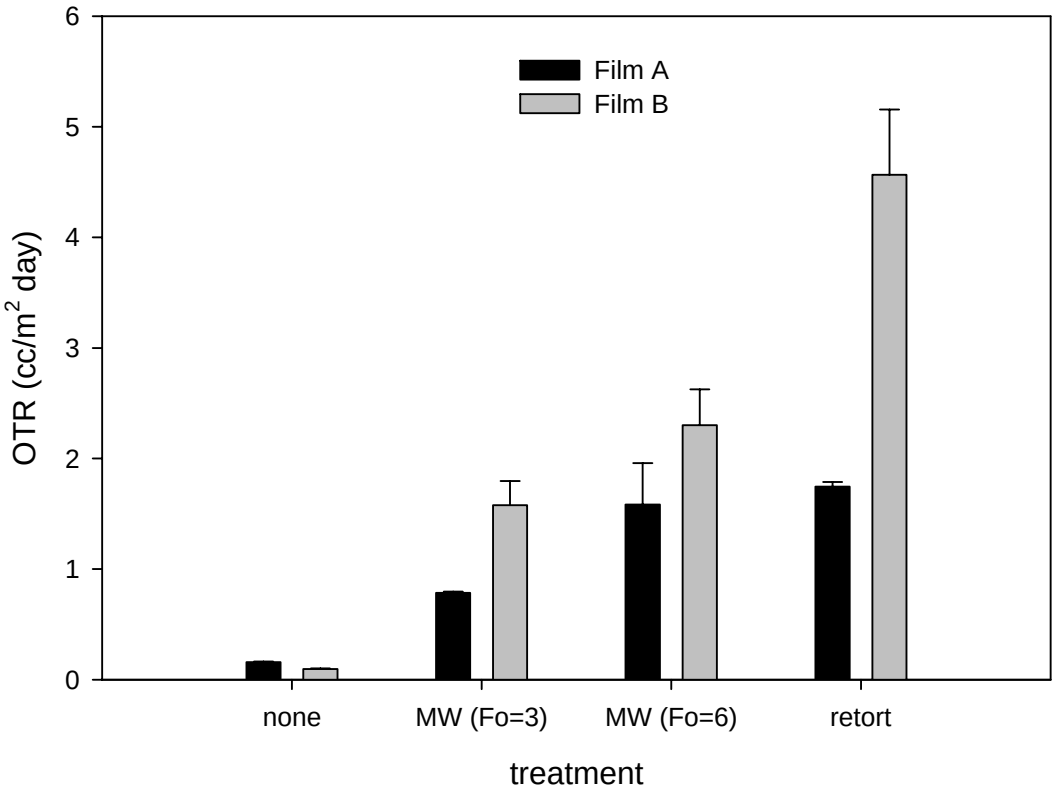

Figure 3.3. Initial post-processing oxygen transmission rate of film A and film B as influenced by microwave (MW) and pressurized hot water treatments

The sharp increase in the oxygen transmission rates due to thermal processing is unique to EVOH laminated films and can be detrimental when used in flexible packages that need to go through conventional retort processing in production of shelf-stable low acid foods. The above results imply that food products processed to a lethality of $F_0 = 6\,min$ by conventional retort would experience more deterioration resulting from oxidation processes during storage when packaged in these types of films, as compared to those processed by $F_0 = 3\,min$ and microwave processes.

The differences in oxygen transmission rate due to the thermal treatments may be explained on the basis of plasticization resulting from water absorption by the EVOH layer during processing. It is possible that the amount of water absorbed by the films was directly proportional to processing time. Due to the short times utilized in microwave heating (i.e., 9 min processing time), the films might have absorbed less moisture than those processed by retort (i.e., 28 min total processing time). The positive correlation between exposure time to water and loss of barrier in the films was also observed for the two microwave processes (i.e. 9 min for $F_0 = 3\ min$ and 12 min for $F_0 = 6\ min$).

To support the above speculation, separate moisture absorption experiments were conducted to determine how much water was absorbed by the two films when immersed in water at 121°C for durations similar to those used in this study. The results from these absorption experiments indicated that exposing film A to water at 121°C for 10 min (similar exposure times to the microwave sterilization treatment used in this study) resulted in moisture uptake of about 4.3% by weight. Exposing film A for 30 min (corresponding to retorting for $F_0 = 3\ min$) resulted in 6.2% moisture uptake. Similarly, film B absorbed about 2.9% and 4.6% moisture when exposed to water for 10 min and 30 min, respectively.

Hernandez and Giacin (1998) reported 60 times increase in oxygen transmission rate for a film structure of 12μm PET/15μm EVOH/60μm cPP (similar to that of film A) after retorting for 20 min at 125°C. The authors also reported very limited effect of thermal treatment on oxygen barrier properties of SiOx coated film (i.e., 12μm PET/SiOx/60μm cPP) and PVDC multilayer film (i.e., 12μm PET/15μm PVDC/15μm

Oriented Nylon /60μm cPP), where oxygen transmission rates increased by only 1.4 times after retort. PVDC and SiOx films are commonly used in lidstock films and flexible pouches. Despite the better performance during retort PVDC contains chlorine and at high temperatures (e.g., during incineration) it undergoes thermal degradation, producing toxic and corrosive products (Wright et al., 1995). PVDC is also more difficult to process and requires special equipment for extrusion. SiOx films have limited flex and crack resistance, which is not easily detected without stress testing of packaging material, and production costs are relatively high (Lange and Wyser, 2003).

3.4.2 Effect of Film Structure

It is evident from Table 3.2 that the oxygen transmission rates of film A and film B before heat treatments were statistically comparable. But after thermal treatments the oxygen transmission rate of film B was higher than that of film A. In particular, after the retort treatment the oxygen transmission of film B was 2.6 times higher than that of film A. For the microwave treatment the ratio of oxygen transmission rate of film B to that of film A ranged from 1.5 to 2 depending on the severity of the process. Film A consisted of a biaxially oriented EF-XL EVOH resin while film B consisted of a non-oriented L171 resin. Molecular alignment that occurs during biaxial orientation generally improves crystallinity, which results in a more tortuous path for oxygen and water vapor permeation, hence the lower oxygen transmission rates observed for film A. The differences between the two films cannot be adequately attributed to plasticization of the EVOH barrier layers by water. It is likely that different factors arising from the individual

layers used in each multilayer film structure combined to influence how the oxygen barrier was affected during thermal processing. The unique multilayer structures of the two films likely provided different mechanisms for protecting the oxygen barrier of the EVOH layers as a result of the thermal processes.

Visual observations of the films after heat treatments have shown some damage in both films, manifested as wrinkling/wavy patterns and clusters of small blister-like swelling. Some of the damage is shown in Figure 3.4 for films exposed to $F_0 = 3\,min$ retort treatment. These observations may be an indication that there were some variations and potential loss of adhesion strength between some adjacent layers within the film structures. However, the visual damage was not unique to or consistent with either film. A sufficient explanation based on changes in internal structures of the films after thermal treatments is not possible without further microstructure examination of the films.

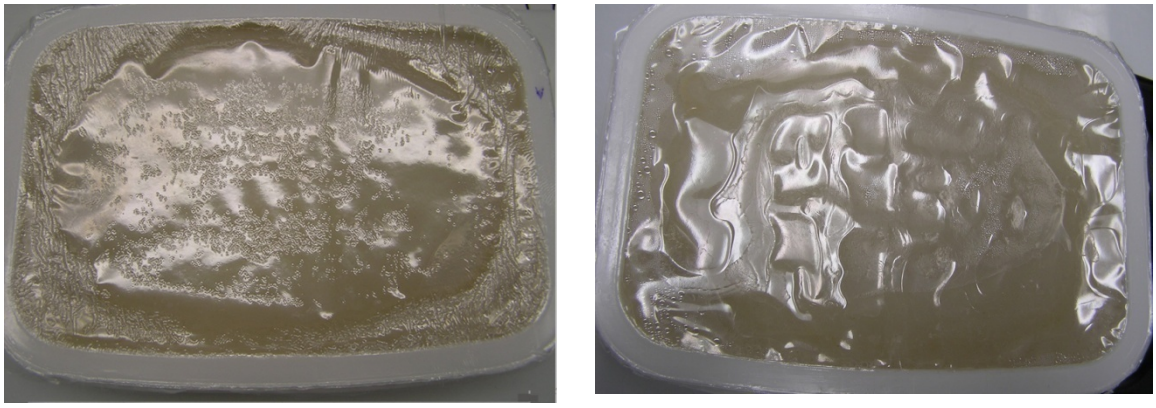

Film A Film B

Figure 3.4. Visual damage of film A and film B after $F_0 = 3$ min retort treatment

3.5 Changes in Oxygen Transmission Rates During Long Term Storage

The changes in oxygen transmission rates of the multilayer EVOH films during storage over 12 months are shown in Figure 3.5. During the entire 12 months storage period, the oxygen barrier of the films was recovered only partially and the pre-processing oxygen transmission rates were not reached. In general, oxygen transmission rates in the multilayer EVOH films decreased between 0 and 2-3 months of storage. The oxygen transmission rate of film A processed by microwave heating decreased to just over half the initial post-processing value for the $F_0 = 3\,min$ process, and decreased by about 2.5 times for the $F_0 = 6\,min$ process during the first 2 months. The oxygen transmission rate for film A processed by retort heating reduced to about half the initial post-processing value. Sharper reductions were observed for film B, especially after the retort treatment with reduction of over five times from 4.57 to 0.83cc/m^2.day. The microwave treatment of film B resulted in reductions of about 1.5 times for $F_0 = 3\,min$ process and almost three times for the $F_0 = 6\,min$ process. It is likely, that during the initial 2-3 month in storage, the much higher vapor pressure in the EVOH layer of the film than that of storage environment forced moisture to migrate through the outer layers to reach equilibrium condition.

Between 2-3 and 12 months the oxygen transmission rates for the films either increased sharply or remained fairly constant. The retort treatment appears to have more effect on the oxygen transmission rate of film A during subsequent storage beyond 2 months as demonstrated by a very high value at 12 months. Conversely, the value for the microwave treated film A increased slightly between 2 and 3 months and remained fairly constant between 3 and 12 months. Film B, on the other hand, revealed a slight increase

in oxygen transmission for both the retort and microwave heated films. It is interesting to note that, except for film A processed by retort treatment, quasi-equilibrium conditions were maintained during long term storage after 2-3 months.

The observed changes in the oxygen transmission rates during entire 12 months storage are controlled by a dynamic process of moisture migration from the EVOH layer through PET to the ambient environment and moisture migration from the mashed potato inside the trays through PP to the EVOH layer. Tsai and Wachtel (1990) stated that equilibrium oxygen permeability of retorted EVOH during storage is determined by both the amount of moisture absorbed during thermal processes and the intrinsic equilibrium moisture content of the EVOH layer at the storage temperature. It is also possible that certain structural changes in the multilayer EVOH films took place during the storage period. In particular, upon cooling from the processing temperature, the EVOH film could have lost an amount of water that was beyond its hold-capacity at the storage temperature. Moisture migration within the film (via slow diffusion until a quasi-equilibrium condition) should be associated with dehydration in some regions of the EVOH films leading to localized re-crystallization of EVOH structure, thus, the observed reduction in the oxygen transmission rates within the first 2 to 3 months. The reason for a steady increase of oxygen transmission rate of film A between 2 and 12 months after retorting (as shown in Figure 3.5) remains unknown.

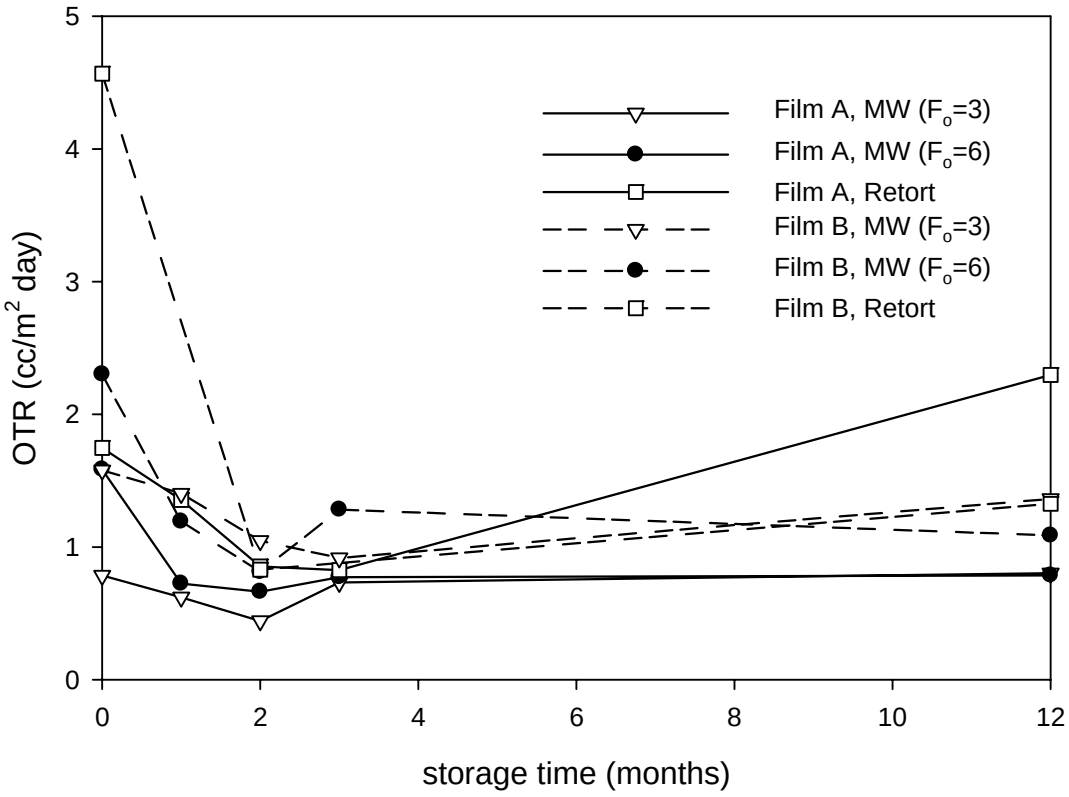

Figure 3.5. Oxygen transmission rate of film A and film B after microwave (MW) and retort processes during storage of mashed potato at 20°C and 65% RH

The differences observed for the two film structures during long term storage could be influenced by properties of the protective layers. The thickness and moisture transmission rates of the protective layers directly influence moisture absorption by the films during thermal processing and moisture loss during storage. The EVOH layer in film A was separated from its outside environment by a 12μm PET layer (i.e., out-12μm PET//12μm EF-XL//75μm PP-food), while additional layers of PP and nylon 6 served as moisture barrier from the external environment in film B (out-12μm PET//50μm PP/6μm

Nylon 6/15μm L171/6μm Nylon 6/50μm PP). Nylon 6 is a poor barrier to moisture, and the moisture transmission rate in PP resin is several times smaller than that of PET (Osborn and Jenkins, 1992). The thinner outer protective layer in film A means that moisture absorption into the EVOH layer was faster during processing, but the moisture also escaped more easily from the film during storage when the ambient environment was at a lower RH than the water activity of the food inside. This might have helped in reducing oxygen transmission rates in film A to a lower level than in film B at the end of the first 2 months of storage. Therefore the positioning of the EVOH layer within the multilayer structure can be a design strategy that can be used to reduce hydration of EVOH layer and consequently limit oxygen permeability into packages as discussed by Zhang (1998).

3.6 Conclusions

The oxygen barrier of the two films deteriorated after treatment by both hot water retort and microwave processing. However the retort treatment resulted in higher oxygen barrier deterioration than the microwave treatment. This implies that microwave processing, with its shorter processing times, can be used to reduce hydration of the EVOH layer during processing which in turn will result in less deterioration of the oxygen barrier property. Although data showed that film A absorbed more water during retort, the oxygen barrier was better than that of film B during storage, possibly due to the location of the EVOH barrier layer in the multilayer structure. For all treatments, the oxygen barrier of the films decreased considerably during the first 2 months of storage

but the original oxygen transmission properties were not recovered during the entire storage period. Over the 12 months storage, the oxygen transmission rates for both films after a $F_0 = 3\,min$ microwave processing remained below the 2cc/m^2.day value comparable to commercially available PVDC laminated films currently used in the USA as lidstock film for shelf-stable products. In practical applications, the lack of full barrier recovery during storage can lead to substantial additional oxygen permeating into the package resulting in possible deterioration of oxygen sensitive foods, especially during the first 2 months of storage.

References

ASTM. 1995. Standard test method for oxygen gas transmission rate through plastic film and sheeting using a coulometric sensor. Annual Book of ASTM Standards. Philadelphia, PA. pp. 532–537.

Ball, C.O. 1923. Thermal process time for canned food. Bulletin 37, Vol. 7, Part 1. National Research Council. Washington, D.C.

Bengtsson, N. E., and Ohlsson, T. 1974. Microwave heating in food industry. Proceedings of the IEEE 62, 44-59.

Chen, H., Liu, F., and Tang, J. 2007. Coupled simulation of microwave heating process using FDTD method and its experiment validation. Journal of Microwave Power and Electromagnetic Energy 41, 50-56.

Downing, D.L. 1996. A Complete Course in Canning and Related Processes: Book II. Microbiology, Packaging, HACCP and Ingredients. 13th ed. CTI Publications, Inc. Baltimore, MD.

EVAL Americas. Technical Bulletin No. 110. Gas barrier properties of EVAL™ Resins. http://www.eval.be/upl/1/default/doc/EA%20-%20Technical%20Bulletin%20No%20110.pdf.

Frey, T. 1986. Coextrusions for flexible packaging. In Baker, M., and D. Eckroth. (Eds.). The Wiley Encyclopedia of Packaging Technology. John Wiley and Sons. New York. pp 199-201.

Guan, D., Plotka, V.C.F., Clark, S., and Tang, J. 2002. Sensory evaluation of microwave treated macaroni and cheese. Journal of Food Processing and Preservation 26, 307-322.

Guan, D., Gray, P., Kang, D.-H., Tang, J., Shafer, B., Ito, K., Younce, F., and Yang, T.C.S. 2003. Microbiological validation of microwave-circulated water combination heating technology by inoculated pack studies. Journal of Food Science 68, 1428-1432.

Hernandez, R.J. and Giacin, J.R. 1998. Factors affecting permeation, sorption and migration processes in package-product systems. In Taub, I.A. and Singh, R.P. (Eds.), Food Storage Stability. CRC Press, Boca Raton, FL. pp. 269-330.

Holdsworth, S.D. 1997. Thermal Processing of Packaged Foods. Blackie Academic & Professional. New York.

Holdsworth, D., and Simpson, R. 2008. Thermal Processing of Packaged Foods. Springer. New York.

Lange, J. and Wyser, Y. 2003. Recent innovations in barrier technologies for plastic packaging – a review. Packaging Technology and Science 16, 149-158.

Lewis, M.J., and Heppell, N.J. 2000. Continuous Thermal Processing of Foods: Pasteurization and UHT Sterilization. Aspen Publishers, Inc. Gaithersburg, MD.

Osborn, K. R. and Jenkins, W.A. 1992. Plastic Films - Technology and Packaging Applications. Technomic Publishing Company, Inc., Lancaster, PA.

Pandit, R. B., Tang, J., Mikhaylenko, G., and Liu, F. 2006. Kinetics of chemical marker M-2 formation in mashed potato - a tool to locate cold spots under microwave sterilization. Journal of Food Engineering 76, 353-361.

Pandit, RB, Tang, J., Liu, F., Mikhaylenko, G. 2007. A computer vision method to locate cold spots in foods in microwave sterilization processes. Pattern Recognition 40, 3667-3676.

Ramaswamy, H.S., and Marcotte, M. 2006. Food Processing: Principles and Applications. Taylor & Francis Group, LLC. Boca Raton, FL.

Sun, T., Tang, T., and Powers, J.R. 2007. Antioxidant activity and quality of asparagus affected by microwave-circulated water combination and conventional sterilization. Food Chemistry 100, 813-819.

Tang, J., Liu, F., Pathak, S., and Eves, G. 2006. Apparatus and method for heating objects with microwaves. US Patent No. 7,119,313.

Tang, Z., Mikhaylenko, G., Liu, F., Mah, J.H., Tang, J., Pandit, R., and Younce, F. 2008. Microwave sterilization of sliced beef in gravy in 7 oz trays. Journal of Food Engineering 89, 375-383.

Teixeira, A.A., and Tucker, G.S. 1997. On-line retort control in thermal sterilization of canned foods. Food Control 8, 13-20.

Tewari, G., and Juneja, V.K. 2007. Advances in Thermal and Nonthermal Food Preservation. Blackwell Publishing Professional. Ames, Iowa.

Tsai, B.C. and Wachtel, J.A. 1990. Barrier properties of ethylene vinyl alcohol copolymer in retorted plastic food containers. In Koros, W.J. (Ed.). Barrier Polymers and Structures. ACS Symposium Series 423, American Chemical Society. Washington, DC. pp 192-202.

Wright, M.D., Lees, G.C., and Hurst, S.J. 1995. Recycling of vinylidene chloride copolymer coated polypropylene film: a study of the thermal degradation of VDC copolymer. Thermochimica Acta 263, 51-58.

Zhang, Z. 1998. Transport and mechanical property studies of barrier plastic food packaging materials. PhD Dissertation. The University of Guelph. Guelph, Ontario, Canada.

CHAPTER 4 CORRELATION OF WATER ABSORPTION WITH OXYGEN TRANSMISSION PROPERTIES OF MULTILAYER EVOH FILMS

4.1 Introduction

The presence of even small amounts of moisture in EVOH has shown to affect a variety of film properties, ranging from mechanical properties (Gaucher-Miri et al., 2002; Cabedo et al., 2006), glass transition temperature, T_g (Aucejo et al., 1999; Zhang et al., 2001; Lagaron et al., 2001; Cabedo et al., 2006) to the gas barrier properties (Zhang et al., 2001; Muramatsu et al., 2003). The combined effect of high relative humidity, high temperatures and long processing times during retort processing has an even more adverse effect on the barrier properties of multilayer EVOH containing films.

The increase in oxygen transmission rates after thermal processing using retort was shown in the previous chapter. These effects were mainly attributed to plasticization of the polymer matrix by water. Plasticization implies intimate mixing in which water is dissolved in a polymer. At molecular level, plasticization leads to increased intermolecular space or free volume, and may involve weakening or breaking of polymer-polymer hydrogen bonds (Levine and Slade, 1988; Hodge et al. 1996a). It has become well established that plasticization by water affects the glass-to-rubber transition of polymers by depressing the T_g of the polymer matrix. The critical effect of plasticization by water leads to increased mobility in the dynamically constrained amorphous component of the polymer (Levine and Slade, 1988). In the simple dilution

mechanism T_g depression is related simply to an increase of the volume, while in the case of specific polymer-water interactions, the sorption process can be related to the distribution of intermolecular physical bonds (e.g. hydrogen bonds) which induce a decrease of T_g and of mechanical properties.

During water absorption, the hydroxyl group in EVOH associates with water through the hydrogen bond. It has been suggested that water penetrates only the amorphous regions of a polymer. At room temperature it is expected that only the non-coupled hydroxyl groups would be associated with water which makes up the amorphous region of the semi-crystalline EVOH copolymer (Min et al., 1994). As recognized, the crystalline phase is made of hydroxyl groups along the chains of EVOH molecules which are attracted to and associated with their closest hydroxyl groups within the polymer chain (i.e. coupled hydroxyl groups). However, some researchers reported that the crystalline regions are also affected by excess quantities of water, an effect more pronounced at high temperatures and pressures used in retort processing (Hodge et al., 1996a; Lopez-Rubio et al., 2005). At elevated temperatures, water would penetrate into the crystalline region to act as a diluent, reducing the strength between the hydroxyl groups of the polymer chains. Therefore, the reduced crystallinity resulting from of excess moisture will lead to increased oxygen permeability of the affected polymer. Lopez-Rubio et al. (2005) reported decrease in crystallinity of EVOH in PP/EVOH/PP films after retort treatments leading to higher oxygen permeability. In comparison, these authors reported no deterioration in structure and oxygen permeability for the outer PP layers. The authors noted that during retorting pressurized water melts and disrupts defective and ill-defined crystals in EVOH crystalline morphology.

Water in polymers usually exists in two or three separate states, classified into different thermodynamic or dynamic properties, commonly as free water, freezable bound water and non-freezing water (Hodge et al., 1996b, Ping et al., 2001). Freezable bound water undergoes a thermal melting transition at a temperature lower than that of bulk water due to the interactions between polymer/water molecules. Freezable bound water is weakly bound to the polymer chain and that melts on heating at temperatures greater than 0 °C due to these bonding interactions. Free water undergoes similar thermal transitions to that of bulk water. Non-freezing bound water is bound water that does not exhibit a detectable phase transition by differential scanning calorimetry (DSC) over the range of temperatures normally associated with bulk water. According to these classifications, water molecules close to hydrophilic surfaces (such as hydroxyl groups in EVOH) are bound to these hydrophilic sites and, thus relatively immobilized (Pissis, 2005). On the other hand, water molecules in sufficient distance from such surfaces are free, behaving like molecules in bulk water. Hodge et al. (1996a) postulated that nonfreezing water is responsible for the majority of plasticization (increase in free volume and chain mobility) in hydrated polyvinyl alcohol.

In order to corroborate the speculation that the duration of thermal processing is related to the extent of oxygen barrier deterioration in multilayer films (as suggested in Chapter 3), simulated retort experiments were carried out to determine the exact amount of water absorbed. The amount of water absorbed at 121°C after specified heating periods was measured gravimetrically and the corresponding oxygen transmission rates were evaluated on the two multilayer EVOH films studied in Chapter 3. The effects of water absorption on possible crystallinity changes were evaluated using DSC experiments. The

behavior/states of water in the two multilayer films were also evaluated from the DSC analysis in order to determine any probable correlation with oxygen transmission rates.

4.2 Materials and Methods

4.2.1 Film Sample Preparation

Two multilayer films (Film A and film B) were used in this study. Detailed descriptions of these films were given in Chapter 3. Films were cut into samples of approximately 5 cm in diameter. Prior to testing, film samples (~5cm in diameter) were dried in a vacuum oven with a vacuum of about 60 cm Hg) at 70 °C for 2-3 days until the weight was constant. Weight of film samples were measured using an analytical balance with a resolution of 0.0001g (Analytical Plus, OHAUS).

4.2.2 Water Absorption Measurements

To simulate retort conditions, water absorption tests were performed at 121°C in an oil bath (HAAKE W13, Thermo Electron Corporation) using ethylene glycol (JT Baker) as a heating medium. A custom made test cell was designed for these tests. The cell consisted of two main cylindrical aluminum parts – the base and top – and a screw cap closure (Figure 4.1). The bottom and top parts are opened and closed along machined threads, and the top has an opening for adding water on the top of the tested film sample. A 0.032 inch type T thermocouple (Omega Inc.) was inserted through the screw cap closure for monitoring temperature inside the cell. In order to obtain a hermetic seal the test cell was fitted with *O*-rings at all closures (i.e., at the sealing faces between the base

and the top, and on the screw cap closure). During testing, film specimens were immersed in water and clamped in place between the two O-rings on the sealing surface (between base and top). This ensured that there was no water absorption at the cut film edge.

After predetermined heating times (i.e. 0, 5, 10, 20, 30 and 60 minutes), test cells were removed from the oil bath and immediately cooled in ice/water mixture to approximately 20°C. The film specimens were removed from the test cell and their surfaces wiped with a paper towel to remove surface water and weighed immediately to obtain the final/wet weight. The percentage water absorption was calculated according to equation 4.1. Three replicates were taken at each measurement time for each of film A and film B. The percentage of water uptake/absorption at any time (M_t) was calculated according to the following equation.

$$M_t = \frac{w_t - w_d}{w_d} \times 100 \qquad (4.1)$$

where w_t is the weight of sample at time t (wet weight) and w_d is the dry weight of sample.

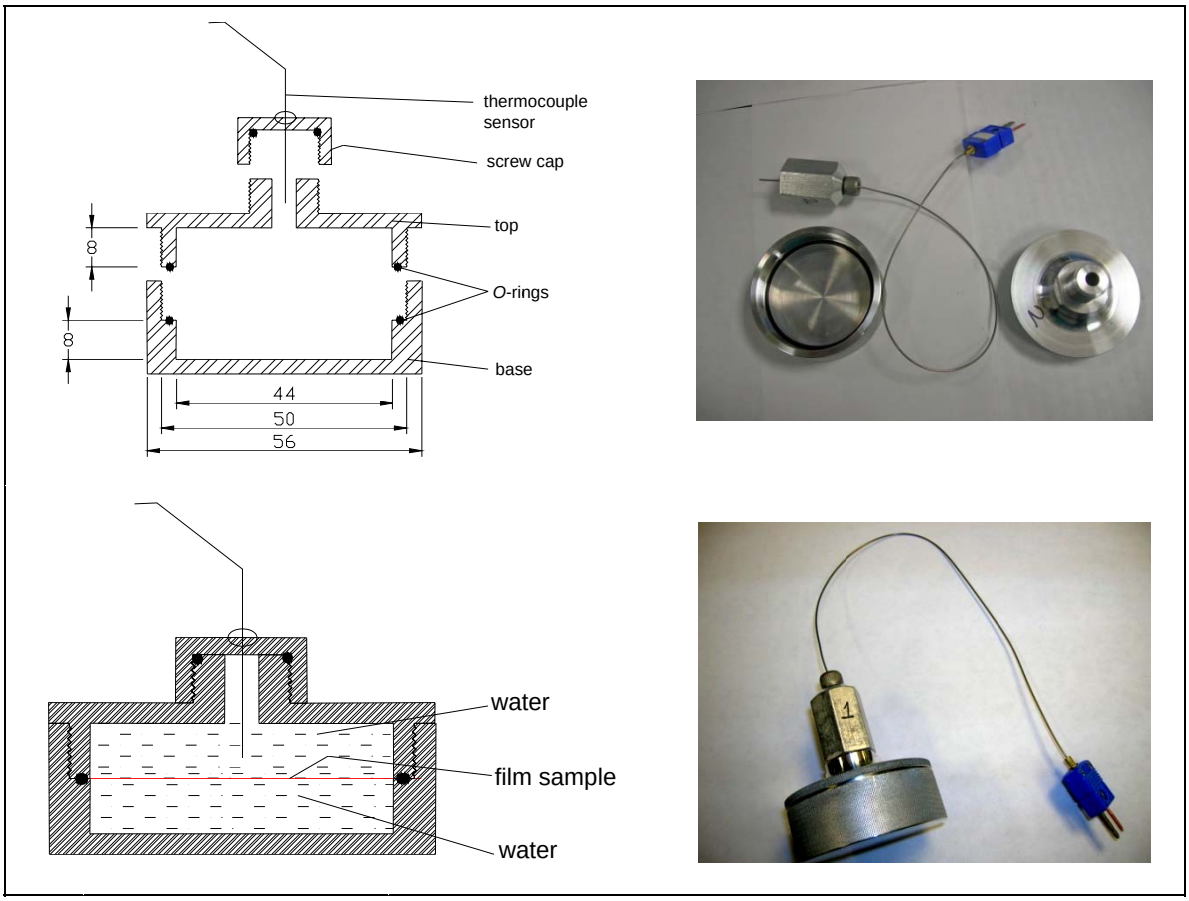

Figure 4.1. Schematic diagram and picture of test cell. Dimensions shown are in mm.

4.2.3 Oxygen Transmission Rates of Multilayer EVOH films

Oxygen transmission rates (OTR) were evaluated on film A and film B using instrumentation (i.e. MOCON OX-TRAN 2/20, MOCON, Inc., USA) and procedures described in Chapter 3, section 3.3.5, at 20°C and 65% RH. OTR measurements were performed immediately following simulated retort treatments at 121°C for various heating times (as described above). The moist film specimens were masked with aluminum foil on both sides exposing a circular measurement area of 5cm^2 and mounted onto the diffusion cells of the instrument. The amount of oxygen contained in the carrier

gas reached equilibrium after approximately 14 days. Duplicate measurements were made.

4.2.4 Differential Scanning Calorimetry

Differential scanning calorimetry (DSC) is the most widely used technique for studying processes that are initiated by either an increase or a decrease in temperature. DSC measures the change in the difference in the heat flow rate to the sample and to a reference sample while subjected to a controlled temperature (Hohne et al., 2003). These measurements provide quantitative and qualitative information about physical and chemical changes that involve endothermic or exothermic processes, such as the glass transition, crystallization, melting, enthalpies of phase transitions, etc., or changes in heat capacity. The original concept of DSC, known as power compensation, involves maintaining sample and reference at the same temperature and measuring the heat flow required to keep the two at a thermal equilibrium (Hilfiker, 2006). In this study a TA Q2000 Series DSC cell (TA Instruments) was used. This is a differential type (heat flux mode) instrument in which the heat differential between the sample pan and the reference pan is measured as a function of temperature and the energy associated with the temperature is calculated from the ratio of the temperature difference between the sample and reference and the thermal resistance of a heating block (Hilfiker, 2006). The temperature differential between the sample and the reference as both are heated and cooled is measured by thermocouples.

DSC determinations were done on film samples which had been exposed to hot water retort treatment at 121°C for different heating times up to 60 minutes. Thus the films were prepared for DSC determinations immediately following heat treatments. The DSC cell was operated with nitrogen flow to determine phase transitions (T_g, melting temperature (T_m)) and enthalpy of melting/fusion. Aluminum sample pans and lids were initially weighed and then filled with about 10 mg sample by piling up several circular pieces cut from polymer film samples using a cork borer. The sample pan was hermetically sealed and the weight of pan plus sample was recorded. The sample pan was then placed in the DSC sample holder, and a sealed empty pan was used as a reference. The pans were cooled from room temperature to -50°C at 10°C/min, held for 1 minute and then heated from -50°C to 300°C at a rate of 10°C/min. After DSC measurements, the lids of the sample pans were pierced at several points and the pans were dried in a vacuum oven at 70°C for 2-3 days to obtain the mass of the dry sample (w_d) using the differences between the initial weight of the pan plus sample (before DSC) and the dry weight of pan plus sample.

DSC raw data (thermograms) show heat flow plotted against temperature. The DSC scans were evaluated using thermal analysis software (Universal Analysis, TA Instruments). A straight baseline would be obtained when no thermal even occurs (i.e. no physical change takes place in the sample). However, when transitions such as glass transition and melting take place, the sample absorbs heat and the temperature is lowered. The area under the curve for a thermal event will be proportional to the energy or heat supplied or released to equalize the temperatures. T_g was determined as the onset of a

glass transition and the melting temperature (T_m) was determined as the maximum of the endothermic melting peak. The enthalpy of melting/fusion (ΔH_f) was determined by calculating the area under the melting endotherm above an arbitrarily drawn baseline. Duplicate analyses were performed.

4.3 Results and Discussion

4.3.1 Performance of Test Can Apparatus

During an experiment, the water temperature inside the test cell required time to reach the desired temperature. This time, referred to as the heating up (or come-up time), should be as short as possible to minimize water absorption during the non-steady heating period and provide isothermal conditions for the main duration of a heat treatment. Therefore the selection of final test cell dimensions was based on the shortest heating up time that could be obtained. One of the critical design considerations during design was to have film samples with sufficient dimensions for use in a MOCON OX/TRAN instrument for oxygen transmission testing. The standard sample size for this instrument is 10.16 × 10.16 cm. However, smaller samples of no less than 5cm^2 surface area can be used with foil masks. Preliminary evaluation of several test cell dimensions was made to obtain a size with the shortest possible time. The final design chosen had an inner diameter of ~4.5cm to provide the minimum 5cm^2 measurement area and allow ease of handling. The inner depth of the cell was 1.6cm (0.8cm each of the top and bottom parts) and the wall thickness was about 0.3cm. A sample of the temperature-time data showing the standard deviations of the measurements from the three cells is presented in Table 4.1, and the

temperature-time profiles of the three test cells figure shown in figure 4.2. The results indicate that the water temperature in the test cell reached 121 ± 0.5°C after 2½ minutes of heating. Statistical analysis using analysis of variance indicated that there was no significant difference between the temperature data for the three cells at the different heating times. The measured temperature data from the three test cells showed good consistency between different cells and repeatability within the same test cell.

Table 4.1. Time-temperature data for three test cells

Heating Time (min)	Temperature (°C)			
	Cell 1	Cell 2	Cell 3	Average*
1	107.09 ± 0.93	104.60 ± 1.65	105.51 ± 1.85	105.74 ± 1.73
1.5	116.27 ± 0.12	114.27 ± 0.13	116.31 ± 0.06	115.57 ± 1.59
2	119.56 ± 0.12	118.30 ± 1.29	119.57 ± 0.02	119.15 ± 0.94
2.5	120.69 ± 0.05	119.99 ± 0.71	120.70 ± 0.04	120.46 ± 0.53
3	121.14 ± 0.05	120.76 ± 0.37	121.17 ± 0.07	121.03 ± 0.29
4	121.36 ± 0.01	121.25 ± 0.09	121.46 ± 0.05	121.35 ± 0.11
5	121.38 ± 0.03	121.33 ± 0.04	121.50 ± 0.08	121.40 ± 0.09
6	121.37 ± 0.01	121.35 ± 0.03	121.50 ± 0.11	121.41 ± 0.10

* Average of three cells based on six measurements, two each from a single cell

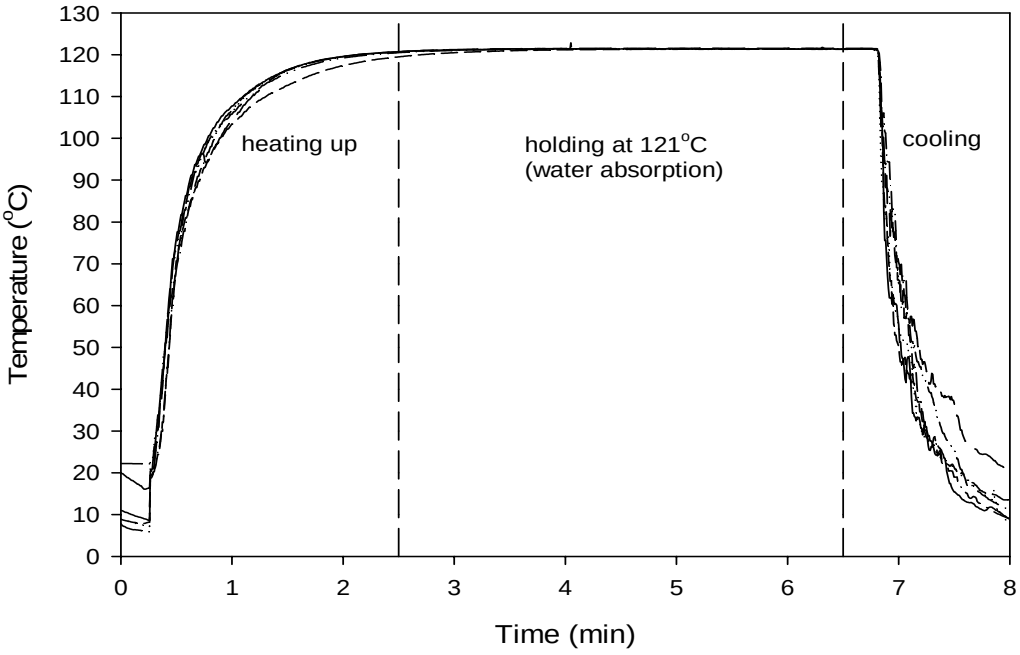

Figure 4.2. Temperature-time profiles inside test cell showing heating and cooling. Graph shows six curves obtained from three test cells.

An essential criterion for the cell design was to ensure no water absorption occurs through the cut film edge. Generally thin films (in which thickness is much smaller than diameter) are used without any edge sealing. It is assumed that the effect on water absorption at the edge is small and can be neglected. However, for water absorption at high temperature conditions like those used in this study, and edge effects may not be negligible. Barrer et al. (1962) showed that errors can arise from neglecting edge effects which may lead to large differences in transport coefficients measured by different methods. Proper sealing of the cut edges was evaluated by visual observation of film samples after heat treatments. In this study a good seal was demonstrated by a clear ring along the edge of the films directly in contact with the *O*-rings. No water was absorbed in

this area as opposed to an opaque area in the rest of the films as shown in figure 4.3. In addition, films from test cans which were not sealed properly do not show these clear regions and their weight gain was much higher, indicating that more water could have entered through the edges.

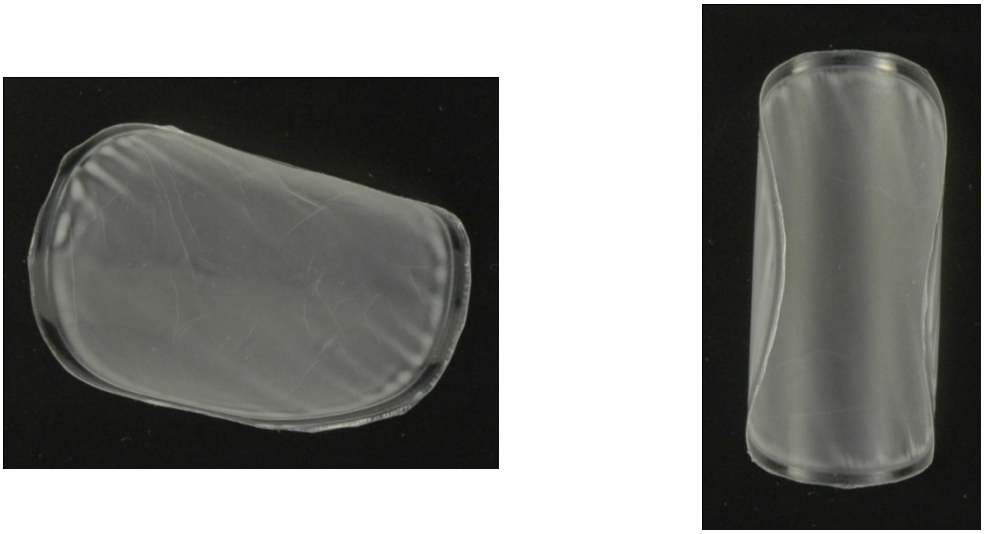

Figure 4.3. Film specimens after retort showing clear region along location of *O*-rings

4.3.2 Effect of Water Absorption on Oxygen Transmission

The results of the effect of water absorption at 121°C oxygen transmission rates of film A and film B are presented in Table 4.2. From Table 4.2 and Figure 4.4 it is clear that film A absorbed more water than film B at the same experimental conditions. It would be expected that film A would absorb less water since it contains a biaxially oriented EF-XL layer in its structure as opposed to the non-oriented L171 layer in film B. Film B also contains biaxially oriented nylon 6 which is also highly hydrophilic. Biaxially oriented films such as EF-XL (in film A) have higher crystalinity as a result of

orientation, and have been shown to absorb less water than their non-oriented counterparts (Zhang et al., 1999). Therefore other factor must be at play to influence the overall water absorption by the two films. It can be argued that film B with its thicker protective layers around the EVOH layer, provided more protection against moisture absorption by the EVOH layer.

Table 4.2. Water absorption at 121°C and oxygen transmission rate (OTR) data for film A and film B

Retort Time	% Water Absorption		OTR (cc/m^2 day)	
(min)	Film A	Film B	Film A	Film B*
0	0	0	0.16 ± 0.006	0.096 ± 0.005
5	3.3 ± 0.01	2.2 ± 0.02	4.57 ± 0.46	-
10	4.3 ± 0.14	2.9 ± 0.02	6.33 ± 0.29	2.86 ± 0.19
20	5.7 ± 0.05	4.1 ± 0.46	6.77 ± 0.69	7.34 ± 0.65
30	6.2 ± 0.12	4.7 ± 0.22	7.20 ± 0.49	17.28 ± 0.50
60	7.3 ± 0.05	5.3 ± 0.40	13.99 ± 1.41	25.25 ± 1.93

* OTR data for film B at 5 min retort time not available

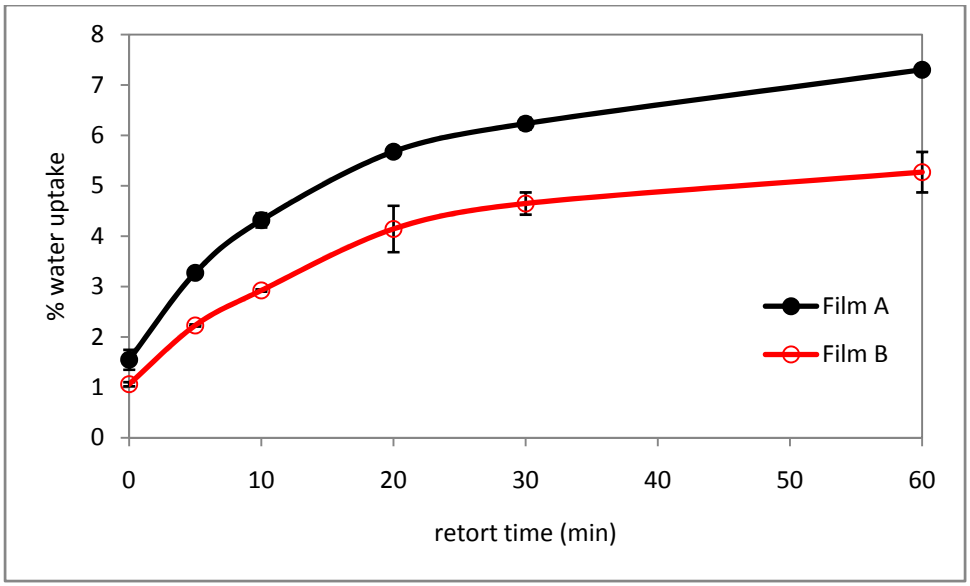

Figure 4.4. Comparison of water absorption by Film A and Film B at 121°C

The oxygen transmission data in Table 4.2 was also plotted in Figure 4.5 to show the relationship between water absorption and oxygen transmission rate. Oxygen transmission rates increased as the amount of water absorbed by both film A and film B also increased. Close observation of Figure 4.5 reveals that there might be two distinct stages describing the change of oxygen transmission rates with water absorption for both film A and film B. Linear fits of these two apparent stages were attempted and yielded R^2 values as indicated on Figure 4.5. The R^2 value for the second stage on the curve for film A was not shown since only two data points were available. The point at which the oxygen transmission behavior changes were indicated by inflection points that occurred at ~6% water absorption for film A and at ~4% for film B. Film A and film B exhibited similar oxygen transmission behavior at lower water contents (up to water content of ~4%), suggesting that water absorption might have a similar mechanism and effect on the two films initially. Above 4% water content the oxygen transmission rate of film B

increased sharply, while that of film A continued to increase in a more gradual manner. It is noted that the inflection points observed in Figure 4.5 are similar to the general curve of polymer specific volume and temperature, where there is a change in slope that corresponds to a sudden increase in free volume as temperature increases above T_g (Nogales et al., 2007). It is therefore speculated that inflection points observed in the current study might be related to the glass-rubber transition in these systems. The inflection points might also be caused by irreversible changes in the polymer structure such as formation of voids, cracks, delamination, etc. This will be discussed in more detail later in section 4.3.4.

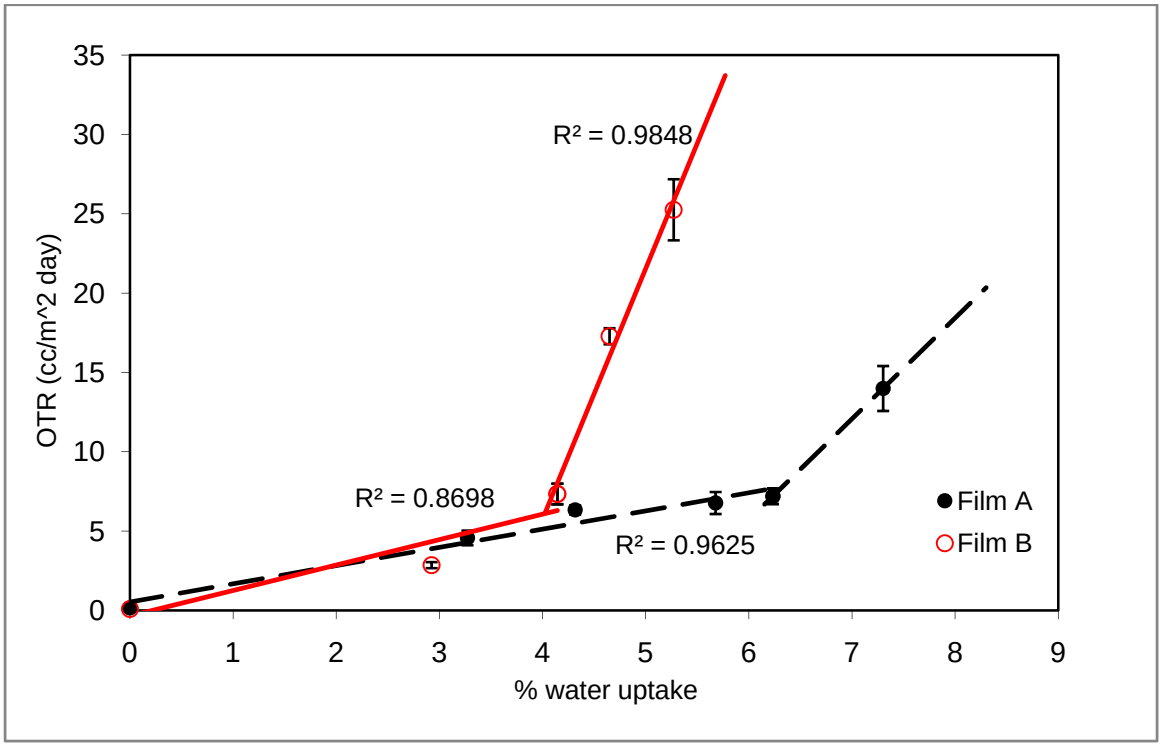

Figure 4.5. Effect of water absorption on oxygen transmission rates of film A and film B

The observation of increasing oxygen transmission rates with water absorption is attributed to the plasticizing effect of water on EVOH (L171 and EF-XL) and nylon 6 layers which are components of film A and film B. Plasticization has been reported to be a strong function of the amount of water absorbed (Hodge et al., 1996a). Plasticization is expected to promote polymer chain mobility, which in turn enhances mobility of oxygen molecules through the polymer matrix. Yamamoto et al. (2009) used nuclear magnetic resonance to correlate molecular mobility of EVOH chains due to water absorption with oxygen permeability. It has already been stated that plasticization of polymers by water is usually reflected in depression of T_g. However, attempts to evaluate the change in T_g with water absorption were futile due to the difficulty in measurement of exact T_g values of EVOH used in film A and film B from differential scanning claorimetry. This difficulty in T_g detection of EVOH components of the film was probably due to the small fraction of EVOH in the overall multilayer films relative to the size of the sample required for DSC measurements. Thus, in 10 mg of sample used in the DSC pans, only about 1 mg was EVOH. Only the apparent T_g regions for PP and PET in DSC scans for film A, and those for PP, PET and nylon 6 for film B were identified (Figure 4.6). These identified T_g values for PP and PET in film A and film B essentially remained unchanged as water absorption increased, suggesting that there was no plasticization of the PP and PET layers by water. In spite of this, it is well known that the T_g values of EVOH films are well below room temperature when saturated with water (Matsui et al., 1996; Cabedo et al., 2006).

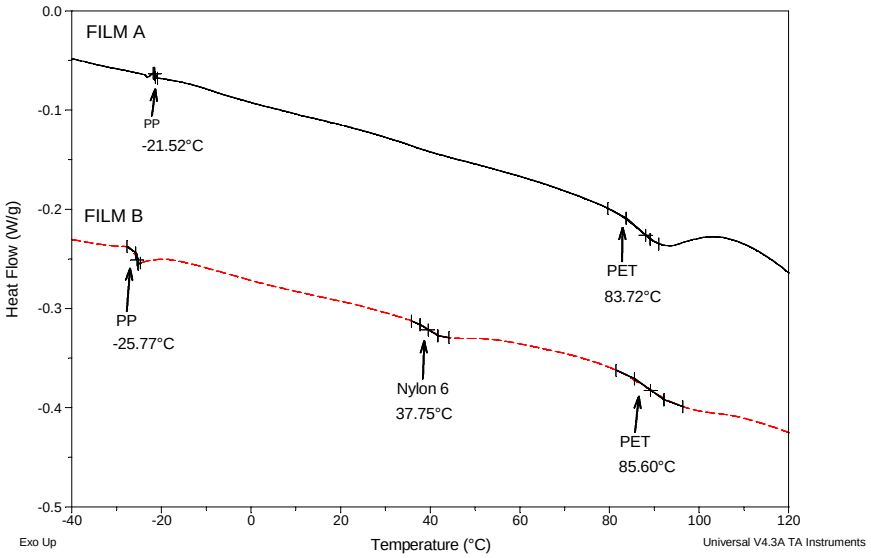

Figure 4.6. T_g and T_m for dry film samples of film A and film B

4.3.3 Water Absorption Effects on Film Morphological Structure

While the plasticization of hydrophilic polymer matrices by water is largely recognized, the effect of water on the crystalline phase of semi-crystalline polymers is not well implicit. It has been suggested by some researchers that water penetrates only the amorphous regions of a polymer and not the crystalline phase. At room temperature it is expected that only the non-coupled hydroxyl groups (which make up the amorphous region of the semi-crystalline EVOH copolymer) would be associated with water (Min et al., 1994). The crystalline phase is thought to be made of coupled hydroxyl groups (i.e. those hydroxyl groups on EVOH chains that are attracted to and associated with their closest hydroxyl groups within the polymer chain). On the other hand, some researchers have asserted that the crystalline regions are also affected by excess quantities of water,

an effect more pronounced at high temperatures and pressures used in retort processing (Hodge et al., 1996a; Lopez-Rubio et al., 2005). At elevated temperatures, water would penetrate into the crystalline region to act as a diluent, reducing the strength between the hydroxyl groups of the polymer chains. Disruption of the crystalline regions may occur in the polymer due to the swelling stresses imposed by increased water uptake thus increasing the effective number of free volume sites available for oxygen permeation (Hodge et al., 1996b). Therefore, the reduced crystallinity resulting from excess moisture will lead to increased oxygen permeability of the affected polymer.

DSC is a standard tool for investigation of crystallization and melting processes in polymers (Reiter and Sommer, 2003). Polymer crystallinity can be defined from DSC measurements by integrating the area under the melting peak to obtain the enthalpy of fusion/melting, and comparing it to a reference value representing the heat of melting of a 100% crystalline material (Reading et al., 2001). The melting temperature (T_m) and enthalpy of fusion/melting (ΔH_m) of the individual film components of film A and film B were determined from DSC experiments as a function of amount of water absorbed after retort heating. The melting peaks are shown in Figure 4.7, and the melting temperature data is shown in Table 4.3 for components of film A and film B. The melting peaks for the different components of film A and film B are observed at the same locations for all water contents studied, indicating no influence of water absorption on T_m. Statistical analysis (using ANOVA) of data in Table 4.3 showed no significant differences between the melting temperatures of components of both film A and film B at the different water contents. In general a depression of T_m with increasing water content, associated with the molecular interaction between water and the polymer, is expected.

The melting point for any polymer crystal is affected by both enthalpy (H) and entropy (S) effects according to the following equation:

$$T_m = \frac{\Delta H_m}{\Delta S_m} \tag{4.2}$$

where ΔH_m is the enthalpy of melting/fusion and ΔS_m is the entropy of fusion. ΔH_m of the polymer-water system reflects the total absorbed energy during hydration process between the hydroxyl group and water molecules (Min et al., 1994). ΔS_m is a parameter related to polymer chain flexibility/stiffness. Water absorption generally decreases ΔH_m due to weakening of the polymer-polymer interactions resulting from disruption of polymer-polymer hydrogen bonds. This effect also makes polymer chains move freely, hence increases ΔS_m. Accordingly the decrease in enthalpy and probable increase in entropy may take place in a competitive manner, and as a consequence T_m remains unchanged. Similar results in which no influence of water absorption on T_m were reported by Aucejo et al. (1999). The authors interpreted the lack of influence of water absorption on T_m as an indication of lack of crystal perfection during the DSC heating process. These authors also stated that the water initially present is removed from the sample before the melting process starts.

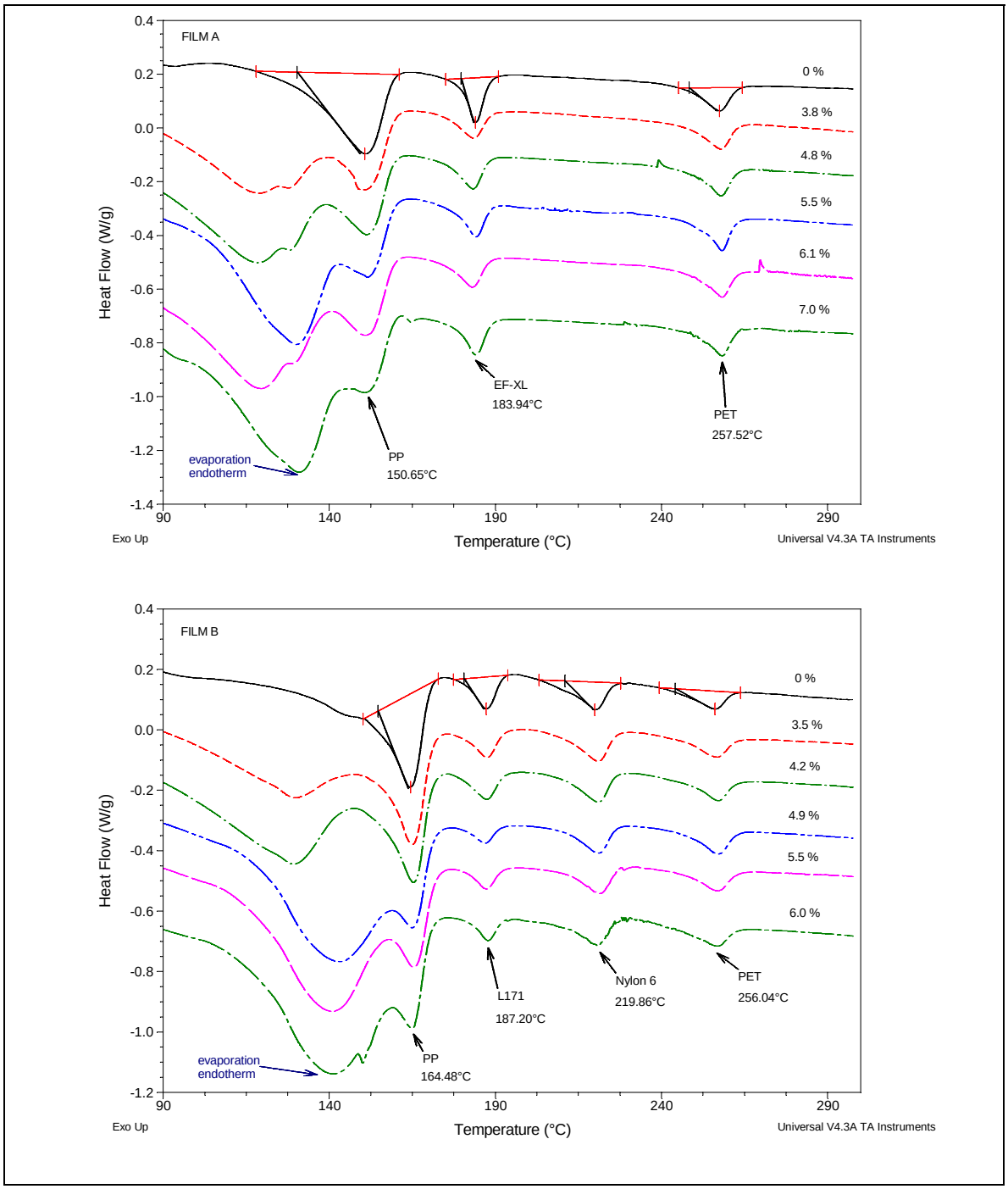

Figure 4.7. DSC scans showing melting behavior of components of film A (top) and film B (bottom) at different moisture contents

Table 4.3. Effect of water absorption on melting temperature (T_m) of components of film A and film B

Retort Time (min)	FILM A			FILM B			
	Water Uptake (%)	T_m (°C)		Water Uptake (%)	T_m (°C)		
		PET	EF-XL		PET	L171	Nylon 6
0	0	258.2 ± 0.1	184.8 ± 0.2	0	256.2 ± 0.2	187.4 ± 0.3	220.1 ± 0.3
5	3.8 ± 0.1	258.3 ± 0.05	183.4 ± 0.03	3.5 ± 0.4	256.7 ± 0.2	187.5 ± 0.3	220.8 ± 0.3
10	4.8 ± 0.03	258.4 ± 0.7	183.1 ± 0.07	4.2 ± 0.02	256.8 ± 0.01	187.3 ± 0.08	221.0 ± 0.01
20	5.5 ± 0.5	258.2 ± 0.2	183.7 ± 0.2	4.9 ± 0.08	256.8 ± 0.2	187.1 ± 0.5	221.0 ± 0.2
30	6.1 ± 0.6	258.2 ± 0.2	183.7 ± 0.3	5.5 ± 0.6	256.7 ± 0.3	187.6 ± 0.5	221.1 ± 0.2
60	7.0 ± 0.2	258.2 ± 0.2	184.2 ± 0.1	6.0 ± 0.1	256.5 ± 0.2	188.0 ± 0.5	221.1 ± 0.9

The ΔH_m, measured by integrating the area under the melting peak, was shown to be affected by moisture content as shown in Table 4.4 for components of film A and film B. The values for PP are not shown due to incomplete integration of the PP melting peak. A wide peak with a maximum around 100°C was observed for hydrated samples and was identified as evaporation endotherm of water. The thermograms for dry film samples (0% water content) did not show this evaporation peak. The end of the water evaporation peak overlapped and obscured the start of PP melting endotherm in the DSC thermogram, making it impossible to integrate the peak. ΔH_m decreased with increasing water content for EF-XL, L171 and nylon 6 but not for PET components in film A and film B. The decrease in ΔH_m might be an indication that the degree of crystallinity of the hydrophilic components of both film A and film B was reduced by water absorption at elevated temperatures. The data is also plotted in Figure 4.8 for EF-XL and L171 components. It is clear that the ΔH_m values for EF-XL (in film A) are higher than those of L171 (in film B). The higher values for EF-XL indicate a higher crystallinity for EF-XL, which is expected because EF-XL is biaxially oriented and L171is non-oriented. It was shown in Figure 4.5 that the oxygen transmission rate for film A was lower than that of film B for samples with more than 4% water content. It is possible that film A was able to withstand the retort process better than film B because of the more robust and well defined crystalline morphology in EF-XL. For both EF-XL, ΔH_m showed a significant decrease was observed from dry samples to samples with 3.8% water content. Afterwards, enthalpy values stayed more or less constant. The same trend was observed for L171 component with a significant decrease observed after 4% water content.

Table 4.4. Effect of water absorption on enthalpy of melting (ΔH_m) of components of film A and film B

Retort Time (min)	FILM A			FILM B			
	Water Uptake (%)	ΔH_m (J/g)		Water Uptake (%)	ΔH_m (J/g)		
		PET	EF-XL		PET	L171	Nylon 6
0	0	5.9 ± 0.3a	8.2 ± 0.6a	0	3.9 ± 0.07a	5.1 ± 0.08a	7.0 ± 0.3a
5	3.8 ± 0.1	5.5 ± 0.06a	5.6 ± 0.03b	3.5 ± 0.4	4.2 ± 0.2a	4.2 ± 0.2ab	6.2 ± 0.3ab
10	4.8 ± 0.03	5.1 ± 0.7a	6.4 ± 0.09c	4.2 ± 0.02	4.3 ± 0.09a	4.2 ± 0.1ab	5.9 ± 0.2ab
20	5.5 ± 0.5	6.1 ± 0.4a	6.1 ± 0.07bc	4.9 ± 0.08	4.7 ± 0.3a	2.7 ± 0.9b	5.5 ± 0.3ab
30	6.1 ± 0.6	4.9 ± 1.1a	6.5 ± 0.04c	5.5 ± 0.6	3.6 ± 0.7a	3.2 ± 0.8b	4.9 ± 0.2b
60	7.0 ± 0.2	5.3 ± 0.7a	6.2 ± 0.2bc	6.0 ± 0.1	3.9 ± 1.29a	1.5 ± 0.8b	4.6 ± 1.5b

Means with the same letters within a column (i.e. at different water contents) are not statistically different

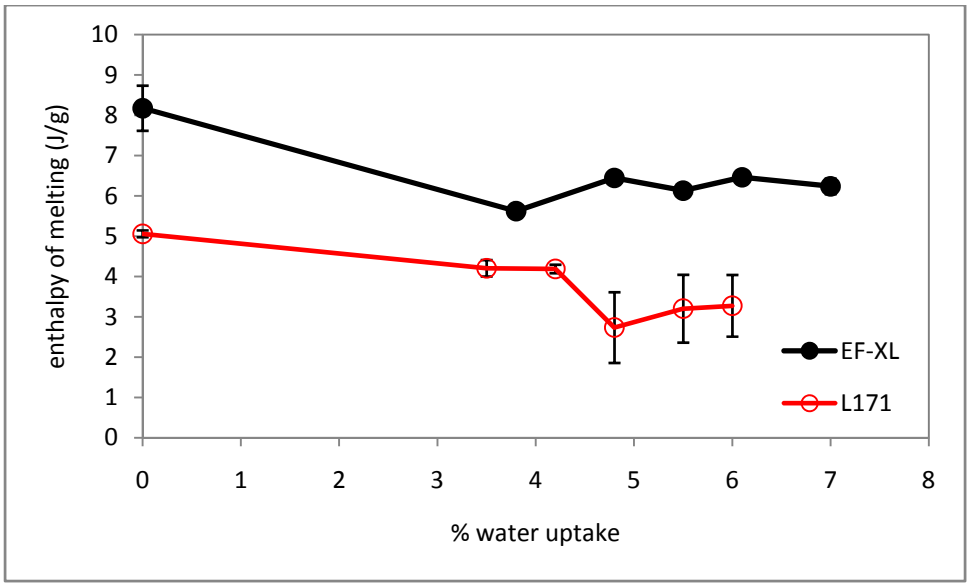

Figure 4.8. Variation of enthalpy of melting (ΔH_m) with water absorption for EF-XL and L171

4.3.4 Visual Changes in Film Structure after Retort Heating

The synergistic effects of high RH and temperature are known to induce irreversible damage in some hydrophilic polymers in the form of voids, cracks, etc. (Pogany, 1976; Apicella and Nicolais, 1981, Fan et al., 2008). Film A and film B showed some visual defects after retort for longer durations (Figure 4.9). An opaque discoloration was observed for film A, at retort durations longer than 30 minutes, which disappeared shortly afterwards when stored at ambient conditions. Film B showed pronounced damage in the form of wrinkles, blisters, etc. after 20 minutes of retort heating, which might indicate possible loss of adhesion (delamination) between some adjacent layers within the film. The damage on film B was rather permanent as it was still visible after extended periods at room conditions. For both films the damage was barely visible at shorter heating times.

Formation of blisters, microvoids, etc. occurs when a polymer film saturated with water at an elevated temperature is rapidly cooled (Hansen, 2000). A rapid quench to a lower temperature can free the dissolved water and the water now becomes in excess of that soluble in the film. The solubility of the polymer is lowered and water condenses in the form of microscopic water-filled cavities, provided the internal pressure which is generated by the excess water exceeds the strength of the polymer. If the excess water cannot rapidly diffuse out of the film it happens as a separate phase, causing failure by blistering or delamination.

The inflection point observed in Figure 4.5 at 6% water absorption for film A corresponds to 30 minutes of retort heating, while the 4% water absorption for film B corresponds to 20 minutes of retort heating, which is about the same times visual damage begins to show on the films. The damage might contribute to higher oxygen transmission rates observed for films at higher water absorption. There is a tendency of water to cluster at high relative humidities leading to microvoid nucleation during the sorption process (Carfagna and Apicella, 1983). This is particularly favored at higher temperatures due to the lower energy required for void formation and the fact that the increased mobility of segments of polymer chains at higher temperatures does not hinder the translational freedom of water molecules (Apicella and Nicolais, 1981). It would be interesting to perform some internal structural analysis to distinguish what types of damage occur in the two films.

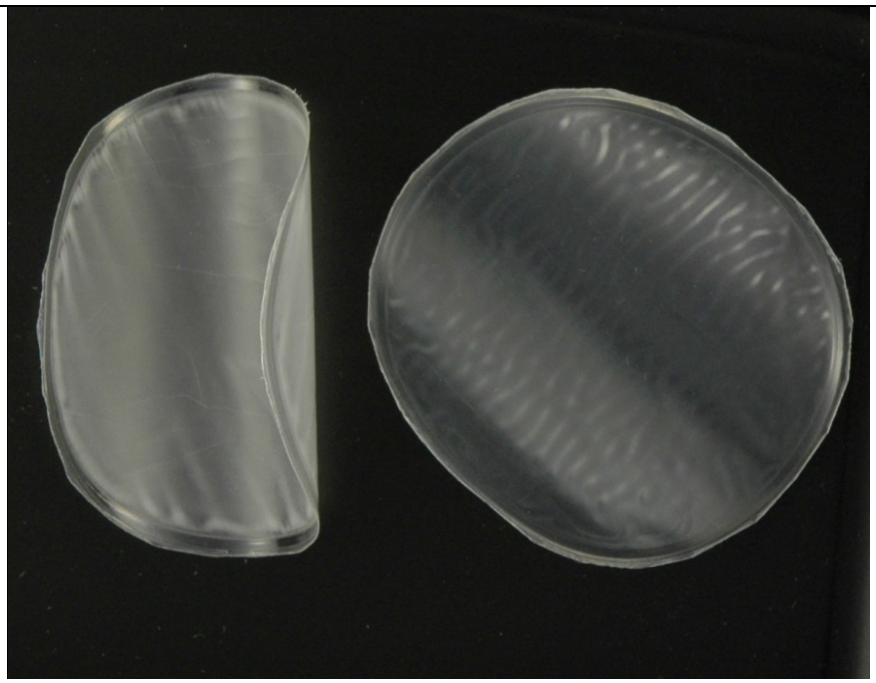

Figure 4.9. Visible defects on film A (left) and film B (right) after 60 minutes of retort at 121°C.

4.3.5 Characterization of States of Water in Film A and Film B by DSC

The thermodynamic states of water are considered to affect the physical properties of polymers. For example, Hodge et al. (1996b) demonstrated that increase in mean free volume cavity size (associated with higher oxygen permeabilities) was most significant during the stages when water in polyvinyl alcohol was contained as non-freezing bound water, concluding that non-freezing water is the fraction responsible for majority of plasticization. The states and proportions of water were evaluated for film A and film B after retort in order to investigate if there is any correlation with oxygen permeability. The amount of water associated with each thermodynamic state was determined from the enthalpy of melting of water as observed from DSC heating scans.

Figure 4.10 shows DSC scans for film A and film B after water absorption at retort conditions. The figure shows that for film A ice melting endotherms/peaks were detected only at water contents of 5.5% and above. The ice melting peaks observed for film A were closer to 0°C, and the water state for these peaks was identified as free water. No peak associated with freezable bound water. On the other hand, for film B a measurable ice melting peak was observed only at a water content of 6%, i.e. after 60 minutes retort. The peak occurred at a temperature around -15°C. Since this peak temperature was much lower than the melting point of free/bulk water, the state was identified as freezable bound water. According to Hatakeyama, et al. (1988) freezable bound water has a melting temperature between -50°C and 0°C. No free water was observed for film B in the range of water contents used. The temperature of ice melting (for film A) also increased as water absorption increased as indicated in figure 4.9 by a gradual shift of the endothermic peak towards higher temperature. The peak temperature shifted from -1.6 ± 0.61°C to 1.6 ± 0.07°C as water absorption increased from 5.5% to 7.0%. The heat of fusion of water melting also increased with water absorption.

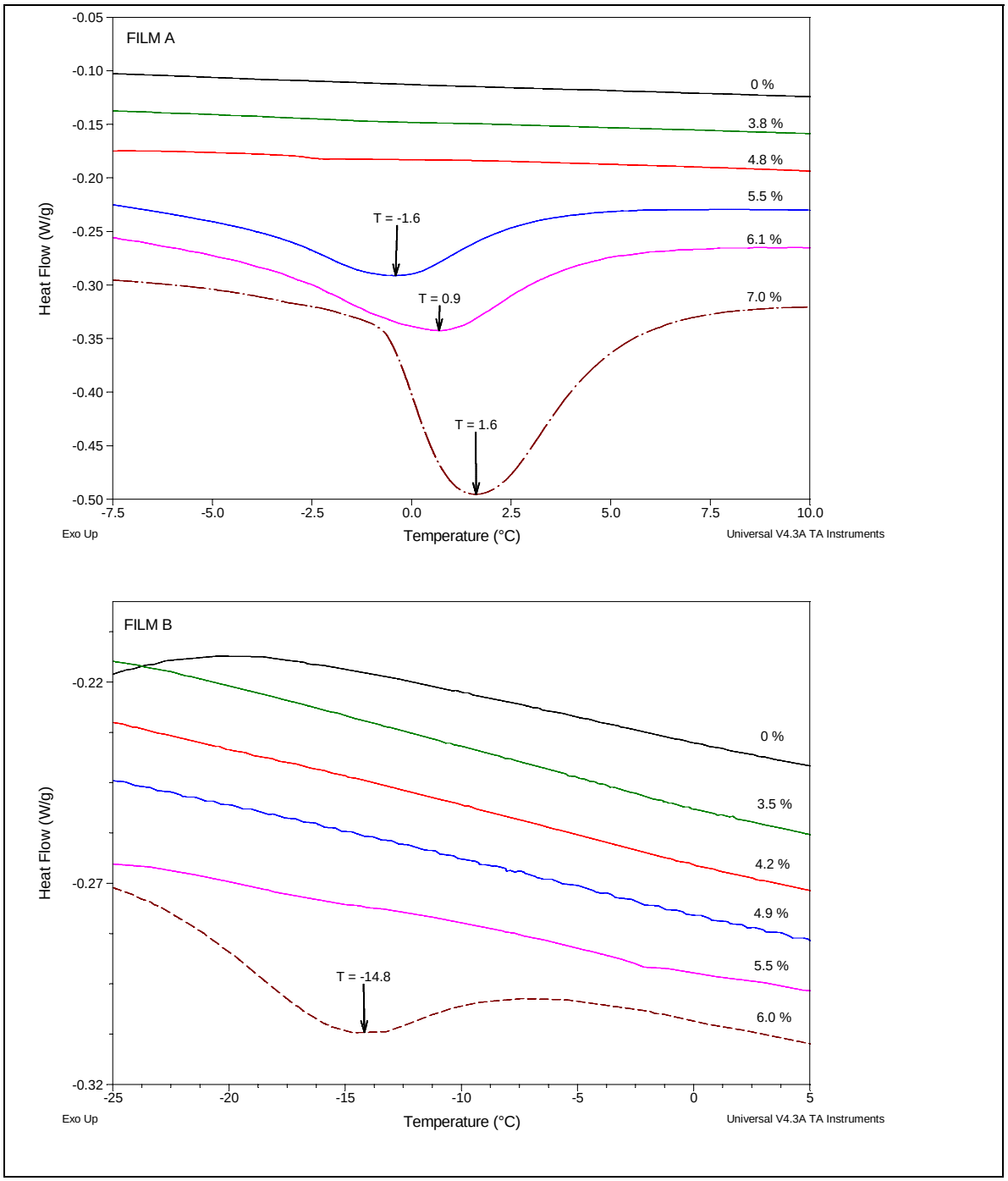

Figure 4.10. DSC heating scans showing ice melting for film A (top) and Film B (bottom)

The amount of free water and freezable bound water was calculated from the melting peaks as % w/w water with respect to dry sample weight using the following equation:

$$w_i = \frac{\Delta H_i}{w_d \times \Delta H_f} \tag{4.3}$$

where w_i is the weight of water calculated from the individual peaks for the different water states on dry weight basis (i stands for free or freezable bound water), ΔH_i is the integrated enthalpy under the ice melting peak (i.e. measured quantity of heat sorbed during melting in J), and ΔH_f is the enthalpy of ice melting transition for free water taken as that of free water (i.e. $\Delta H_f = 334 J/g$ according to Nakamura et al. (1983), and w_d is the dry weight of DSC sample (in g). The amount of non-freezing bound water was then calculated by subtracting the sum of free water and freezable bound water (i.e. those water fractions detected on the DSC scans) from the total water content according to the equation:

$$w_{nf} = w - \left(w_{free} + w_{fb}\right) \tag{4.4}$$

where w_{nf} is the non-freezing bound water, w_{free} is free water, w_{fb} is freezable bound water, and w is the total water absorbed by film during retort heating. The calculated data for the various water fractions are shown in Table 4.5 for both film A and film B. The data shows that for film A the amount of non-freezing bound water increased and reached a constant value of about 0.05g/g after only 10 minutes of retort. For film B a constant value was not reached in the water contents measured, but a value of about 0.058g/g was reached after 60 minutes of retort and 6% total water content. The amount of non-freezing bound water increases with increasing total water content as polymer-polymer

hydrogen bonds are disrupted, resulting in increased primary binding sites available for water molecules. According to Liu and Yao (2001) after a certain water content level, polymer chains have strengthen out to their fullest, and the cavity size of the polymer becomes constant, and hence the non-freezing bound water attains a maximum value. An increase in the amount of non-freezing bound water can be an indirect indication of an increase in free volume, explaining the increase in oxygen transmission rates with water absorption observed in Figure 4.5. However, the existence of the different states does not correlate with the break in slope observed in Figure 4.5. Lien et al. (2002) also found no correlation between oxygen permeability and presence of water in any particular state within polyvinyl alcohol films. These authors concluded that either all forms/states of water in the film matrix contribute in a simple additive manner to increase oxygen permeability, or the effect of polymer structure obscures the contribution due to bound water.

Table 4.5. Quantities of water fractions for film A and film B evaluated by DSC

FILM A					
Retort time (min)	5	10	20	30	60
Total water absorbed, W (g/g)	0.038 ± 0.0006	0.048 ± 0.003	0.055 ± 0.003	0.061 ± 0.007	0.070 ± 0.003
Free water, W_{free} (g/g)	ND	ND	0.0063 ± 0.0009	0.013 ± 0.001	0.019 ± 0.0006
Freezing bound water, W_{fb} (g/g)	ND	ND	ND	ND	ND
Non-freezing bound water, W_{nf} (g/g)	0.038 ± 0.0006	0.048 ± 0.003	0.049 ± 0.002	0.048 ± 0.006	0.051 ± 0.003
FILM B					
Retort time (min)	5	10	20	30	60
Total water absorbed, W (g/g)	0.035 ± 0.004	0.042 ± 0.0002	0.049 ± 0.0008	0.055 ± 0.006	0.060 ± 0.001
Free water, W_{free} (g/g)	ND	ND	ND	ND	ND
Freezing bound water, W_{fb} (g/g)	ND	ND	ND	ND	0.0020 ± 0.0002
Non-freezing bound water, W_{nf} (g/g)	0.035 ± 0.004	0.042 ± 0.0002	0.049 ± 0.0008	0.055 ± 0.006	0.058 ± 0.003

ND means Not Detected

4.4 Conclusions

Oxygen transmission rates of multilayer EVOH films increased with increasing water absorption. Two distinct regions in the curve of oxygen transmission rate versus water absorption were observed with change of slope at 6% water content for film A and 4% for film B. Analysis of effect of water absorption at retort conditions revealed a reduction in melting enthalpy as water content increases for EF-XL in film A, and L171 and nylon 6 in film B, suggesting there might be some reduction on crystallinity of these components. The non-freezing water content increased with increasing total water content, indicating increasing availability of primary binding sites, hence free volume of the polymer. This correlates with increased higher oxygen transmission observed with increased water contents. However, presence of water in any particular state could not be correlated to the change of slope observed at water contents of 4% for film A and 6% for film B. These results emphasize that longer durations of retort processes result in significant increases in oxygen transmission rates due to possible irreversible damage and reduction in crystallinity of the films. As shown in Chapter 3, the duration of microwave treatments was only 9 minutes for the $F_0 = 3\ min$ and 12 minutes $F_0 = 6\ min$ processes, while the retort treatment lasted 28 minutes for $F_0 = 3\ min$ process. Therefore the microwave process times were well below the values that correspond to dramatic increases in oxygen transmission rates and observed damage on the films. Similarly the lesser oxygen barrier deterioration for film A underscores the importance of proper design of the multilayer films in terms of the types, properties and placement of polymers used.

References

Apicella, A. and Nicolais, L. 1981. Environmental aging of epoxy resins: synergistic effect of sorbed moisture, temperature and applied stress. Industrial and Engineering Chemistry, Product Research and Development 20, 138-144.

Aucejo, S., Marco, C., and Gavara, R. 1999. Water effect on morphology of EVOH copolymers. Journal of Applied Polymer Science 74, 1201-1206.

Barrer, R.M., Barrie, J.A., and Rodgers, M.G. 1962. Permeation through a membrane with mixed boundary conditions. Transactions of Faraday Society 58, 2473-2483.

Cabedo, L., Lagaron, J.M., Cava, D., Saura, J.J., and Gimenez, E. 2006. The effect of ethylene content on the interaction between ethylene vinyl alcohol copolymers and water – II: Influence of water sorption on the mechanical properties of EVOH copolymers. Polymer Testing 25, 860-867.

Carfagna, C. and Apicella, A. 1983. Physical degradation by water clustering in epoxy resins. Journal of Applied Polymer Science 28, 2881-2885.

Fan, X., Zhang, G.Q., van Driel, W.D., and Ernst, L.J. 2008. Interfacial delamination mechanisms during soldering reflow with moisture preconditioning. IEEE Transactions on Components and Packaging Technologies 31, 252-259.

Gaucher-Miri, V., Jones, G.K., Kaas, R., Hiltner, A., and Baer, E. 2002. Plastic deformation of EVA, EVOH and their multilayers. Journal of Materials Science 37, 2635-2644.

Hansen, C.M. 2000. Hansen Solubility Parameters: A User's Handbook. CRC Press LLC. Boca Raton, FL.

Hatakeyama, T., Nakamura, K., and Hatakeyama, H. 1988. Determination of bound water content in polymers by DTA, DSC and TG. Thermochimica Acta 123, 153-161.

Hilfiker, R. 2006. Polymorphism in the Pharmaceutical Industry. Wiley-VCH Verlag GmbH & Co. KGaA. Weinheim, Germany.

Hodge, R.M., Bastow, T.J., Edward, G.H., Simon, G.P., and Hill, A.J. 1996a. Free volume and mechanism of plasticization in water swollen polyvinyl alcohol. Macromolecules 29, 8137-8143.

Hodge, R.M., Edward, G.H., and Simon, G.P. 1996b. Water absorption and states of water in semi-crystalline poly(vinyl alcohol) films. Polymer 37, 1371-1376.

Hohne, G., Hemminger, W., and Flammersheim, H.-J. 2003. Differential Scanning Calorimetry. Springer Verlag Berlin Heidelberg, New York.

Lagaron J.M., Powell, A.K., and Bonner, G. 2001. Permeation of water, methanol, fuel and alcohol containing fuels in high barrier ethylene vinyl alcohol copolymer. Polymer Testing 20, 569-577.

Levine, H., and Slade, L. 1988. Water as a plasticizer: physic-chemical aspects of low moisture polymeric systems. In Franks, F. (Ed.). Water Science Reviews, Vol. 3. Cambridge University Press. Cambridge, England. pp 79-185.

Lien, L., Fellows, C.M., Copeland, L., Hawkett, B.S., and Gilbert, R.G. 2002. Water binding and oxygen permeability in polyvinyl alcohol films. Australian Journal of Chemistry 55, 507-512.

Liu, W.G., and Yao, K.D. 2001. What causes frozen water in polymers: hydrogen bonds between water and polymer chains? Polymer 42, 3943-3947.

Lopez-Rubio, A., Hernadez-Munoz, P., Gimenez, E., Yamamoto, T., Gavara, R., and Lagaron, J.M. 2005. Gas barrier and morphological alterations induced by retorting in ethylene vinyl alcohol based food packaging structures. Journal of Applied Polymer Science 96, 2192-2202.

Matsui, T., Fukamachi, M., Koyase, J., Shimoda, M., Tanaka, Y., and Osajima, Y. 1996. Sorption behavior of flavors with water sensitive ethylene vinyl alcohol copolymer film in aqueous solution. Food Science and Technology International 2, 113-115.

Min, B.G., Son, T.W., Kim, B.C., Lee, C.J., and Jo, W.H. 1994. Effect of solvent or hydrophilic polymer on the hydration melting behavior of polyacrylonitrile. Journal of Applied Polymer Science 54, 457-462.

Muramatsu, M., Okura, M., Kuboyama, K., Ougizawa, T., Yamamoto, T., Nishihara, Y., Saito, Y., Ito, K., Hirata, K., and Kobayashi, Y. 2003. Oxygen permeability and free volume hole size in ethylene vinyl alcohol copolymer film: temperature and humidity dependence. Radiation Physics and Chemistry 68, 561-564.

Nakamura, K., Hatakeyama, T., and Hatakeyama, H. 1983. Relationship between hydrogen bonding and bound water in polyhydroxystyrene derivatives. Polymer 24, 871-876.

Nogales, A., Sanz, A., Sics, I., Garcia-Gutierrez, M-C., and Ezquerra, T.A. 2007. Order and segmental mobility in crystallizing polymers. In Reiter, G. and Strobl, G.R. (Eds.). Lecture Notes in Physics: Progress in Understanding of Polymer Crystallization. Volume 714. Springer Verlag Berlin Heidelberg. New York. pp 435-456.

Ping, Z.H., Nguyen, Q.T., Chen, S.M., Zhou, J.Q., and Ding, Y.D. 2001. States of water in different hydrophilic polymers – DSC and FTIR studies. Polymer 42, 8461-8467.

Pissis, P. 2005. Water in polymers and biopolymers studied by dielectric techniques. In Kupfer, K. (Ed.). Electromagnetic Aquametry: Electromagnetic Water Interaction with Water and Moist Substances. Springer-Verlag Berlin Heidelberg. New York. pp 39-70.

Pogany, G.A. 1976. Anomalous diffusion of water in glassy polymers. Polymer 17, 690-694.

Reading, M., Price, D.M., and Orliac, H. 2001. Measurement of crystalinity in polymers using modulated temperature differential scanning calorimetry. In Riga, A.T. and Judovits, L.H. (Eds.). Material Characterization by Dynamic and Modulated Thermal Analytical Techniques. ASTM STP 1402. American Society for Testing Materials. West Conshohocken, PA. pp 17-31.

Reiter, G., and Sommer, J.-U. 2003. Polymer Crsystallization: Observations, Concepts and Interpretations. Spinger-Verlag Berlin Heidelberg. New York.

Yamamoto, T., Kanda, T., Nishihara, Y., Ooshima, T., and Saito, Y. 2009. Correlation study among oxygen permeability, molecular mobility, and amorphous structure change of poly(ethylene vinyl alcohol) copolymers by moisture. Journal of Applied Polymer Science. Part B: Polymer Physics 47, 1181-1191.

Zhang, Z., Britt, I.J., and Tung, M.A. 1999. Water absorption in EVOH films and its influence on glass transition temperature. Journal of Polymer Science. Part B: Polymer Physics 37, 691-699.

Zhang Z., Britt, I.J. and Tung, M.A. 2001. Permeation of oxygen and water vapor through EVOH films as influenced by relative humidity. Journal of Applied Polymer Science 82, 1866-1872.

CHAPTER 5 WATER ABSORPTION AND DIFFUSION CHARACTERISTICS OF POLYMER FILMS

5.1 Introduction

The transport behavior of water is of utmost interest in food packaging because packages are often exposed to various environments of moisture during food processing and storage. The total amount of water accessible to the hydrophilic EVOH layer in multilayer films is limited by the types, thickness and water transport characteristics of the outer layers. A better understanding of the water transport characteristics (thermodynamic and kinetic data) in the different polymer materials that make up multilayer films is necessary to identify the optimum conditions for use of packaging structures.

Transport of small molecular weight substances, including water, through polymers is generally described by the 'solution-diffusion' mechanism (Wijmans and Baker, 1995). In this mechanism permeation of penetrant molecules is thought to occur by dissolution of molecules at the polymer surface (described by the solubility coefficient), followed by diffusion through the polymer matrix (described by the diffusion coefficient). Figure 5.1 is a schematic visualization of the permeation process. The driving force for transport of molecules from one surface to another is a difference in the amount of penetrant molecules between the two surfaces (i.e. a gradient), which can be expressed in terms of partial pressure, concentration, fugacity or chemical potential. Hence, a basic expression representing the solution-diffusion mechanism of gases

through homogeneous dense polymer films relates permeability, solubility and diffusivity as follows:

$$P = DS \tag{5.1}$$

where P is the permeability coefficient which denotes the quantity of penetrant molecules passing through a specimen of a given surface area and thickness during a fixed amount of time. D is diffusivity or diffusion coefficient, a kinetic parameter which reflects penetrant mobility through the polymer matrix. S is the solubility coefficient which is a thermodynamic term that depends on the penetrant-polymer interactions.

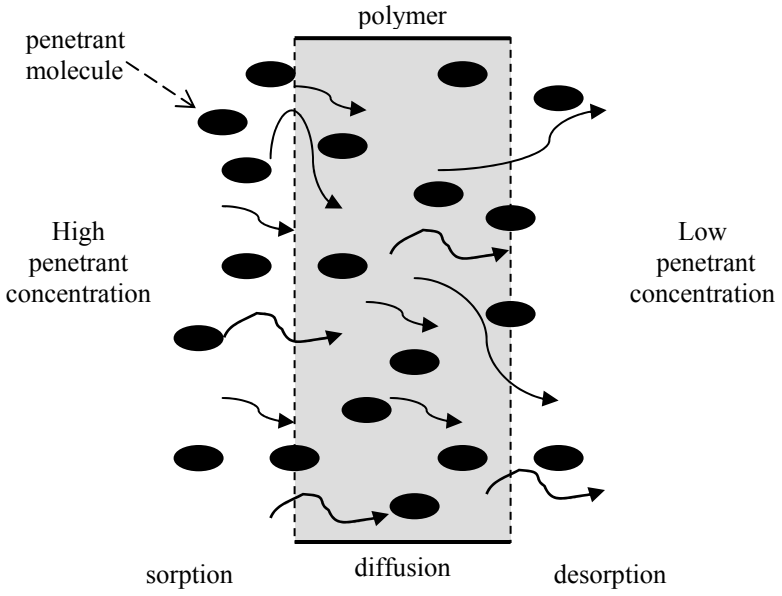

Figure 5.1. Illustration of permeation process through a polymer film

The behavior of water in polymers presents a special case, due to the nature of the water molecule. The water molecule is relatively small and has a strong tendency towards hydrogen bond formation with itself as well as with other polar groups (van Krevelen,

1990). While the polymer-penetrant interactions are quite small for gases, the same is not true for water. The objective of this study is to evaluate water sorption and diffusion characteristics of monolayer and multilayer films are evaluated at different temperatures ranging from room temperature to 121°C. Equilibrium water contents and temperature effects were evaluated for two multilayer films and in comparison with some monolayer films. Solubility and diffusion coefficients were evaluated for monolayer films. Sorption isotherms of EVOH films of different copolymer composition were investigated to assess the mechanisms of interactions of water and the polymers.

5.2 Theoretical Background

The general mechanisms of sorption and diffusion of penetrant molecules in polymers is described in the following sections.

5.2.1 Sorption

When a penetrant comes into contact with the polymer part of it is taken by the polymer. The penetrant molecules can enter the polymer (absorption) or remain attached to the polymer surface (adsorption) (Brunauer, 1943). Often the two phenomena occur simultaneously, and the total uptake is then designated by the term sorption. Sorption also includes trapping of penetrant molecules in microvoids and clustering of molecules into aggregates (Crank and Park, 1968; Rogers, 1985; Naylor, 1989). The quantity of penetrant molecules dispersed in the polymer matrix at equilibrium and the sorption mode are governed by the thermodynamics of the polymer/penetrant system and the

nature and strength of interactions between penetrant molecules and the polymer. The intensity of these interactions depends strongly on the polarity of polymer chains. Polymers are generally characterized as either hydrophilic or hydrophobic depending on the amount of water absorbed at equilibrium. Generally, polymers which at 25°C and 100% RH absorb more than 10% of water are usually classified as hydrophilic, while those absorbing less than about 1% of moisture are classified as hydrophobic (Zaikov, et al., 1988). The 10% criterion is not an absolute one and it is not in any way a measure to characterize the mechanism of water transport. Water absorption by hydrophilic polymers is attributed to specific associations between water molecules and the polar groups in the polymer chains (e.g., hydroxyl (OH) groups in EVOH, amide groups (CONH) in nylon 6). Water molecules absorbed by hydrophilic polymers form hydrogen bonding networks with the polar groups causing plasticization of the polymer matrix (Levine and Slade, 1988). At molecular level, plasticization leads to increased intramolecular and intermolecular space or free volume, and may involve weakening or breaking of polymer-polymer hydrogen bonds. When polar groups are fully occupied, subsequent water molecules start bonding with each other, forming water clusters. The hydrophilic nature of EVOH copolymers is well known. At room temperature and 100% RH EVOH copolymer absorbs up to 13% moisture at equilibrium (Aucejo et al., 1999). For the less polar polymers the sorption sites for water is assumed to be the existing free volume within the polymer matrix. The first water molecules to be sorbed are distributed among the polymer chain units without any significant energy exchange with the polymer segments (Zaikov, et al., 1988). Further adsorption of water by the polymer results in preferential interaction between water molecules leading to cluster formation. As a result

hydrophobic (such as polyolefins) and moderately hydrophilic polymers (such as polyesters), have low water absorption capacities because the interactions between water molecules are stronger than those between polymer chains and water molecules. Water uptake by PE at room temperature and saturated RH conditions was reported in the range 0.002-0.006% (Myers et al., 1961; McCall et al., 1984), while that for PP was less than 0.5% (McKnight et al., 1997; Yi and Pellegrina, 2002; Tajvidi et al., 2006).

When penetrant molecules come in contact with the polymer, the molecules adsorb to the surface in quantities that are a function of their partial pressure in the bulk. The amount of penetrant molecules adsorbed over a range of partial pressures (or water activity) at a constant temperature is graphically represented in a sorption isotherm. Sorption isotherms are classified on the basis of the relative strengths of the interactions between penetrant molecules and the polymer, or between the penetrant molecules themselves within the polymer (Naylor, 1989). The simplest type of sorption is Henry's law sorption which arises when polymer/penetrant and penetrant/penetrant interactions are weak relative to polymer/polymer interactions (Naylor, 1989; Rodgers, 1985). This is the case of ideal solution behavior where the sorbed penetrant molecules are randomly dispersed within the polymer. According to this mode the solubility coefficient (S) is constant and independent of sorbed concentration at a given temperature. For low pressures and ideal gases, the sorption isotherm is a linear relation of concentration versus pressure (or vapor activity):

$$C = Sp \tag{5.2}$$

Henry's law sorption behavior is observed when penetrant gas are sorbed by rubbery polymers at low pressures (< 1 atm) and arises from the low solubility (< 0.2%) of the

penetrant gases in the polymer (Naylor, 1989). Several other situations exist where penetrant concentrations may deviate from ideal and sorption mechanisms cannot be represented by Henry's law. Brunauer et al. (1940) introduced a systematic interpretation of adsorption isotherms and classified five different types as shown in figure 5.2. This classification has become one of the most commonly used in literature. According to this classification, Type I isotherms, also known as Langmuir isotherms, assumes monolayer adsorption on a homogeneous surface (Rodgers, 1985). The Langmuir isotherm assumes that adsorption takes place only at specific localized sites on the surface and saturation corresponds to complete occupancy of these sites. Type I isotherms reduce to Henry's law at low pressures. Type II isotherms describe adsorption on polymers with strong interactions between specific sites (e.g. polar groups) followed by a more or less random distribution of penetrant when the specific sites are nearly all occupied (Rodgers, 1985; Naylor, 1989). Type III sorption behavior occurs in systems where there are no specific site interactions with penetrant molecules, i.e. systems where penetrant/penetrant interactions are inherently stronger than corresponding polymer/penetrant interactions (e.g. water in hydrophobic polymers or hydrophilic polymers at higher penetrant concentrations). The first molecules sorbed tend to plasticize the polymer structure locally making it easier for subsequent molecules to enter in the same neighborhood than to go elsewhere. Type IV and type V isotherms usually occur when multilayers of penetrant are absorbed onto the surface of the pores in a porous solid (Masel, 1996). Initially, the isotherm looks like type II or type III, respectively, but eventually the absorbed layer gets so thick and fills up the pores. As a result no more penetrant can be absorbed at the isotherm levels of as the polymer is saturated with penetrant. No single

sorption isotherm can describe the entire range of water activity because water is associated with a polymer matrix by different mechanisms in different water activity regions. The above physical interpretations are just simplifications, and it is likely that two or more modes of sorption will occur concurrently.

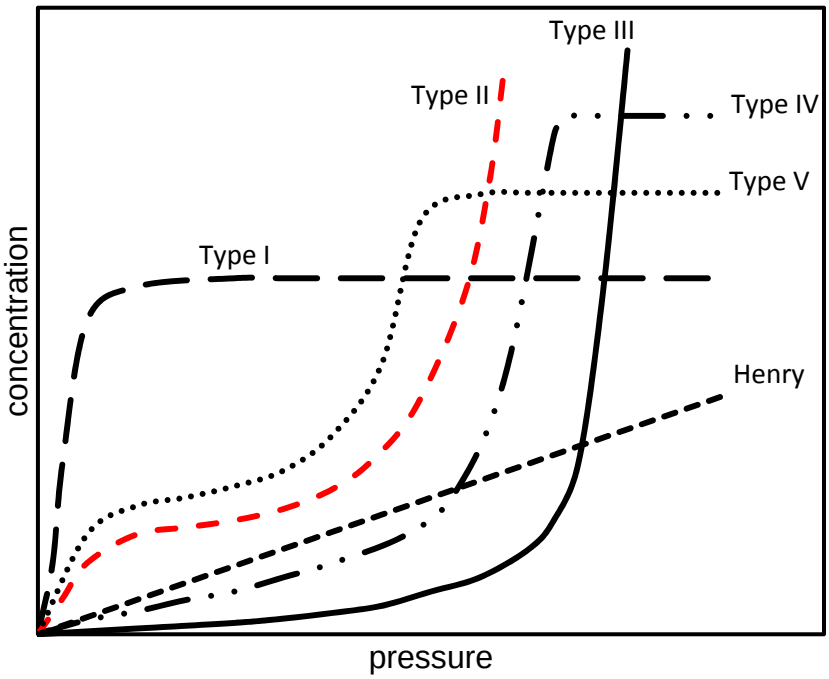

Figure 5.2. Schematic of adsorption isotherms (adapted from Brunauer et al., 1940)

5.2.2 Diffusion of Water in Polymers

Diffusion is the process by which small molecules are transported through a polymer as a result of random molecular motions without appreciable displacement of the macromolecules of polymer (Crank and Park, 1968). The mathematical theory of diffusion in isotropic materials is based on the hypothesis that the rate of transfer of

diffusing substance through unit area of a section of the material is proportional to the concentration gradient measured normal to the section (Crank. 1975):

$$F = -D\frac{\partial C}{\partial x} \tag{5.3}$$

where F is the flux, (the rate of the diffusing substance transferred per unit area of section), C is the concentration and x is the space coordinate. The negative sign arises because diffusion occurs in the direction opposite to that of the increasing concentration. Equation (5.3) is known as Fick's first law of diffusion. The fundamental differential equation of diffusion (referred to as Fick's second law) is derived from the mass balance of a volume element as follows (Crank, 1975):

$$\frac{\partial C}{\partial t} = D\left(\frac{\partial^2 C}{\partial x^2} + \frac{\partial^2 C}{\partial y^2} + \frac{\partial^2 C}{\partial z^2}\right) \tag{5.4}$$

where D is a constant diffusion coefficient. In other situations though, the diffusion coefficient may not be constant and may depend on the concentration. Those situations will not be considered in this study. In equation (5.4) the diffusion occurs in three directions (x, y, z). Many situations can be approximated as one dimensional diffusion problems. An example is the case for thin polymer films where the thickness is very small as compared to the length. Equation 5.4 is then reduced to the following:

$$\frac{\partial C}{\partial t} = D\left(\frac{\partial^2 C}{\partial x^2}\right) \tag{5.5}$$

Solutions of equation (5.5) to give concentration profiles of penetrants in polymers depend on the initial and boundary conditions for the particular problem and the geometry of the sample being evaluated. The case considered in this study is for an initially dry film sample of thickness l that is fully immersed in water. Figure 5.3 is a schematic of a one dimensional diffusion problem for a thin film fully immersed in a

penetrant. Ignoring water penetration through the edge of the film, this system can be treated as a one-dimensional diffusion problem.

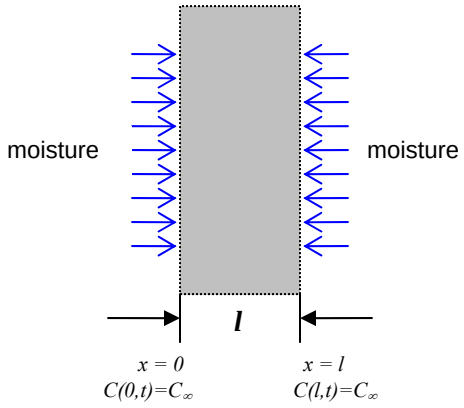

Figure 5.3. Graphical representation of one dimensional diffusion problem

If equilibrium between the bulk fluid and the film surface is attained rapidly by comparison with the rate of diffusion, the surface concentration can be kept effectively constant throughout the experiment (Chainey, 1989). Based on this assumption and that the concentration of penetrant is uniform within the film (i.e. initially zero) the initial and boundary conditions are:

$$C = C_0, \qquad 0 < x < l, \qquad t = 0$$

$$C = C_\infty, \qquad x = 0\,, \qquad x = l, \qquad t > 0 \tag{5.6}$$

where C_0 is the moisture concentration initially (i.e. when $t = 0$) and C_∞ is the equilibrium (saturated) moisture concentration. From these conditions, the concentration profiles of penetrant within the plane sheet/film can be expressed in terms of space (x) and time (t) by the following series:

$$\frac{C(x,t)}{C_\infty} = 1 - \frac{4}{\pi}\sum_{n=0}^{\infty} \frac{1}{(2n+1)^2} exp\left[-\frac{(2n+1)^2\pi^2 Dt}{l^2}\right] \tag{5.7}$$

At any time t, the total amount of moisture that has entered the film (i.e., M_t) is given by:

$$M_t = \int_0^l (C - C_0) dx \tag{5.8}$$

Equation (5.8) can be integrated with respect to time to derive an expression of moisture uptake (M_t):

$$\frac{M_t}{M_\infty} = 1 - \frac{8}{\pi^2} \sum_{n=0}^{\infty} \frac{1}{(2n+1)^2} exp\left[-\frac{(2n+1)^2 \pi^2 Dt}{l^2} \right] \tag{5.9}$$

For small times, when the value of the ratio $\frac{M_t}{M_\infty}$ is less than 0.5-0.6 equation (5.9) can be approximated with very little error by the following equation:

$$\frac{M_t}{M_\infty} = \frac{4}{l} \sqrt{\frac{Dt}{\pi}} \tag{5.10}$$

5.3 Materials and Methods

5.3.1 Description of Film Materials

Monolayer films and multilayer films were evaluated to study transport properties of water. The films evaluated include film A and film B as described in Chapter 3 (section 3.3.2.), and monolayer films of biaxially oriented PET (Mylar), cast nylon 6, EF-XL (a biaxially oriented EVAL® resin with 32 mol % ethylene), and L171 (a non-oriented EVAL® resin with 27 mol % ethylene). The films were all supplied by EVAL Company of America, Houston, TX.

5.3.2 Water Absorption Measurements

Prior to testing, film samples (~5cm in diameter) were dried in a vacuum oven (60 cm Hg) at 70 °C for 2-3 days until constant weight. Initial dry weight (w_d) was taken before each measurement using an analytical balance with a resolution of 0.0001g (Analytical Plus, OHAUS).Water absorption was measured gravimetrically by immersing films in deionized water at 25°C, 60°C, 90°C and 121°C. For EF-XL and L171 immersion tests were done at 25°C only because the films could not withstand water immersion at high temperatures and data was very unpredictable. Water absorption at 121°C was measured using the test cell and procedure described in Chapter 4 (section 4.2.2). Water absorption at 25°C, 60°C, and 90°C was done by directly immersing film samples in beakers containing deionized water placed in a thermostated bath set at the desired temperature. Samples were periodically taken out, wiped with paper towel to remove surface water and weighed immediately to obtain the final/wet weight (w_d). For film A, film B, and PET, the same film samples were used for the entire sorption period (i.e., samples were placed back into the beakers and used for the next weight measurement). For nylon 6, EF-XL, and L171 measurements, different samples were used at each sorption time to avoid underestimation of amount of water absorbed. Water absorption and desorption in these films is very fast, and some water was lost very quickly during the weighing period (which lasted about 1 minutes per sample). Three replicates were used for each measurement time for films. The percentage of water uptake/absorption at any time (M_t) was calculated according to the following equation.

$$M_t = \frac{w_t - w_d}{w_d} \times 100 \qquad (5.11)$$

where w_t is the weight of sample at time t (wet weight) and w_d is the dry weight of sample. The percentage equilibrium water absorption (M_∞) was calculated as an average of several constitutive measurements that showed no appreciable additional absorption (about 3 or 4 successive measurements).

5.3.3 Determination of Solubility and Diffusion Coefficients

In order to compare transport coefficients of hydrophobic and hydrophilic polymers, diffusion and solubility coefficients were determined for PET, nylon 6, EF-XL and L171 films at 25°C. The solubility coefficient (S in mol/m^3/Pa) was calculated from the equilibrium water content according to the following formula (Launay et al., 1999):

$$S = \frac{W_\infty \times \rho}{M_w \times p} \tag{5.12}$$

where W_∞ is the weight of water in the polymer at equilibrium (g water/ g dry polymer), ρ is the density of the polymer, M_w is the molecular weight of water (18 g/mol), and p is the vapor pressure of water at the experimental temperature.

To evaluate whether diffusion of moisture followed Fick's laws, the moisture uptake ($\frac{M_t}{M_\infty}$) data were plotted against the square root of time $\sqrt{t}$ according to equation (5.10). For Fickian diffusion, the plot must be linear up to at least 50-60% of the equilibrium moisture content for both absorption and desorption (Frisch, 1980, Illinger and Schneider, 1980). Following the linear portions both absorption and desorption curves must be concave to the time axis until equilibrium moisture content is reached. The diffusion coefficient D was calculated from the slope of the initial linear portion of the curve as follows:

$$D = \pi \frac{l^2}{16} \times [slope]^2 \quad (5.13)$$

where l is the thickness of the film.

5.3.4 Sorption Isotherms

Sorption isotherms of EF-XL and L171 films were obtained by exposing films to various water activity levels maintained with saturated salt solutions at 25°C. Eight salts were chosen to cover a range of water activity (a_w) between 0.11 and 0.94. The salts used were lithium chloride (a_w = 0.11), potassium acetate (a_w = 0.23), magnesium chloride (a_w = 0.33), potassium carbonate (a_w = 0.43), magnesium nitrate (0.53), sodium chloride (a_w = 0.75), potassium chloride (a_w = 0.84), and potassium nitrate (a_w = 0.94) (Greenspan, 1977). Film samples were weighed daily to determine the amount of water absorbed until equilibrium was reached. The equilibrium water content was determined when 3-5 consecutive weight measurements showed a difference of less than 0.0001g. The time required to reach equilibrium for both films was about 7-10 days. Two replicates were used at each water activity level. The equilibrium water content (M_∞) was calculated as:

$$M_\infty = \frac{w_f - w_i}{w_i} \times 100 \quad (5.14)$$

where w_f is final weight of sample, w_i is the initial weight of sample. The sorption isotherm was obtained by plotting M_∞ as a function of water activity for both L171 and EF-XL films.

5.4 Results and Discussion

5.4.1 Water Absorption Characteristics of Films at 25°C

Figure 5.4 shows water absorption as a function of immersion time at 25°C for all films studied. For all films, there was an initial period of rapid water absorption, where the amount of water absorbed increased linearly with time. The rate of water absorption reduced as equilibrium/saturation was approached. The data on equilibrium water content and time taken to reach equilibrium are presented in Table 5.1. The data showed that the hydrophilic films (EF-XL, L171, nylon 6) absorbed the most amount of water, while PET, which is hydrophobic, absorbed the least amount. The amount of water absorbed by polymer films depends on the extent of the interactions between the polymer and water molecules. Among the hydrophilic films L171 absorbed more water, followed closely by nylon 6, while EF-XL absorbed less. Water absorption among EVOH copolymers is strongly related to the ethylene and vinyl alcohol content in the copolymer and orientation. L171 contains a higher content of vinyl alcohol (i.e., 73 mol % vinyl alcohol compared to 68 mol % vinyl alcohol in EF-XL). As a result more hydrophilic sites (OH groups) exist in L171 to interact with water molecules. In addition, EF-XL is biaxially oriented which further improves its water barrier property due to existence of more ordered crystal morphology. The multilayer films absorbed amounts intermediate between that of PET and the hydrophilic films. Both film A and film B contain hydrophobic PET and PP as outer layers that help to limit water penetration to the inner hydrophilic EVOH layers. However, despite the protection offered by PP and PET layers some water still penetrates into the film and interacts with the polar sites of EVOH and

nylon 6 to allow more water absorption by the polymer films. Film A contains EVAL® resin EF-XL, while film B contains the EVAL® resin L171 and nylon 6. Film B absorbed more water at equilibrium than film A because it contains both L171 and nylon 6, which Table 5.1 shows absorbed the highest amount of water.

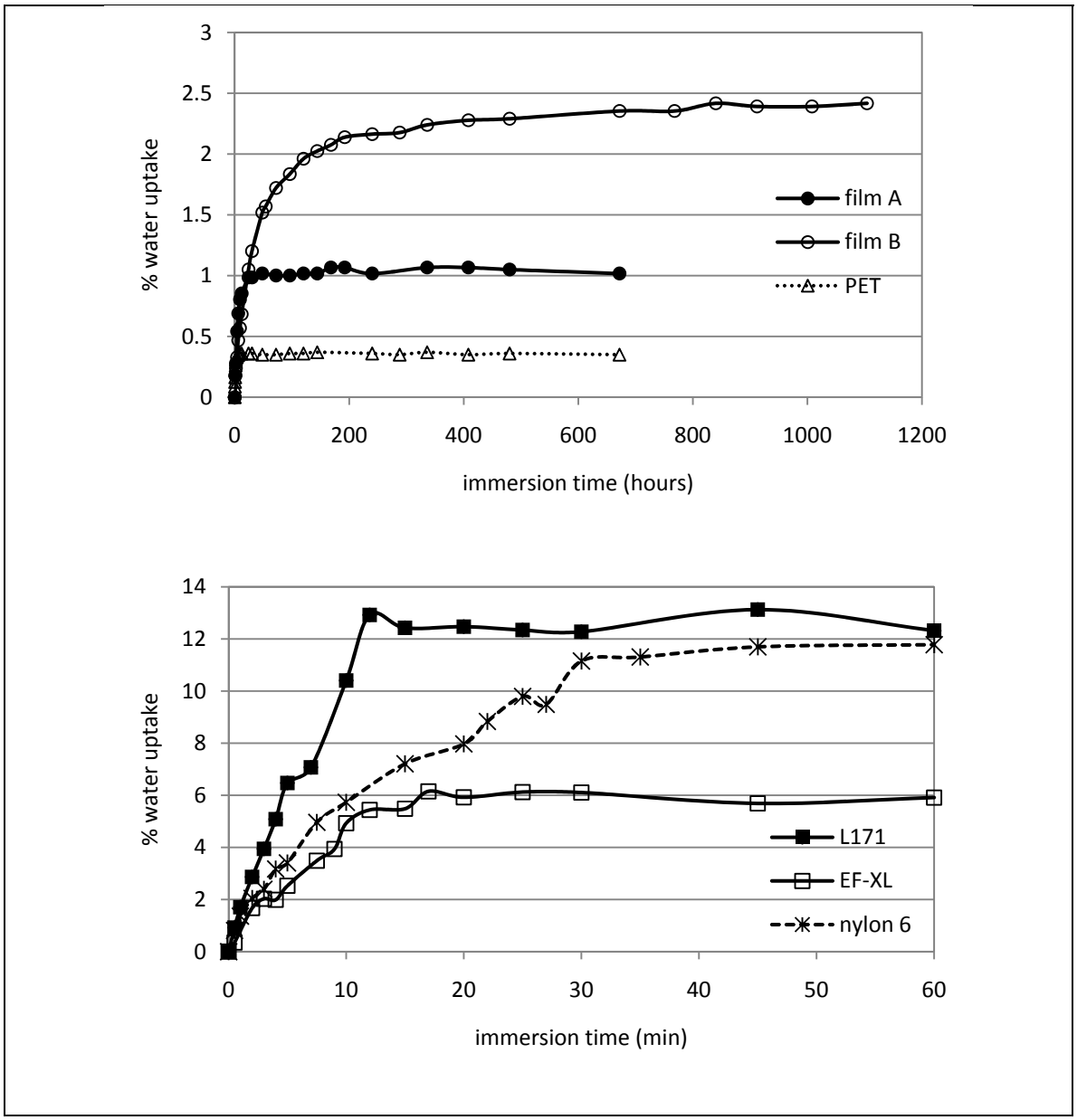

Figure 5.4. Water absorption as a function of time by film A and film B at 25°C

Table 5.1. Equilibrium water content of films at 25°C

Film	Thickness (mm)	Equilibrium water content M_∞ (%)	Time to reach equilibrium t_∞
Film A	0.111	1.0	1 day
Film B	0.140	2.3	10 days
PET	0.132	0.36	6 hours
L171	0.071	12.6	12 minutes
EF-XL	0.023	6.0	17 minutes
Nylon 6	0.112	11.5	30 minutes

5.4.2 Effect of Temperature on Water Absorption

Water absorption curves for film A and film B at 25°C, 60°C, 90°C, and 121°C are presented in Figures 5.5. At all temperatures, film A reached equilibrium faster than film B. The time taken to reach equilibrium decreased as temperature increases for both films. At 25°C film A reached an equilibrium value of only 1% within one day, and film B reached a value of 2.3% in more than 10 days. Similarly, at 60°C film A attained an equilibrium value of 1.4% in about 12 hours, while film B attained 3% in about 30 hours. At 90°C film A reached approximately 1.9% equilibrium water content in 5 hours, while film B reached 3.7% equilibrium value in 12 hours. At 121°C it took only 3 hours for film A to reach 8.3% equilibrium and 6 hours for film B to reach equilibrium value of 9.5%.

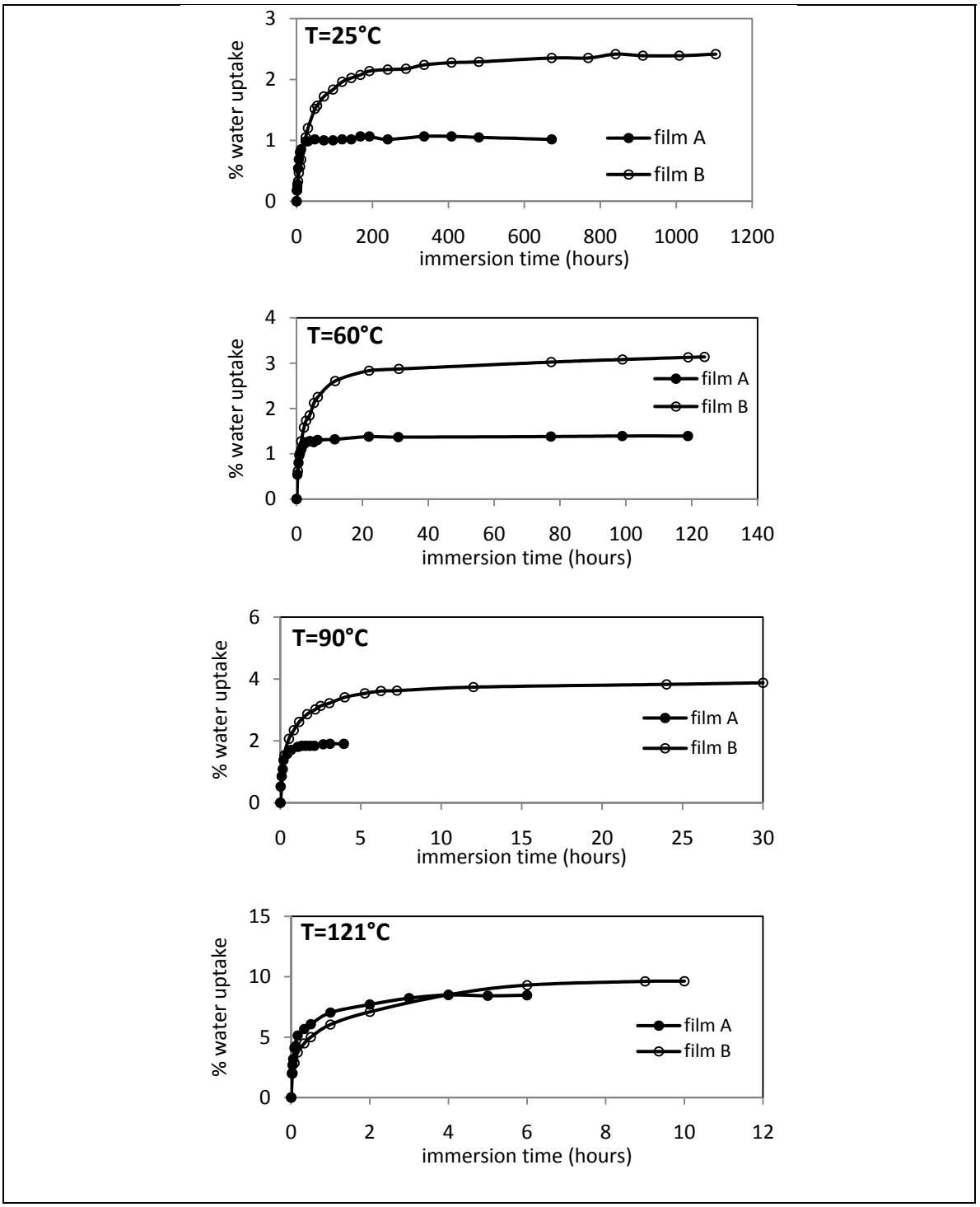

Figure 5.5. Water absorption as a function of time for film A and film B at different temperatures

Figure 5.6 is a plot of equilibrium water content (M_∞) as a function of temperature for film A and film B. Values for PET and nylon 6 are also shown for comparison. It has already been indicated that it was difficult to measure water sorption gravimetrically in EVOH films (EF-XL and L171) at higher temperatures as they could not withstand these conditions. Hence nylon 6 was used to represent the behavior of hydrophilic films. The figure shows that M_∞ increased linearly with temperature between 25°C and 90°C for both film A and film B, and increased considerably between 90°C and 121°C. In comparison, M_∞ for PET increased linearly in the entire temperature range studied. In contrast, M_∞ for nylon 6 decreased from 25°C to 60°C, and remained relatively unchanged between 60°C and 121°C.

An increase of equilibrium water absorption with temperature observed for film A and film B has been reported as a general behavior for low polarity polymers such as polyethylene, PET, etc. (McCall et al., 1984, Launay et al., 1999). Higher equilibrium absorption values are expected at higher temperatures, since the saturated vapor pressure (the driving force) increases with temperature faster than the solubility decreases with temperature. On the other hand, a decrease of equilibrium water absorption with temperature in hydrophilic polymers such as nylon 6 may be due to the disruption of hydrogen bonds resulting from increased thermally induced molecular vibrations. Decrease in equilibrium water content with temperature was previously reported for EVOH and nylon 6 (Zhang et al., 1999; Cava et al., 2006b; Hernandez and Gavara, 1994). The similarity between film A and film B and low polarity polymers may be due to the fact that the outer layers of these multilayer films essentially control and limit the

amount of water penetrating the films. The abrupt increase in equilibrium water content for film A and film B between 90°C and 121°C might be due to possible damage on the films due to the synergistic effects of high RH and temperature for extended periods of time as described in Chapter 4. It was observed that film A samples turned opaque after immersion in water at 121°C for time periods longer than 30 minutes. Film B showed more damage in the form of bubbles/blisters appearing on the films.

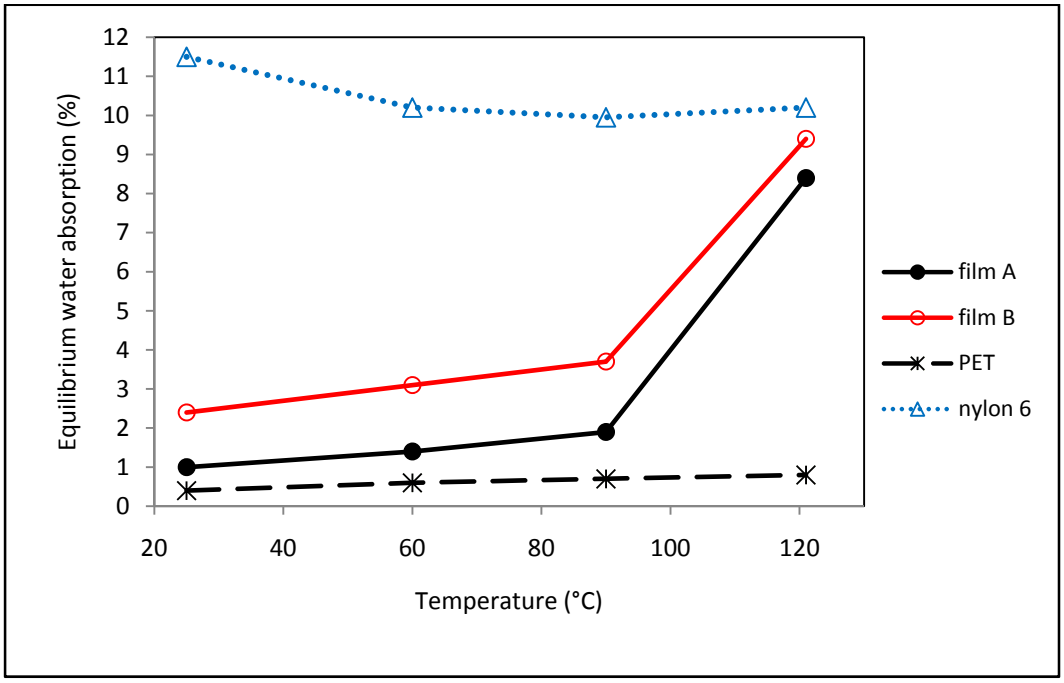

Figure 5.6. Equilibrium water content as a function of temperature for selected films

5.4.3 Solubility and Diffusion Coefficients for Monolayer Films

Solubility and diffusion coefficients were analyzed for monolayer films using Fick's laws. Similar analysis was not done for the multilayer films (film A and film B) since the assumption of constant diffusion coefficient in Fick's laws does not apply for multilayer films. Plots of $\frac{M_t}{M_\infty}$ versus $\sqrt{t}$ for L171, EF-XL, nylon 6 and PET are shown

in Figure 5.9. For all the films the plots showed an initial linear region from which the diffusion coefficient is calculated according to equation (5.13).

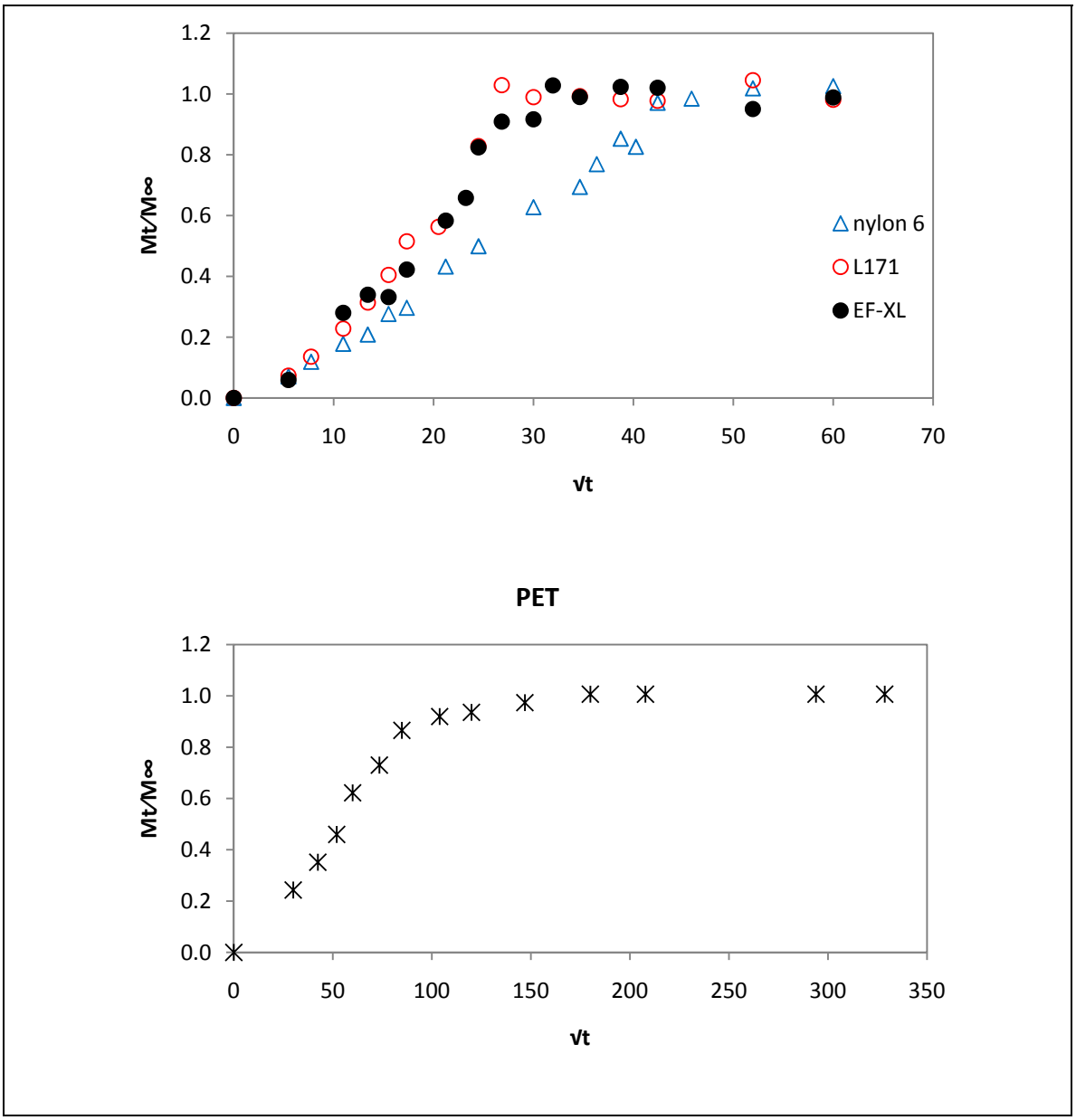

Figure 5.7. Water diffusion curves for monolayer films at 25°C

The solubility and diffusion coefficients of the films are summarized in Table 5.2. The table shows that the diffusion coefficient is higher for PET than for the hydrophilic films (EF-XL, L171, nylon 6). On the other hand the solubility coefficients of the hydrophilic films are higher than that of PET. Lower diffusion coefficients are generally reported for hydrophilic polymers. This is due to the considerable immobilization of water molecules at highly polar sites in hydrophilic polymers that hinder mobility of water molecules, resulting in low diffusion coefficients (Marais, et al., 1998). As expected, solubility coefficients are higher for the hydrophilic films than for PET due to the strong interaction between the hydroxyl groups in EVOH and amide groups in nylon 6.

Literature data on diffusion of water in EVOH is scarce, and available data are often inconsistent. For instance, Lagaron et al (2001) and Cava et al. (2006b) reported that diffusion of water in EVOH films follows Fickian behavior. However, in an earlier study by Zhang et al. (1999) Fickian behavior was only observed for water sorption at 25°C and deviations from Fickian sorption were observed at higher temperatures (35°C and 45°C) and high water activities. Cava et al. (2006b) reported diffusion coefficients of 7.84×10^{-12} m^2/s for EVOH with 29 mol% ethylene, while Lagaron et al. (2001) reported values as low as 0.02×10^{-12} m^2/s for EVOH films with 32 mol % ethylene. In this study, a diffusion coefficient of 0.16×10^{-12} m^2/s was reported for L171 (27 mol % ethylene), and 0.078×10^{-12} m^2/s for EF-XL (32 mol % ethylene). The considerable variation in data among different studies is possibly because of the inherent variations in the materials and the different experimental conditions used.

Table 5.2. Solubility and diffusion coefficients of water in monolayer films at 25°C

Film	Solubility coefficient, S (mol/m^3 Pa)	Diffusion coefficient, D ($\times 10^{-12}$ m^2/s)
PET	0.088	0.37
Nylon 6	2.41	0.20
L171	2.64	0.16
EF-XL	1.26	0.078

5.4.4 Sorption Isotherms for EVOH Films at 25°C

The sorption behavior of water in EVOH films (EF-XL and L171) was further evaluated from sorption isotherms at 25°. As shown in figure 5.10 the isotherms of both EF-XL and L171 films are sigmoid in shape, corresponding to type II isotherm according to the classification of Brunauer et al. (1940). This type is typical of hydrophilic polymers as reported by various authors (Del Nobile et al., 1997; Zhang et al., 1999; Aucejo et al., 2000; Cava et al., 2006a, Starkweather, 1980; Fukuda et al., 1987; Murase et al., 2002; Hernandez and Gavara, 1994). The different regions of the sorption isotherm correspond to the different mechanisms of interaction between water molecules and the polymer, and between water molecules themselves. The initial regions of the isotherms (at low and moderate water contents) are ascribed to the strong hydrogen bonding interactions between water and the highly polar hydroxyl groups of EVOH chains. As polar sites for begin to saturate, water molecules increasingly tend towards locations formed by spaces between polymer chains, and begin to come together to hydrogen bond with each other

forming water clusters (Hernandez and Gavara, 1994; Aucejo et al., 2000). Therefore, the exponential part of the sorption curve (at higher water activities) is said to correspond to a region when water condenses into clusters due to predominant water/water interactions. Free water begins to manifest itself clearly in this region and considerable structural changes such as increase of chain spacing (free volume) may take place.

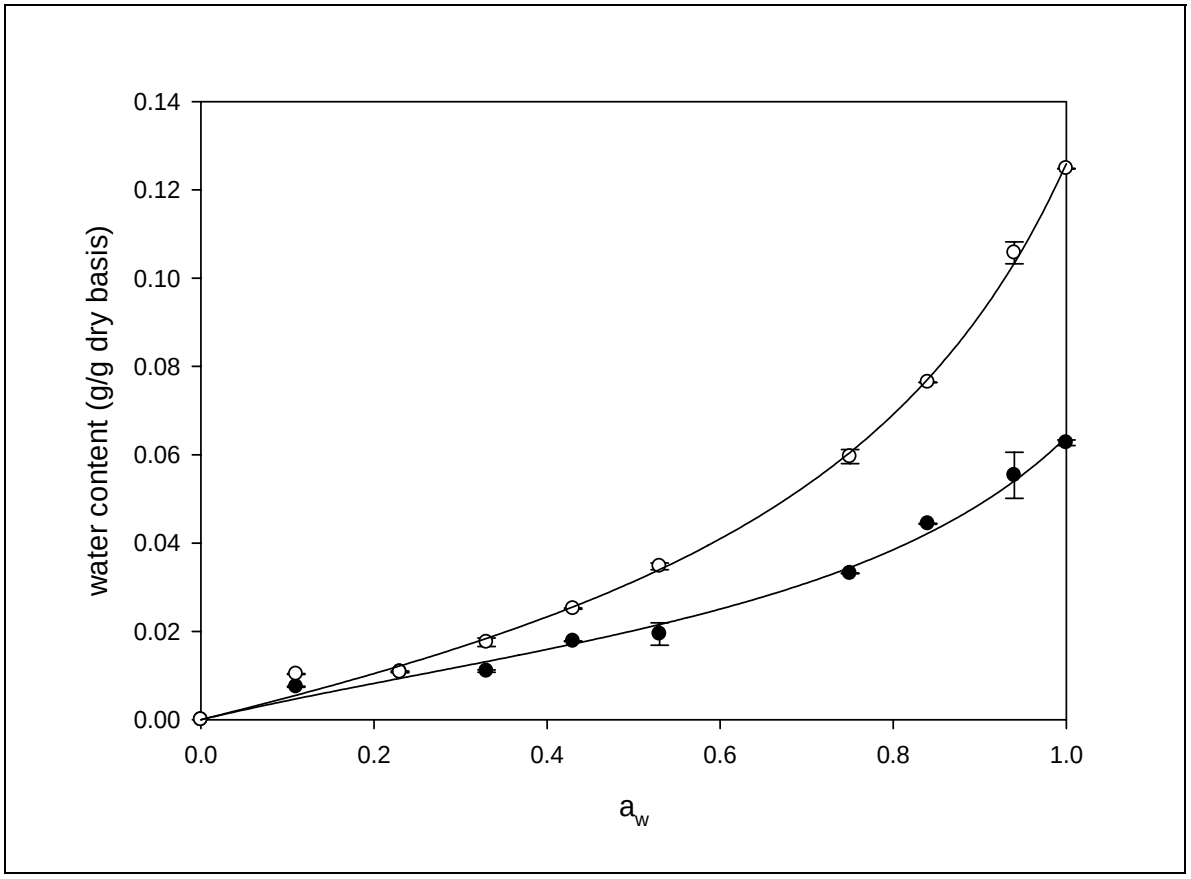

Figure 5.8. Water sorption isotherms at 25°C for L171 (o) and EF-XL (•). Data points are averages of three replicates and solid lines represent GAB model fit.

The sorption data was fitting using the Guggenheim-Anderson-de Boer (GAB) model. This model has been shown to be valid over a wide range of water activities

(Rahman and Labuza, 1999), and has shown to fit sorption data for EVOH films very well (Zhang et al., 1999). The GAB model is a three-parameter equation expressed as follows (Sun, 2002):

$$W_{\infty} = \frac{W_m C K a_w}{(1-Ka_w)(1-Ka_w+CKa_w)} \tag{5.15}$$

where W_{∞} is the water content absorbed at equilibrium (in g water per g dry polymer), a_w is the water activity, W_m is the monolayer water content corresponding to the amount of moisture which would completely occupy all available sorption sites (in g water per g dry polymer), C is a parameter related to the monolayer enthalpy of sorption (i.e. the energy difference between water molecules of the first sorption layer and those absorbed in successive layers), and K is a constant related to the multilayer heat of sorption (i.e. the energy difference between water molecules absorbed in the second and successive layers and the free water molecules of the surrounding environment). The constants C and K are temperature-dependent coefficients. The GAB model is based on the assumptions that water molecules are sorbed into primary sorption sites forming a monolayer, and subsequently into identical multilayers of much more loosely held water (Kent and Meyer, 1984). The GAB model fitting parameters for EF-XL and L171 films are given in Table 5.3.

Table 5.3. Parameters of GAB equation for EF-XL and L171 at 25°C

Parameter	EF-XL	L171
W_m (g water/ g dry polymer)	0.0157	0.0261
C	4.861	3.828
K	0.786	0.821
R^2	0.990	0.994

R^2 is the correlation coefficient

As mentioned previously, formation of water clusters in hydrophilic is possible at high water activities. To evaluate the formation of water clusters in L171 and EF-XL films studied, the widely recognized cluster theory of Zimm and Lundberg cluster theory was used to evaluate the water activity level at which clusters begin to form in these films (Zimm and Lundberg, 1956). The Zimm and Lundberg function uses a mathematical formula based on statistical mechanics to calculating the degree of clustering for two-component systems such as water in polymers. For component 1 (i.e. water), a cluster integral can be written as:

$$\frac{G_{11}}{v_1} = -(1 - v_1)\left[\frac{\left(\frac{\partial a_w}{v_1}\right)}{\partial a_w}\right] - 1 \qquad (5.16)$$

where $\frac{G_{11}}{v_{11}}$ is the clustering function, v_1 is the partial molar volume of water, φ_1 is the volume fraction of water in the polymer film, and a_w is the water activity. The quantity $\frac{G_{11}}{v_{11}}$ denotes the water-water interactions as a function of water content and indicates the tendency of water molecules to form clusters. For ideal solutions, the activity coefficient

($\frac{a_w}{v_1}$) does not vary with concentration and $\frac{G_{11}}{v_{11}}$ is equal to −1. Specific associations between water molecules and polar groups in polymer and between water molecules result in situations where the activity coefficient decreases with increasing φ_1 and $\frac{G_{11}}{v_{11}}$ becomes greater than −1. Therefore, extent of clustering is indicated by the extent to which $\frac{G_{11}}{v_{11}}$ exceeds −1.

To apply the Zimm and Lundberg cluster function, the GAB model (equation 5.15), is re-written in terms of volume fractions instead of weight fractions. Assuming volume additivity and considering the density of sorbed water to be 1g/cm^3, the relationship between volume fraction and weight gain per dry samples is as follows (Sun, 2002):

$$W_\infty = \frac{v_1\rho_1}{v_2\rho_2} \tag{5.17}$$

Substituting equation (5.17) into equation (5.15), the GAB model may be re-written as:

$$\frac{a_w}{v_1} = \frac{(1-Ka_w)(1-Ka_w+CKa_w)}{W_mCK\rho_2 v_2} \tag{5.18}$$

The cluster function is then expressed as follows:

$$\frac{G_{11}}{v_1} = \frac{(2K-CK-W_mCK)+(2CK^2-2K^2)a_w}{W_mCK} \tag{5.19}$$

$\frac{G_{11}}{v_{11}}$ values were obtained after substituting values of W_m, C and K in Table 5.3. The plot of the cluster function ($\frac{G_{11}}{v_{11}}$) as a function of water activity is shown in Figure 5.11 for both EF-XL and L171 films. The cluster integral $\frac{G_{11}}{v_{11}}$ was found to be greater than -1 at water activities greater than 0.38 for L171 and 0.47 for EF-XL, suggesting that clustering of water takes place after these water activity levels are reached. Zhang et al. (1999) and Aucejo et al. (2000) have previously used the Zimm and Lundberg cluster theory to

evaluate clustering in EVOH. Aucejo et al. (2000) reported cluster formation at water activity of 0.38 for several EVOH copolymers studied at 23°C.

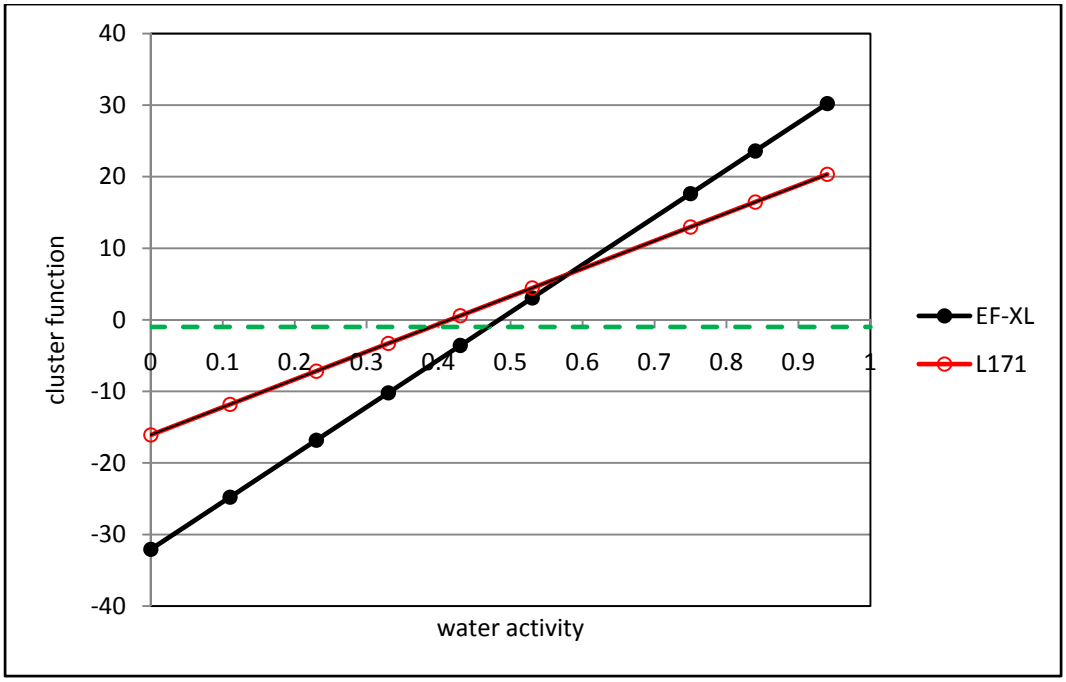

Figure 5.9. Variation of cluster function with water activity at 25°C

5.5 Conclusions

Hydrophilic films (EF-XL, L171 and nylon 6) absorbed more water at equilibrium than the hydrophobic PET. Equilibrium water content values for multilayer films were intermediate between those of hydrophilic and hydrophobic films. These results indicate the importance of using hydrophobic layers as the outer layers in multilayer films in order to protect the hydrophilic EVOH barrier layers from extensive water absorption. Equilibrium water absorption by film A and film B increased with increasing temperature linearly between 25°C and 90°C in a similar manner to low polarity polymers such as PET. However, an abrupt increase was observed between 90°C and 121°C possibly due

to structural damage caused by high temperatures. Diffusion coefficients of water in hydrophilic polymers were lower due to possible immobilization of water molecules at the polar sites. Sorption Isotherms of EVOH were sigmoidal (type II) typical of hydrophilic polymers. Analysis of the isotherms showed that formation of water clusters occurred at water activities exceeding 0.38 for L171 films and 0.47 for EF-XL films.

References

Aucejo, S., Marco, C., and Gavara, R. 1999. Water effect on morphology of EVOH copolymers. Journal of Applied Polymer Science 74, 1201-1206.

Aucejo, S., Catala, R., and Gavara, R. 2000. Interactions between water and EVOH food packaging films. Food Science and Technology International 6, 159-164.

Brunauer, S., Deming, L.S., Deming, W.E., and Teller, E. 1940. On a theory of the van der Waals adsorption of gases. Journal of the American Chemical Society 62, 1723-1732.

Brunauer, S. 1943. The Adsorption of Gases and Vapors. Vol. 1 – Physical Adsorption. Princeton University Press. Princeton, NJ.

Cava, D., Cabedo, L., Gimenez, E., Gavara, R., and Lagaron, J.M. 2006a. The effect of ethylene content on the interactions between ethylene vinyl alcohol copolymers and water: (I) Applications of FT-IR spectroscopy to determine transport properties and interaction in food packaging films. Polymer Testing 25, 254-261.

Cava, D., Sammon, C., and Lagaron, J.M. 2006b. Water diffusion and sorption induced swelling as a function of temperature and ethylene content in ethylene vinyl

alcohol copolymers as determined by attenuated total reflection Fourier transform infrared spectroscopy. Applied Spectroscopy 60, 1392-1398.

Chainey, M. 1989. Transport phenomena in polymer films. In Cheremisinoff, N.P. (Ed.). Handbook of Polymer Science and Technology: Vol. 4. Composites and Specialty applications. Marcel Dekker. New York. pp 498-540.

Crank, J. 1975. The Mathematics of Diffusion. Oxford University Press, Inc. New York.

Crank, J. and Park, G.S. 1968. Methods of measurement. In. Crank, J. and Park, G.S. (Eds.). Diffusion in Polymers. Academic Press. New York. pp 1-39.

Del Nobile, M. A., Laurienzo, P., Malinconico, M., Mensitieri, G., and Nicolais, L. 1997. New functionalized ethylene/vinyl alcohol co-polymers: synthesis and water vapor transport properties. Packaging Technology and Science 10, 95-108.

Frisch, H.L. 1980. Sorption and transport in glassy polymers - a review. Polymer Engineering and Science 20, 2-13.

Fukuda, M., Ochi, M., Miyagawa, M., and Kawai, H. 1991. Moisture sorption mechanism of aromatic polyamide fibers: stoichiometry of the water sorbed in poly(paraphenylene terephthalamide) fibers. Textile Research Journal 61, 668-680.

Greenspan, L. 1977. Humidity fixed points of binary saturated aqueous solutions. Journal of Research of the National Bureau of Standards – A. Physics and Chemistry 81A, 89-96.

Hernandez, R.J. and Gavara, R. 1994. Sorption and transport of water in nylon 6 films. Journal of Food Engineering 22, 495-507.

Illinger, J.L., and Schneider, N.S. 1980. Water-epoxy interactions in three epoxy resins and their composites. In Rowland, S.P. (Ed). Water in Polymers. ACS Symposium Series 127. American Chemical Society. Washington, D.C. pp 571-583.

Kent, M., and Meyer, W. 1984. Complex permittivity spectra of protein powders as a function of temperature and hydration. Journal of Physics. D: Applied Physics 17, 1687-1698.

Lagaron, J.M., Powell, A.K., and Bonner, G. 2001. Permeation of water, methanol, fuel and alcohol containing fuels in high barrier ethylene vinyl alcohol copolymer. Polymer Testing 20, 569-577.

Launay, A., Thominette, F., and Verdu, J. 1999. Water sorption in amorphous polyethylene terephthalate. Journal of Applied Polymer Science 73, 1131-1137.

Levine, H., and Slade, L. 1988. Water as a plasticizer: physic-chemical aspects of low moisture polymeric systems. In Franks, F. (Ed.). Water Science Reviews, Vol. 3. Cambridge University Press. Cambridge, England. pp 79-185.

Marais, S., Nguyen, Q.T., Devallencourt, C., Metayer, M., Nguyen, T.U., and Schaetzel, P. 1998. Permeation of water through polar and nonpolar polymers and copolymers: determination of the concentration dependent diffusion coefficient. Journal of Polymer Science. Part B. Polymer Physics 38, 1998-2008.

Masel, R.I. 1996. Principles of Adsorption and Reaction on Solid Surfaces. John Wiley & sons. Hoboken, NJ.

McCall, D.W., Douglas, D.C., Blyler, L., Johnson, G.E., Jelinski, L.W., and Bair, H.E. 1984. Solubility and diffusion of water in low density polyethylene. Macromolecules 17, 1644-1649.

McKnight, S.H., and Gillespie Jr., J.W. 1997. In situ examination of water diffusion to the polypropylene-silane interface using FTIR-ATR**.** Journal of Applied Polymer Science 64, 1971-1985.

Murase, S., Inoue, A. Miyashita, Y., Kimura, N., and Nishio, Y. 2002. Structural characteristics and moisture sorption behavior of nylon 6/clay hybrid films. Journal of Polymer Science. Part B: Polymer Physics 40, 479-487.

Myers, A.W., Meyer, J.A., Rogers, C.E., Stannett, V., and Szwarc, M. 1961. Studies in the gas and vapor permeability of plastic films and coated papers: part VI. the permeation of water vapor. TAPPI 44, 58–64.

Naylor, T.V. 1989. Permeation Properties. In Allen, G. and Bevington, J.C. (Eds.). Comprehensive Polymer Science: The Synthesis, Characterization, Reactions and Applications of Polymers. Volume 2: Polymer Properties. Pergamon Press. Oxford, England. pp 643-668.

Rahman, M.S. and Labuza, T.P. 1999. Water activity and food preservation. In Rahman, M.S. (Ed.). Handbook of Food Preservation. Marcel Dekker. New York. pp 339-382.

Rodgers, C.E. 1985. Permeation of gases and vapors in polymers. In Comyn, J. (Ed.). Polymer Permeability. Elsevier Applied Science Publishers. New York. pp 11-73.

Starkweather, H.W. 1980. Water in nylon. In Rowland, S.P. (Ed.). Water in Polymers. ACS Symposium Series, American Chemical Society, Washington, DC. pp 433-440.

Sun, W.Q. 2002. Methods for study of water relations under desiccation stress. In Black, M. and Pritchard, H.W. (Eds.). Desiccation and Survival in Plants: Drying Without Dying. CABI Publishing. New York. pp 47-91.

Tajvidi, M., Najafi, S.K., Moteei, N. 2006. Long-term water uptake behavior of natural fiber/polypropylene composites. Journal of Applied Polymer Science 99, 2199-2203.

van Krevelen, D.W. 1990. Properties of Polymers: Their Correlation with Chemical Structure; Their Numerical Estimation and Prediction from Additive Group Contributions. Elsevier. Amsterdam, The Netherlands.

Wijmans, J.G. and Baker, R.W. 1995. The solution-diffusion model: a review. Journal of Membrane Science 107, 1-21.

Yi, X., and Pellegrina, J. 2002**.** Diffusion measurements with Fourier transform infrared attenuated total reflectance spectroscopy: water diffusion in polypropylene. Journal of Polymer Science. Part B: Polymer Physics 40, 980-991.

Zaikov, G.E., Iordanskii, A.L., and Markin, V.S. 1988. Diffusion of Electrolytes in Polymers. VSP BV. Utrecht, The Netherlands. pp 41-71.

Zimm, B.H. and Lundberg, J.L. 1956. Sorption of vapors by high polymers. Journal of Physical Chemistry 60, 425-428.

Zhang, Z., Britt, I.J., and Tung, M.A. 1999. Water absorption in EVOH films and its influence on glass transition temperature. Journal of Polymer Science. Part B: Polymer Physics 37, 691-699.

CHAPTER 6 DIELECTRIC CHARACTERIZATION OF WATER ABSORPTION IN MULTILAYER FILMS

6.1 Introduction

Due to the significant role of water in polymer properties, both quantitative and qualitative determination of water content in polymers is important. The gravimetric technique is a common experimental method for measurement of water absorption by polymers. The technique offers a direct measure of the water content, the accuracy is excellent and repeatability is guaranteed. However, the method is time consuming and destructive. Several other experimental techniques are available that provide indirect measure of water absorption and hydration properties in polymers. The various methods differ in complexity, sensitivity, precision, cost etc. Examples include differential scanning calorimetry (DSC), dynamic mechanical analysis (DMA), nuclear magnetic resonance (NMR), X-ray scattering techniques, infrared and Raman spectroscopy, positron annihilation lifetime spectroscopy (PALS), etc.

In this work, dielectric characterization is considered for evaluation of the dependence of the dielectric properties of polymers on water content. Measurement of water behavior in polymers by dielectric techniques is based on the systematic variation of the dielectric properties of the polymer material with its water content (Kraszewski, 1996a; Kraszewski, 2001). The dielectric properties are measured and the unknown water content of the material is determined on the basis of these measurements. A more fundamental concept thereby involves the independent measurement of both dielectric

properties and water content and the investigation of the relationship between the measured quantities. Dielectric techniques such as dielectric spectroscopy (e.g., time domain spectroscopy, time domain reflectrometry), capacitance bridges, impedance and network analyzers, etc., have been used for investigation of behavior of water in polymers. The techniques for measuring dielectric properties are chosen based on several factors including frequency range, accuracy, suitability and sample geometry and preparation.

The split post dielectric resonator (SPDR) is one of the easiest and most convenient techniques for measuring dielectric properties of laminar materials at microwave frequencies (Clarke, 2007). Theoretical error analysis has shown that the SPDR technique enables measurements of permittivity of low-loss dielectric materials with accuracy of 0.3% and dielectric loss tangent with a resolution of 2×10^{-5}. The SPDR technique was chosen as the dielectric property measurement method for this study. The objective of this study is to carry out a preliminary investigation of the possible use of the SPDR technique to measure water content in polymer films. This was done by evaluating the relationship between dielectric properties and water content in multilayer films.

6.2 Theoretical Background

Most plastics are dielectrics, which are materials which contain no free electrons so that no electric current flows through them, i.e., they are non-conductors. A dielectric material has an arrangement of electric charges in which the positive charges and negative charges are equally distributed and therefore cancel each other out. When a

dielectric material is placed in an external electric field, the positive and negative charges move in opposite directions. This movement of charged particles in response to the applied electric field gives rise to induced dipoles (Kraszewski, 1996a). This process is called polarization and a dielectric material in such a state is said to be polarized.

At the microscopic level, several mechanisms can contribute to the polarization of dielectric materials. The total polarization of a molecule can result from electronic polarization, atomic/nuclear polarization, dipole or orientation and Maxwell-Wagner polarization. Electronic polarization arises from the slight displacement of electrons with respect to the nuclei caused by an electric field (Blythe and Bloor, 2005). An electric field can also distort the arrangement of atomic nuclei in a molecule. Thus, atomic polarization arises from the relative displacement of atomic nuclei because of the unequal distribution of charge in molecule formation. Some dielectric materials contain permanent dipoles as a result of the asymmetric charge distribution of differently charged particles in a molecule, in addition to induced dipoles. These permanent dipoles tend to re-orient and re-align themselves under the influence of a changing electric field, thus giving rise to dipolar or orientation polarization. Maxwell-Wagner (or interfacial) polarization occurs in heterogeneous systems where there may be some charge buildup at interfaces between components (Kraszewski, 1996a).

The interaction between electromagnetic (EM) fields and dielectric materials is commonly described by the complex permittivity of the material, ε, which is defined as the absolute permittivity divided by the permittivity of free space $\varepsilon_0 = \frac{1}{36\pi} \times 10^{-9} F/m$. The relative complex permittivity can be expressed as:

$$\varepsilon = \varepsilon' - j\varepsilon'' \tag{6.1}$$

where $j = \sqrt{-1}$. The real part of the relative permittivity, ε', is known as the dielectric constant, and the imaginary part, ε'', is known as the loss factor. The loss factor is zero for a lossless material. The dielectric constant describes the ability of a material to store electrical energy in response to an electric field (Erbulut, et al., 2008). The loss factor describes the ability of the material to dissipate heat, which typically results in heat generation. Another descriptive parameter is the loss tangent, $\tan \delta$, which indicates the ability of the material to convert dielectric energy into heat, is represented as follows:

$$\tan \delta = \frac{\varepsilon''}{\varepsilon'} \tag{6.2}$$

When complex permittivity is drawn as a simple vector diagram (Figure 6.1), the real and imaginary components are 90° out of phase. The vector sum forms an angle δ with the real axis (ε'). The relative "lossiness" of a material is the ratio of the energy lost to the energy stored.

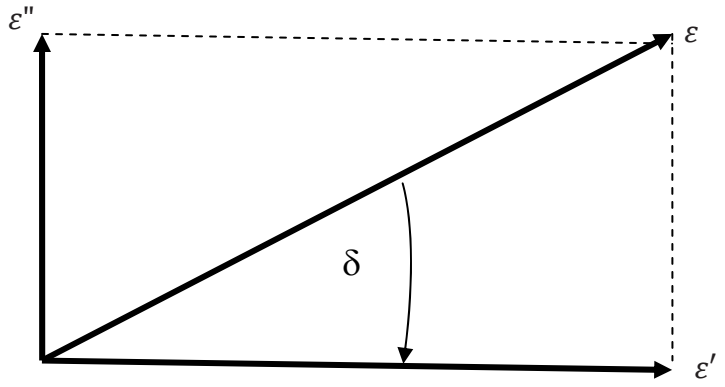

Figure 6.1 Loss tangent vector diagram

Dielectric properties of some of the polymers commonly used in packaging are presented in Table 6.1. In general, the dielectric constant and loss factor of polymer materials are very low. The dielectric properties are influenced by chemical structural units, especially polarity (Putintsev and Putintsev, 2007). In general, the values of dielectric properties increase with the polarity of the polymer. Non-polar polymers such as polyethylene (PE) and polypropylene (PP) have low dielectric constant and dissipation factor, while the values for polar polymers such as polyvinyl alcohol are high. The dielectric properties of non-polar materials are mainly due to electronic polarization only. Because polar materials contain permanent dipoles the values of their dielectric properties are higher. Water molecules are permanent dipoles, and so water has a large value of equilibrium permittivity (Li et al., 2003). The dielectric constant of water at room temperature is about 78 (Misra, 1999). As a result presence of absorbed water has a large effect on the dielectric properties of polymers.

Table 6.1. Dielectric constant and loss tangent for selected polymers (at 1kHz and 23°C)

Material	Dielectric Constant, ε'	Loss tangent, $\tan\ \delta$	Reference
Polyethylene	2.28	0.0001	1
Polypropylene	2.2 -2.6	<0.0005	1
Polyethylene terephthalate	3.25	0.005	1
Polyacrylonitrile	5.5	0.033	1
Polyvinyl alcohol	10.40	0.185	2
Nylon 6	3.5	0.01	1
Polyvinyl acetate	3.07	0.005	2
Polyvinyl chloride	3.1	0.0185	2

1. Brandrup and Immergut (1989)
2. Bicerano (1993)

6.3 Dielectric Property Measurement by Resonance Techniques

Various techniques are widely used for measurement of dielectric properties. The correct choice of measurement technique is important, and is generally based on factors such as the values of dielectric properties (dielectric constant, loss factor), the form of the sample such as shape and dimensions (Sheen, 2009). An ideal method should have good measurement accuracy, a simple and easy procedure, among others. Among the wide variety of available methods, resonant techniques provide high measurement accuracy for low-loss materials at high frequencies (Baker-Jarvis et al., 1998). Dielectric resonance techniques are based on different geometrical arrangements of metal shields and signals

measured. The resonators used are low loss, high dielectric constant material. The high dielectric constant of the resonators ensures that most of the fields are contained within the dielectric (Pozar, 1990). The resonance is supported by the metal walls of a metal cavity and the presence of a sample in the cavity causes only a 'perturbation' in the field distributions in the metal cavity. For small gaps and thin samples, such a resonator operates in the transverse electric (TE) resonant mode. A TE wave is an electromagnetic wave in which the electric field is everywhere perpendicular to the direction of propagation (*z*-direction), i.e. the TE mode does not contain electric fields in the axial or *z*-direction (ASTM, 2007). Parameters of the cavity depend upon the volume, geometry, and mode of operation of the cavity, as well as on the permittivity, shape, dimensions, and location of the object inside the cavity (Kraszewski, 1996b).

6.3.1 The Split Post Dielectric Resonator (SPDR) Technique

The SPDR technique is already well established for measurements of complex permittivity of samples at frequencies ranging between 1 and 10 GHz (Krupka et al., 2001). The SPDR technique uses a fixed geometry resonant measurement cell (i.e. cavity or resonator) to measure dielectric constant and loss tangent of laminar dielectrics such as films at a fixed frequency (Clarke, 2007). Figure 6.2 shows a schematic diagram of a SPDR cavity. It consists of two identical cylindrical disc shaped dielectric resonators, surrounded by a metal enclosure split into two halves. The dielectric resonators are placed coaxially along the resonator axis, leaving a small laminar gap between them into which the specimen is placed for measurement (Clarke, 2007). The two dielectric pucks

resonate together in a coupled resonance in the $TE_{01\delta}$ mode, and so a circularly polarized evanescent electric field exists in the gap between them. A coupling loop excites the $TE_{01\delta}$ mode, which has only an azimuthal electric field component (Baker-Jarvis et al., 1998; Krupka, et al., 2001). As a result, the electric field remains continuous at the dielectric interfaces and it is also very uniform in the *z*-direction. This makes the system insensitive to the presence of air gaps perpendicular to the z-axis of the fixture.

The main sample requirements for PSDR measurements are that sample should be flat (i.e. two parallel faces) and the thickness of the sample h must be less than the fixture air gap (hG in Figure 6.2a). The sample, which can be rectangular or circular, must have enough area to cover the inside of the fixture. For easy handling of the sample it is recommended that the sample area dimension L be bigger than the dimension of the minimum measurable area, l, the active area of the fixture (Figure 6.2a). The electric field in the resonator is parallel to the surface of the sample as shown in Figure 6.2b. The air gap between the sample and the dielectric resonator does not affect the accuracy of the measurement.

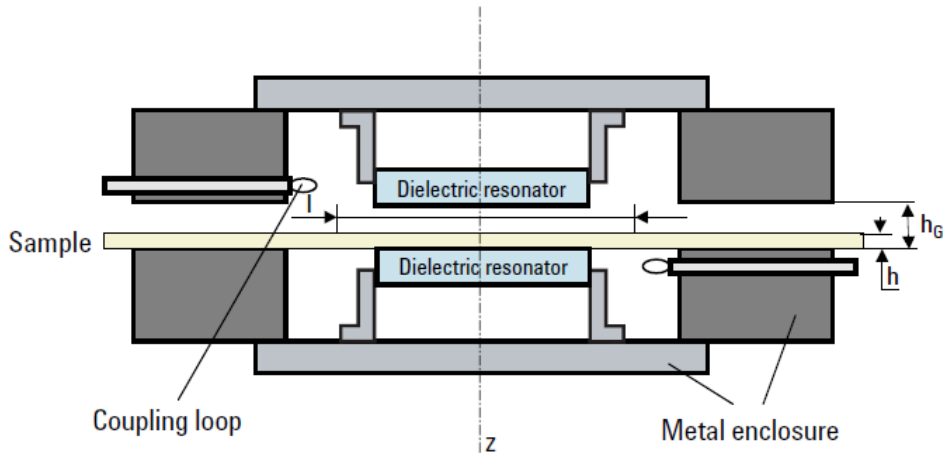

(a) Cross section of SPDR cavity

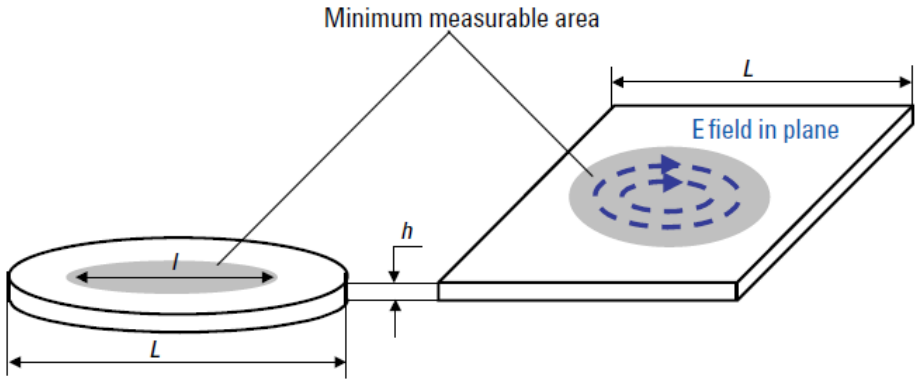

(b). Sample geometry and dimensions

Figure 6.2. Cross section and sample geometry for SPDR cavity (taken from Agilent Technologies Application Note 5989-5384EN)

Once the SPDR is fully characterized, only three parameters are needed to determine the complex permittivity of the specimen: the sample thickness, the changes in resonant frequency and changes in the quality factor (***Q*** factor) obtained when a sample is

placed in the resonator. The sample permittivity is evaluated from the shift of the resonant frequency and ***Q*** factor values of an empty (unloaded) cavity and those of the cavity containing the test sample. The dielectric constant is determined from the shift in the resonant frequency, while the loss tangent is determined from the shift in ***Q*** factor, for the cavity with and without a sample (Kraszewski and Nelson, 1992). The ***Q*** factor is a method of characterizing the rate of dissipation of energy from an oscillating system and it represents the ratio of energy stored in the material to energy dissipated (Helfrick, 1999). The ***Q*** factor is defined in the frequency domain for resonating systems as follows (Kraszewski, 1996b; Helfrick, 1999):

$$Q = 2\pi \times \frac{energy\ stored\ in\ the\ resonance}{energy\ lost\ per\ cycle\ of\ oscillation} \tag{6.3}$$

In the resonators the 'energy stored' is the EM energy stored in the fields in the resonator, the 'energy lost' refers to a cycle of sinusoidal resonating EM signal at the frequency that is present in the resonator. For a typical resonator:

$$\frac{1}{Q} = \frac{1}{Q_{specimen}} + \frac{1}{Q_{resonator\ walls}} + \frac{1}{Q_{coupling}} + \cdots \tag{6.4}$$

where $Q_{specimen}$ accounts for dielectric loss in the specimen – this is the parameter being measured, $Q_{resonator\ walls}$ accounts for the power lost in the metal walls of the resonator due to conduction losses, $Q_{coupling}$ accounts for power lost through all coupling mechanisms into the resonators. There are usually many other sources of loss in resonators.

The Rayleigh–Ritz method is used to compute the resonant frequencies, the unloaded ***Q*** factors, and all other related parameters of the SPDR (Sebastian, 2008). The real part of permittivity (i.e. dielectric constant) of the sample is calculated on the basis of

measurements of the resonant frequencies and thickness of the sample as an iterative solution to the following equation:

$$\varepsilon' = \frac{1+f_0-f_s}{hf_0K_s(\varepsilon',h)} \tag{6.5}$$

where h is the sample thickness, f_0 is the resonant frequency of the empty cavity, f_s is the resonant frequency of the cavity loaded with the dielectric sample, K_s is a function of sample dielectric constant ε' and thickness h. The function K_s is computed and tabulated for every specific SPDR.

The loss tangent of a sample is directly related to the $\boldsymbol{Q}$ factor of the resonator with the sample present. To compute the loss tangent of the sample ($\tan\delta$), equation (6.4) can be further refined as follows (Clarke, 2007):

$$\frac{1}{Q_l} = F_f \tan\delta + \frac{1}{Q_{resonator\ walls}} + \frac{1}{Q_{coupling}} + \cdots \tag{6.6}$$

where Q_l is the unloaded Q-factor of the resonant fixture containing the dielectric sample F_f is the filling factor of the specimen in the resonator defined as follows:

$$F_f = \frac{average\ EM\ energy\ contained\ in\ the\ specimen\ (W_s)}{average\ EM\ energy\ contained\ in\ the\ whole\ resonator\ (W_r)} \tag{6.7}$$

The filling factor (F_f) depends on the cavity and specimen dimensions and on the specimen positioning. It affects the extent to which the resonant frequency is shifted when a specimen is placed in the resonator. Uncertainty of the permittivity measurements of a sample of thickness h can be estimated as $\frac{\Delta\varepsilon}{\varepsilon}=\pm\left(0.0015+\frac{\Delta h}{h}\right)$ and uncertainty in loss tangent measurements is estimated as $\Delta\tan\delta = 2\times10^{-5}$ or $\pm0.03\tan\delta$ (Sebastian, 2008).

During measurement a sample is inserted into the cavity and the sample is subjected to an incident electromagnetic field. When microwaves are directed towards a dielectric material, part of the energy is reflected and part of it is transmitted through the surface. Scattering parameters (or S-parameters) are then measured, which are complex numbers consisting of either the reflection or transmission coefficient of a component at a specified set of input and output reference planes with all other planes terminated by a non-reflecting termination (ASTM, 2007). The S-parameters are directly measured with a vector network analyzer. Scattering equations are then used relate the measured S-parameters to the permittivity of the material (Baker-Jarvis et al., 1990). The systems of equations contain as unknowns the complex permittivity, the calibration reference plane positions, and the sample thickness. The scattering equations are found from analysis of the electric field at the sample surfaces. Error corrections are then applied to compensate for the errors.

6.3.2 Network Analysis

At microwave frequencies it is common to use network analyzers connected to the dielectric measurement cells (such as SPDR) as source/detector combinations. A vector network analyzer consists of a signal source, a receiver and a display (Pollard, 2007). The source launches a known signal at a single frequency to the material being tested. The receiver is tuned to that frequency to detect the reflected and transmitted signals from the material. The measured response produces the magnitude and phase data at that frequency. The network analyzers are equipped with software that converts the measured

data to permittivity. The permittivity of a material is characterized by measurement of the reflection from and/or transmission through the material, and the physical dimensions of the material. A measurement is taken at each specified frequency point over the required bandwidth and then a curve based on those measurements is plotted. Network analyzers measure S-parameters of measurement cavity and frequency changes and Q factors of resonant cavities. The S-parameters relate amplitudes (magnitude and phase) of travelling waves incident on the ports to those reflected from the ports. An example of the resonance curve is shown in Figure 6.3.

Before measurements, network analyzers are calibrated by a procedure in which standard devices are connected to the test ports to characterize the systematic errors in the measurement system which are caused by imperfections in the test equipment and test setup (Instone, 2007). These errors are characterized through calibration and mathematically removed during the measurement process. Systematic errors encountered in network measurements are related to signal leakage, signal reflections, and frequency response (Venkatesh and Raghavan, 2005). Examples of types of systematic errors include directivity and crosstalk errors relating to signal leakage, source and load impedance mismatches relating to reflections, frequency response errors caused by reflection and transmission tracking within the test receivers. The calibration also establishes mathematical reference plane for the measurement test ports. Random errors vary randomly as a function of time and since they are not predictable, they cannot be removed by calibration. The main contributors to random errors are instrument noise (e.g., sampler noise, and the IF noise floor), switch repeatability, and connector

repeatability. Noise errors can often be reduced by increasing source power, narrowing the IF bandwidth, or by using trace averaging over multiple sweeps.

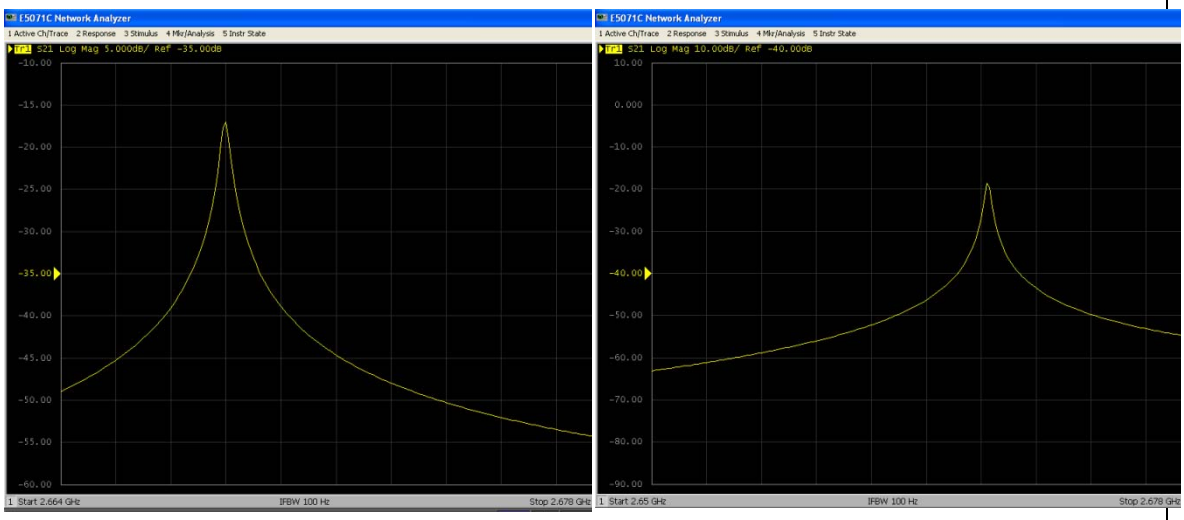

Figure 6.3 Examples of resonant curves from network analyzer

6.4 Materials and Methods

6.4.1 Film Sample Preparation

Film A and film B, and monolayer films of PET, PP, nylon 6, EF-XL and L171 are used in this study. The descriptions of these films were given in Chapter 3 for film A and film B, and in Chapter 5 for the monolayer films. Film samples were cut to a size of about 90mm×85mm to fit into the SPDR cavity. The samples were dried in a vacuum oven at 60 cm Hg and 70 °C for 2-3 days to reach constant weight. The thicknesses of the films were measured using a digital micrometer (Flexbar Co.). An average of thickness measurements taken at five different points was used.

6.4.2 Gravimetric Water Absorption Measurement

Initial dry weight of samples was taken before each measurement using an analytical balance with a resolution of 0.0001g (Analytical Plus, OHAUS). Samples were immersed in beakers containing distilled water and placed in a water bath set at 90°C. After predetermined time periods, they were removed from water bath, dried with paper towels (Kim wipes) and immediately weighed. Triplicate measurements were used for each of the films. The percentage water uptake/absorption at any time (M_t) was calculated according to the following equation:

$$M_t = \frac{w_t - w_d}{w_d} \times 100 \tag{6.8}$$

where w_t is the weight of sample at time t (wet weight) and w_d is the dry weight of sample. Weight change measurements were taken on the same film samples until equilibrium was reached. The percentage equilibrium water absorption (M_∞) was calculated as an average of several constitutive measurements that showed no appreciable additional absorption.

6.4.3 Dielectric Property Measurement

The measurement system consisted of a SPDR cavity operating at a frequency of 2.668 GHz. The cavity was connected to a two port network analyzer (model E5071C ENA Series, Agilent Technologies) as shown in Figure 6.4. The network analyzer was equipped with 85071E Material Measurement software Option 300 (Agilent Technologies) for determination of permittivity and loss tangent. Calibration of the network analyzer was performed using the following standards: **s**hort circuit, **o**pen

circuit, and precision **l**oad impedance and **t**hrough (also referred to as SOLT). The procedure for determining dielectric properties consists of first measuring the resonant frequency f and quality factor Q of an empty cavity (without the sample). Then the cavity was loaded with the sample and the sample resonant frequency f_s and quality factor Q_s are also measured. The material measurement software controls the network analyzer and calculate the dielectric constant, the loss factor or loss tangent of the film materials, and displays them in an easy to use interface.

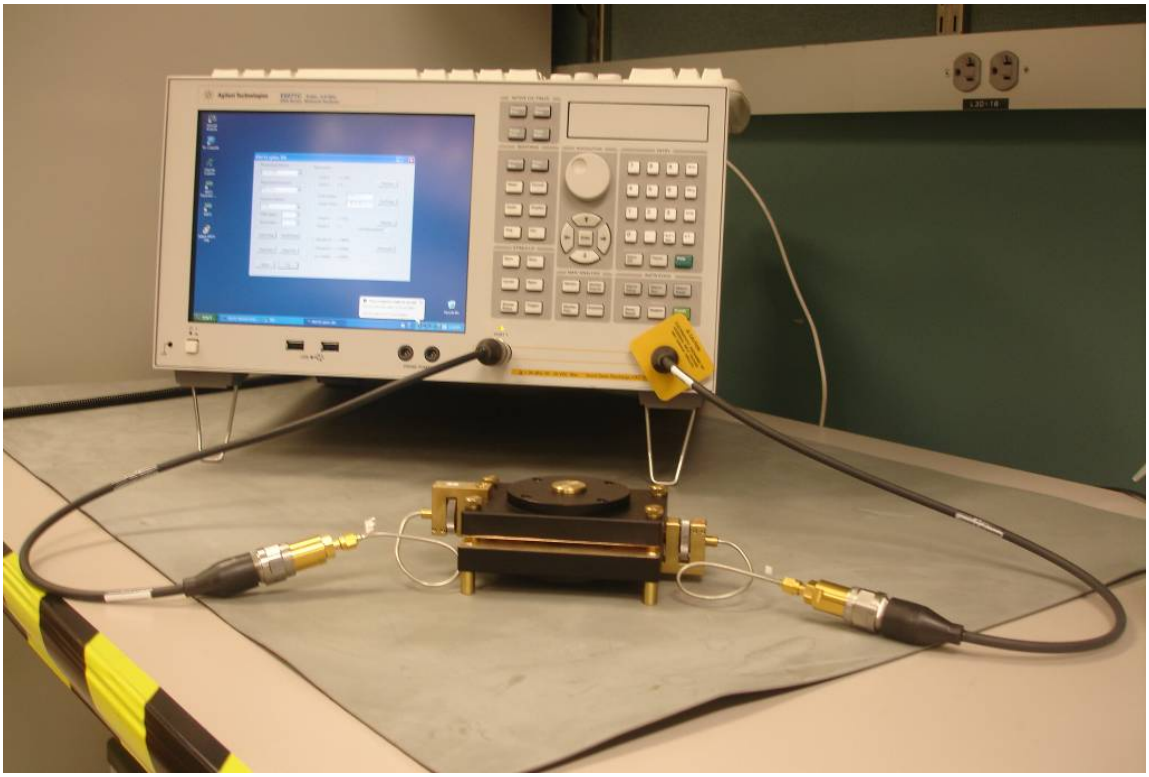

Figure 6.4. Measurement set up showing SPDR cavity connected to network analyzer

6.5 Results and Discussion

6.5.1 Dielectric Properties of Dry and Hydrated Films

Table 6.2 shows values of the dielectric properties of dry and water saturated samples of film A and film B. Values obtained for monolayer films (dry samples only) of PET, PP, EVOH (EF-XL and L171), are also given for comparison. The dielectric constant of film A is slightly lower than that of film B, while the dielectric loss for film A is much greater than that of film B. The difference among the values of $\varepsilon'$and ε'' observed for film A and film B is probably related to the different characteristics of their components. Both film A and film B contain PET and PP as their outer most layers. The oxygen barrier layer in film A is biaxially oriented EVOH (i.e., EF-XL), while film B contains the non-oriented EVOH (i.e., L171) and nylon 6. From Table 6.2 it is observed that the dielectric constant of EF-XL is lower than that of L171 and nylon 6, which might explain the lower value measured for film A relative to that of film B. The measured ε' values for EF-XL and nylon 6 are lower than that of PP despite their high polarity. Both of these films are biaxially oriented, which is likely to affect the film properties by either increasing or decreasing the values of the dielectric constant. Biaxial orientation stretches the polymer in two directions perpendicular to each other, aligning the chains preferentially in the direction of stress. The higher chain packing resulting from biaxial drawing can cause an increase in dipole density (associated with high ε'). However, it may also restrain chain mobility, hampering the orientation of dipoles during during polarization (Gregorio, Jr. and Ueno, 1999). Drawing may also favor formation of

defects in the material that may reduce density and slightly reduce dc conductivity and consequently the values of ε' and ε''.

Water absorption by film A and film B increased the values of the dielectric properties substantially. The effect of water absorption was higher for film B than film A, and for both film, the effect on the loss factor (and loss tangent) was higher than the effect on the dielectric constant. The dielectric constant of film A increased from 2.40 when dry to 2.64 when saturated moisture was ~2%, while that of film B increased from 2.46 to 2.90 with 3.6% moisture at saturation. On the other hand, the dielectric loss increased by more than 5 times for film A and more than 10 times for film B when the films were saturated with moisture. Water molecules are permanent dipoles, having a very large dielectric constant, i.e. 78.5 at 25°C (Weast, 1985). Therefore, as the water content in the composite material increases, the concentration of mobile dipoles is increased, which raises the permittivity of the films (Li et al., 2003). The plasticizing effect of water on the hydrophilic components of the polymers also increases segmental mobility of polymer chains and thus enhances the value of the dielectric constant of the polymer (Brydson, 1970).

Table 6.2. Dielectric properties of dry and hydrated films at 2.668GHz and 25°C

Film	Thickness (mm)	Water content	Dielectric constant	Dielectric loss	Loss tangent
Film A	0.111	Dry	2.40 ± 0.02	0.028 ± 0.0005	0.0118 ± 0.0002
		Saturated (2%)	2.64 ± 0.008	0.16 ± 0.008	0.061 ± 0.003
Film B	0.140	Dry	2.46 ± 0.01	0.023 ± 0.0003	0.0092 ± 0.0001
		Saturated (3.6%)	2.90 ± 0.04	0.26 ± 0.01	0.091 ± 0.004
PET	0.132	Dry	3.16 ± 0.02	0.018 ± 0.0004	0.0055 ± 0.0001
PP	0.120	Dry	2.28 ± 0.02	0.0005 ± 0.0001	0.0002 ± 0.0001
BON	0.027	Dry	2.25 ± 0.02	0.0227 ± 0.0004	0.0101 ± 0.0001
EF-XL	0.023	Dry	2.18 ± 0.03	0.0878 ± 0.007	0.0402 ± 0.0032
L171	0.071	Dry	2.91 ± 0.02	0.1158 ± 0.010	0.0398 ± 0.0033

BON is biaxially oriented nylon 6; EF-XL is biaxially oriented EVOH with 32 mol % ethylene; L171 is non-oriented EVOH with 27 mol % ethylene

6.5.2 Correlation of Water Absorption with Dielectric Properties

Figures 6.5 to 6.8 show the profiles of % water absorption and dielectric properties as a function of immersion time for film A and film B. The graphs for dielectric properties followed similar trend to that of water absorption. All graphs show rapid and relatively linear change of properties with time at the initial stages, followed by a plateau when equilibrium was reached. Film B absorbed more water at equilibrium than film A, and film B approached equilibrium rather slowly (i.e. over a longer time period) than film A. This behavior was also reported in Chapter 4 when water absorption by film A and film B was measured at temperatures between 25°C and 121°C. Film A reached an equilibrium value of about 2% after 2 hours, while film B reached equilibrium water absorption of about 3.6% after 5 hours.

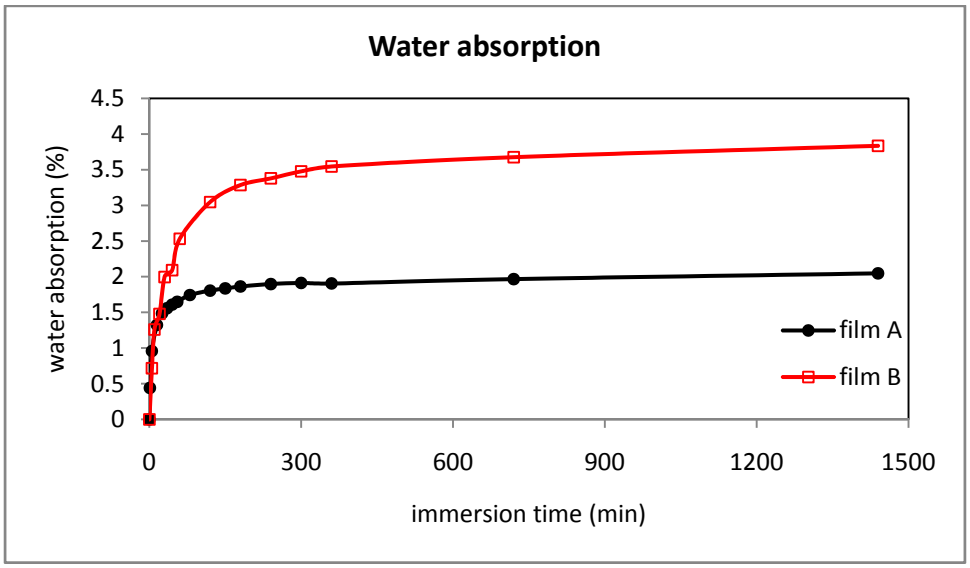

Figure 6.5. Water absorption at 90°C as a function of time for film A and film B

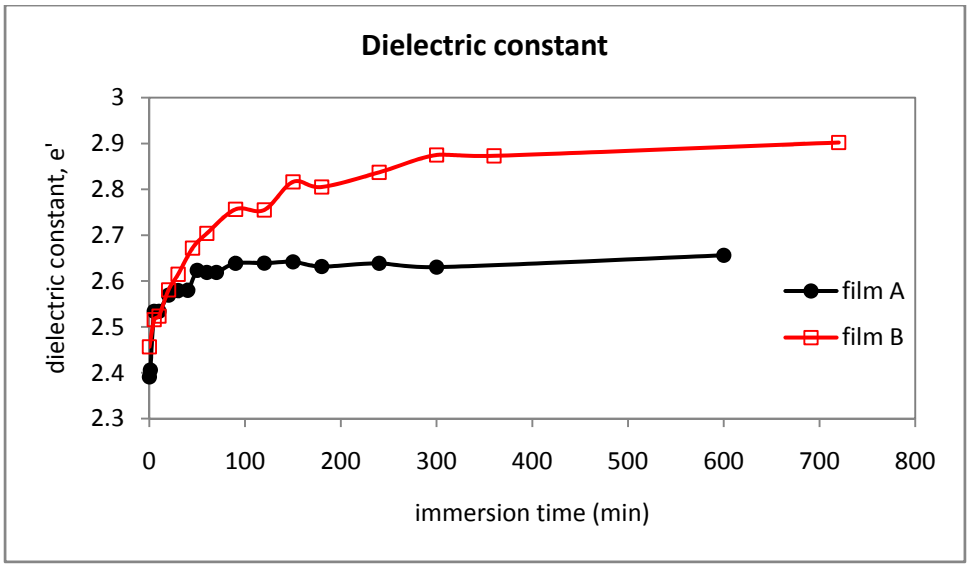

Figure 6.6. Dielectric constant as a function of time for film A and film B

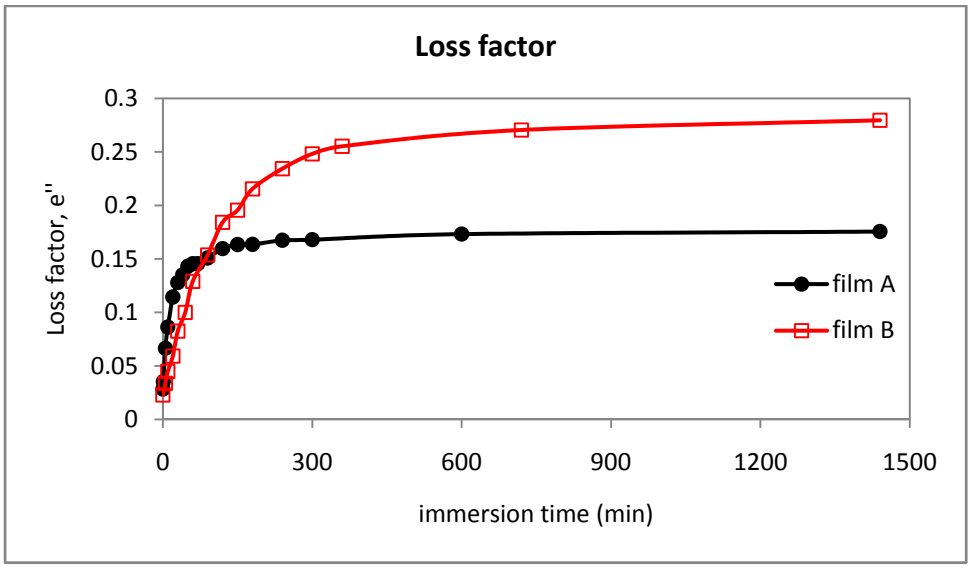

Figure 6.7. Loss factor as a function of time for film A and film B

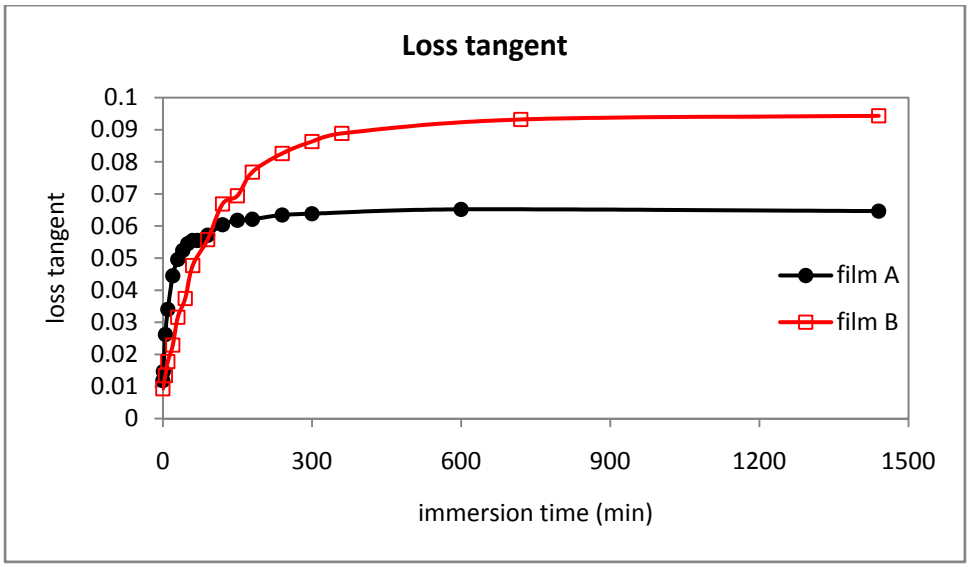

Figure 6.8. Loss tangent as a function of time for film A and film B

In order to obtain the correlation coefficients to measure the strength of the association between water absorption data and dielectric properties data, the data was normalized to bring them to a common scale. All the data was re-scaled to the range [0,1] as using the following formula:

$$Data_{Norm} = \frac{(Data)_t - (Data)_0}{(Data)_f - (Data)_0} \quad (6.9)$$

where $Data_{Norm}$ is the normalized data (water absorption or dielectric property), $(Data)_t$ is the value of data at any time t, $(Data)_0$ is the initial data value, and $(Data)_f$ is the final data value. Li et al. (2003) used similar normalization procedure to evaluate the correlation between water uptake and permittivity of E-glass/epoxy composites. The representative profiles of normalized data as a function of immersion time are shown in figures 6.9 and 6.10 for film A and film B, respectively. The correlation coefficients of the normalized data are shown in the respective figures. As observed from the figures, the

normalized data for water absorption and dielectric property data coincides with each other very well. High correlation coefficients (values shown on the curve) were obtained for both films, e.g., for the dielectric constant $r = 0.979$ for film A and $r = 0.977$ for film B. These high correlation coefficients demonstrate that dielectric characterization using the SPDR technique can be used for measuring water uptake in polymers similar to the ones used in this study.

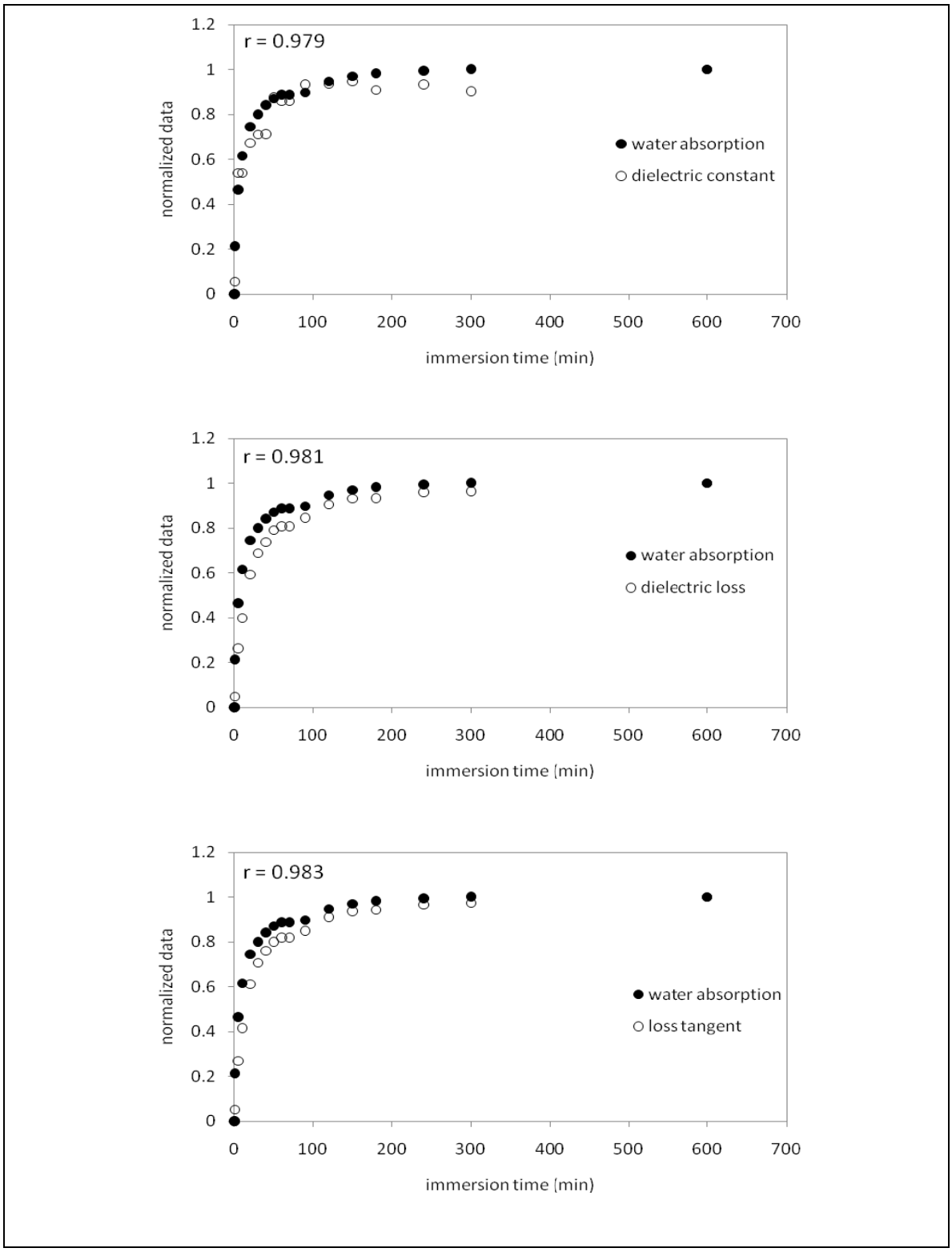

Figure 6.9. Correlation between water absorption and dielectric properties of film A

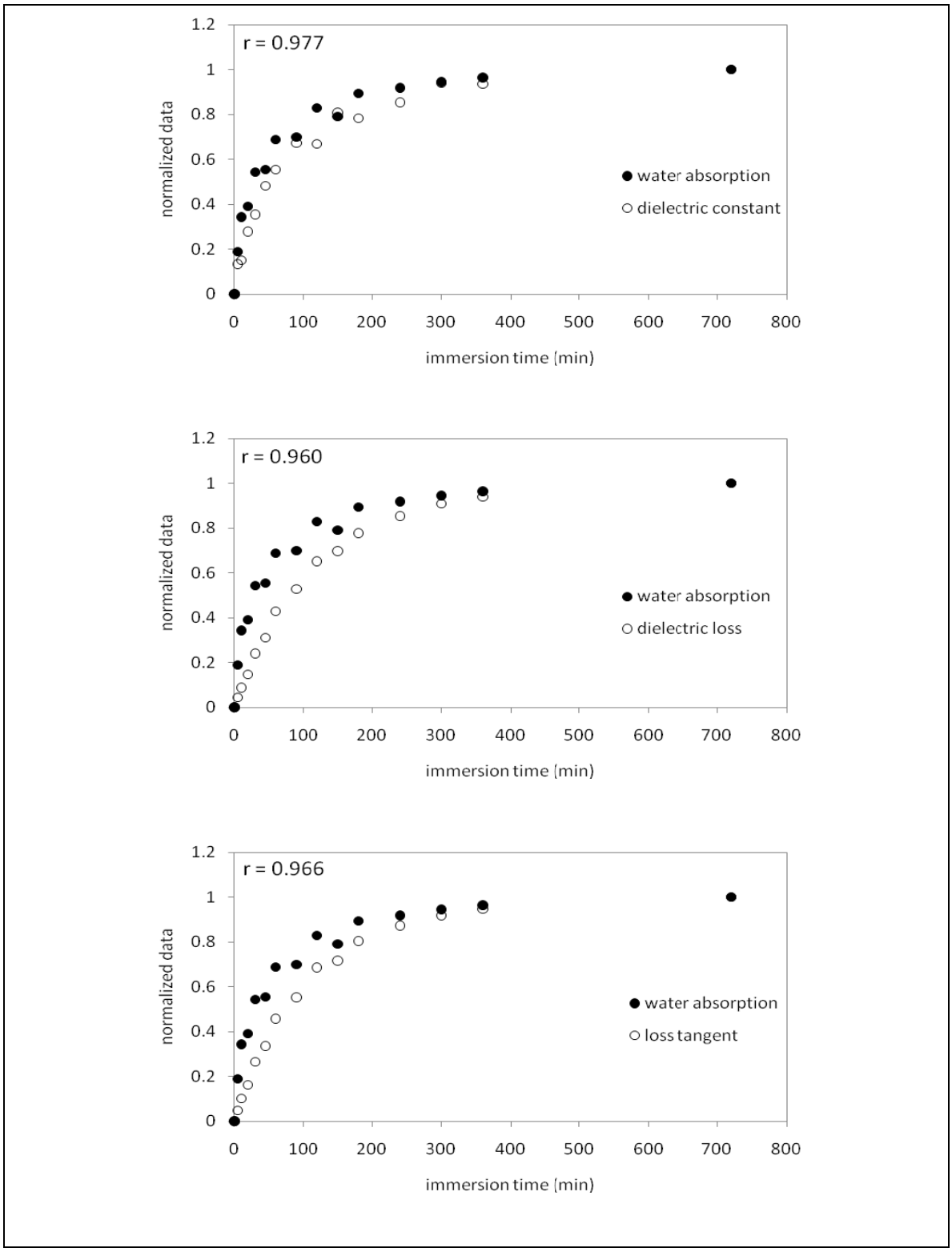

Figure 6.10. Correlation between water absorption and dielectric properties of film B

6.5.3 Dependence of Dielectric Properties on Water Absorption

Figures 6.11, 6.12 and 6.13 show the dielectric constant, dielectric loss and loss tangent, respectively, as a function of water absorption. The figures reveal two apparent regions of the curve describing the change of dielectric properties with water absorption for both film A and film B. The increase in properties was slow in the initial stage, and increased rapidly during the second stage. The change in slope of the curve of dielectric properties occurs at a water content of 0.5% for film A, and 1.5% for film B. Therefore at water content below 0.5% for film A and 1.5% for film B the effect of water absorption on dielectric behavior was small, while a strong linear relationship is observed above these levels of water content.

Figure 6.11 shows that the dielectric constant of film B was higher than that of film A during the initial stage. These higher values are consistent with the higher initial (dry) dielectric constant values observed for film B as compared to that of film A. After water content of 1.5% the dielectric constants of the two films were similar (i.e., the curves overlap each other after 1.5% water absorption). On the other hand, Figures 6.12 and 6.13 show that the loss factor and loss tangent for film A and film B were similar during the initial stage up to 0.5% water content. After this water content, the values of dielectric loss factor and loss tangent for film A were greater than that of film B for the same water content. The curves for the two films seem to be parallel to each other during the second stage.

The observation of two distinct slopes in the graph of dielectric properties as a function of water content has been reported before. Yasufuku (2003) reported similar general trends for various films including PET, polyethylene naphthalate, polyimide,

aramid films, etc. The two different slopes were related to the various stages of water binding with the polymer as expressed by Kraszewski (1996a). At low water contents, water exists in hydrophilic polymers in bound form where it is physically absorbed to the polar sites. Water molecules thus attached to the polymer exhibit lower rotational mobility than molecules of free water. Therefore, this implies at water contents below 0.5% for film A and 1.5% for film B, all the absorbed water molecules are strongly bound to the polymer, and free water begins to form after these water content levels. Strongly bound water molecules are less mobile than free water, hence their small influence of the dielectric properties.

The equations for the curves during the second stage are shown in the respective figures. The slopes of the curves for film A and film B are similar for both properties (i.e. dielectric loss and loss tangent. The equations for the first stage were not included due to lack of enough points for their calculations.

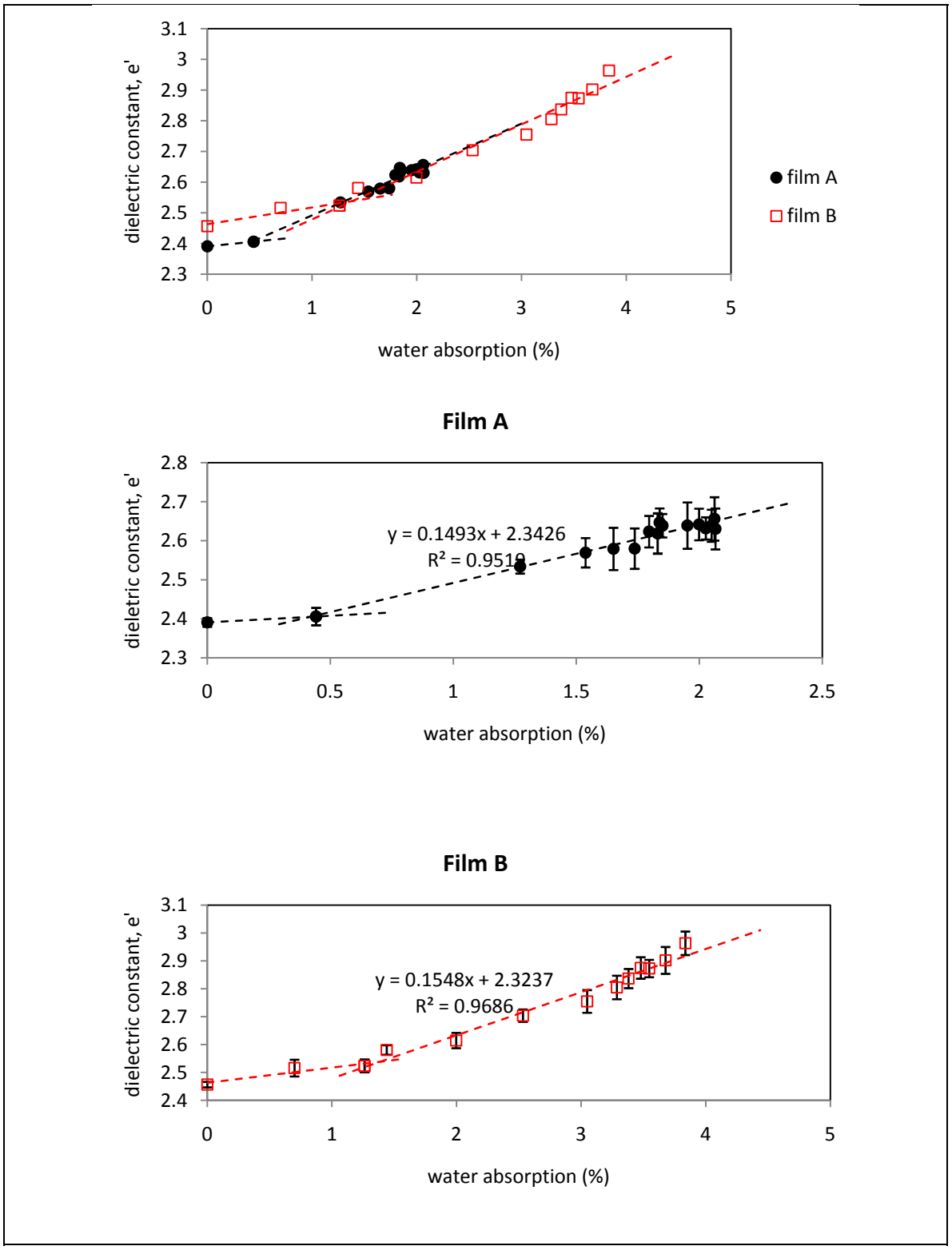

Figure 6.11. Dielectric constant of film A and film B as a function of water absorption

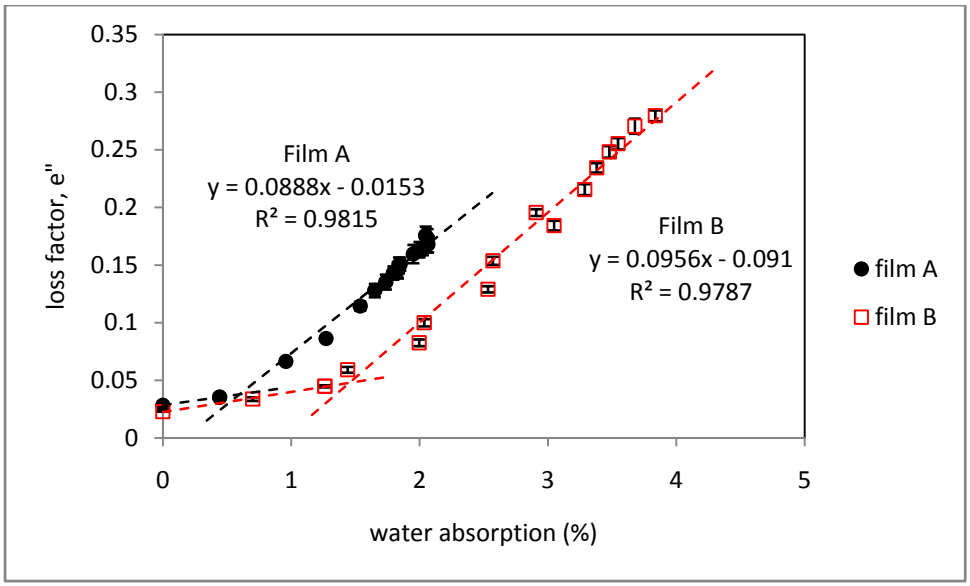

Figure 6.12. Loss factor for film A and film B as a function of water absorption

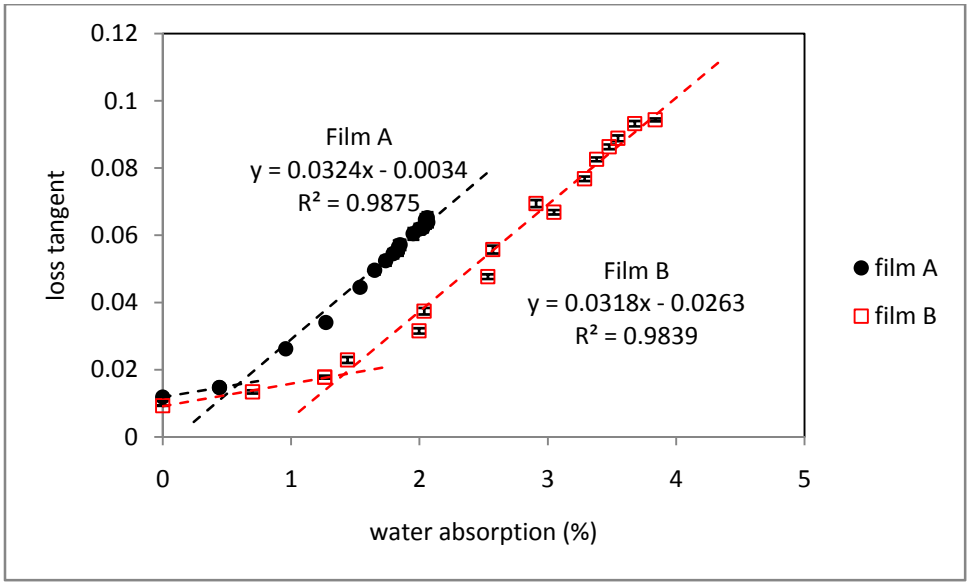

Figure 6.13. Loss tangent for film A and film B as a function of water absorption

6.6 Conclusions

The effect of water absorption on the dielectric properties of film A and film B were successfully evaluated using the SPDR technique. The values of the dielectric constant, dielectric loss and loss tangent for both film A and film B all increased with water absorption. Two apparent stages (i.e. two linear regions) were observed in the profiles of the dielectric properties as a function of water absorption. The first region was very small for both films, corresponding to only small changes in the dielectric properties. The dielectric property data correlated well with water absorption, indicating that water absorption by the films can be studied by dielectric analysis using the SPDR technique. The method can be useful as a simple, quick and non-destructive, requiring little sample preparation (no sample machining is necessary). This is a much better alternative to the gravimetric technique that not only is destructive and slow, but also comes with potential errors associated with handling and measurement of very small changes in weight of representative samples. One limitation of the method is that measurements are done only at one frequency, and different SPDR cavities are needed for each frequency.

References

Agilent Technologies. Application Note, Literature number 5989-5384EN. Split post dielectric resonators for dielectric measurements of substrates.

ASTM. 2007. ASTM D5568-01: Standard test method for measuring complex permittivity and relative magnetic permeability of solid materials at microwave frequencies. Annual Book of ASTM Standards. Philadelphia, PA. pp. 551–565.

Baker-Jarvis, J., Vanzura, E.J., and Kissick, W.A. 1990. Improved technique for determining complex permittivity with the transmission/reflection method. IEEE Transactions on Microwave Theory and Techniques 38, 1096-1103.

Baker-Jarvis, J., Geyer, R.G., Grosvenor Jr., J.H., Janezic, M.D., Jones, C.A., Riddle, B., Weil, C.M., and Krupka, J. 1998. Dielectric characterization of low-loss materials: a comparison of techniques. IEEE Transactions on Dielectrics and Electrical Insulation 5, 571-577.

Bicerano, J. 1993. Prediction of Polymer Properties. Marcel Dekker, Inc. New York.

Blythe, T., and Bloor, D. 2005. Electrical Properties of Polymers. Cambridge University Press. New York.

Brandrup, J., and Immergut, E.H. 1989. Polymer Handbook. John Wiley and Sons, Inc. New York.

Brydson, J.A. 1970. Plastics Materials. Van Nostrand Reinhold. New York.

Clarke, B. 2007. Measurement of dielectric properties of materials at RF and microwave frequencies. In Collier, R.J. and Skinner, A.D. (Eds.). Microwave Measurements. The Institute of Engineering and Technology. London, UK. pp 409-458.

Erbulut, D.U., Masood, S.H., Tran, V.N., and Sbarski, I. 2008. A novel approach of measuring the dielectric properties of PET performs for stretch blow molding. Journal of Applied Polymer Science 109, 3196-3203.

Gregorio Jr., R., and Ueno, E.M. 1999. Effect of crystalline phase, orientation and temperature on dielectric properties of polyvinylidene fluoride (PVDF). Journal of Materials Science 34, 4489-4500.

Helfrick, A.D. 1999. *Q* factor measurement. In Webster, J.G. (Ed.). The Measurement, Instrumentation, and Sensors Handbook. CRC Press. Boca Raton, FL. Springer-Verlag GmbH&Co KG. Heidelberg, Germany.

Instone, I. 2007. Calibration of automatic network analyzers. In Collier, R.J. and Skinner, A.D. (Eds.). Microwave Measurements. The Institute of Engineering and Technology. London, UK. 263-289.

Kraszewski, A.W. 1996a. Microwave aquametry: introduction to the workshop. In Kraszewski, A. (Ed). Microwave Aquametry: Electromagnetic Wave Interaction with Water-Containing Materials. IEEE Press. Piscataway, NJ. pp 3-34.

Kraszewski, A.W. 1996b. Moisture content determination in single kernels and seeds with microwave resonant sensors. In Kraszewski, A. (Ed). Microwave Aquametry: Electromagnetic Wave Interaction with Water-Containing Materials. IEEE Press. Piscataway, NJ. pp 177-203.

Kraszewski, A. 2001. Microwave aquametry: an effective tool for nondestructive moisture sensing. Subsurface Sensing Technologies and Applications 1, 365-376.

Kraszewski, A.W., and Nelson, S.O. 1992. Observations on resonant cavity perturbation by dielectric objects. IEEE Transaction on Microwave Theory and Techniques 40, 151-155.

Krupka J., Gregory, A.P., Rochard, O.C., Clarke, R.N., Riddle, B., and Baker-Jarvis, J. 2001. Uncertainty of Complex Permittivity Measurement by Split-Post Dielectric Resonator Techniques, Journal of the European Ceramic Society 10, 2673-2676.

Li, Y., Cordovez, M., and Karbhari, V.M. 2003. Dielectric and mechanical characterization of processing and moisture uptake effects in E-glass/epoxy composites. Composites: Part B 34, 383-390.

Misra, D. 1999. Permittivity measurement. In Webster, J.G. (Ed.). The Measurement, Instrumentation, and Sensors Handbook. CRC Press. Boca Raton, FL. Springer-Verlag GmbH&Co KG. Heidelberg, Germany.

Pollard, R.D. 2007. Microwave network analyzers. In Collier, R.J. and Skinner, A.D. (Eds.). Microwave Measurements. The Institute of Engineering and Technology. London, UK. pp 207-216.

Pozar, D.M. 1990. Microwave Engineering. Addison-Wesley Publishing Company, Inc. Reading, MA.

Putintserv, N.M., and Putintserv, D.N. 2007. The permittivity of polar dielectrics. Russian Journal of Physical Chemistry A 81, 572-576.

Sebastian, M.T. 2008. Dielectric Materials for Wireless Communications. Elsevier. The Netherlands.

Sheen, J. 2009. Comaprisons of microwave dielectric property measurements by transmission/reflection techniques and resonant techniques. Measurement Science and Technology 20, 1-11.

Venkatesh, M.S., and Raghavan, G.S.V. 2005. An overview of dielectric properties measuring techniques. Canadian Biosystems Engineering 47, 7.15-7.30.

Weast, R.C. 1985. CRC Handbook of Chemistry and Physics. CRC Press, Inc. Boca Raton, FL.

Yasufuku, S. 2003. Dielectric and thermomechanical and spectroscopic and kinetic evaluation of water in heat resistant electrical insulating films. IEEE Electrical Insulation Magazine 19, 23-39.

CHAPTER 7 CONCLUSIONS AND RECOMMENDATIONS

The major findings of this research are summarized below:

1. The oxygen barrier of multilayer films is deteriorated by both thermal treatments studied. Thermal processing utilizing a combination of microwave and hot water heating reduced deterioration of oxygen barrier substantially as compared to retort heating.

2. Although the two films studied had similar initial oxygen barrier properties, they responded quite differently to the effects of water absorption at high temperatures, especially after relatively long heating durations. It is, therefore, important that specific evaluations be performed on individual films to assess how they perform at the specific conditions that they are exposed to. Data from literature cannot be extrapolated for planning purposes.

3. The oxygen barrier of films decreased considerably during the first 2 months of storage but the original O_2 barrier of the films could not be fully recovered. However, during 12 months storage, the O_2 transmission rates for both films after a $F_0 = 3\,min$ microwave processing remained below the 2cc/m^2.day value comparable to commercially available PVDC laminated films currently used in the USA as lidstock film for shelf-stable products.

4. Oxygen transmission rates of multilayer EVOH films increased with increasing water content, with two separate regions observed in the curve of oxygen transmission rate versus water absorption. At the lower water contents, the two films showed similar oxygen transmission rates, suggesting that water absorption by the two films might have a similar mechanism and effect on the two films. It was suggested that the change in slope on the curves of both films might occur where the polymer systems change from the glassy to the rubbery state in a manner. On the other hand, possible irreversible structural damage (formation of voids, delamination, etc.) that might occur due to stress created by high temperature and moisture conditions can also deteriorate the oxygen barrier more.

5. Equilibrium water absorption by the multilayer films increased with increasing temperature in a similar manner to low polarity polymers such as PET. Diffusion coefficients were found to be lower in hydrophilic films (EVOH and nylon 6) due to possible immobilization of water molecules at the hydrophilic sites of these polymers.

6. A preliminary study showed promises for using dielectric characterization as an indirect measure of water content in polymer films was done. The values of the dielectric constant, dielectric loss and loss tangent for both film A and film B all increased with water absorption. The dielectric property data correlated well with water absorption. From this it was concluded that the method can be useful as a

simple, quick and non-destructive method which requires very little sample preparation.

The following areas need further evaluation in order to understand fully the influence of water on oxygen barrier properties of EVOH packaging films:

1. Microstructural analysis to reveal actual mechanisms and effect of water absorption on internal structure of multilayer films.

2. Modeling and simulation using numerical techniques to gain insight on water transport properties and concentration distribution in multilayer films.

3. Better and more efficient methods of measuring transport coefficients of water in polymers are essential. Available literature data on water transport (solubility and diffusivity) in polymer films is inconsistent. Further evaluation of the dielectric characterization using the split post dielectric resonator method to establish its accuracy and reliability is recommended.

4. Lipid oxidation is the primary cause of loss of quality and reduction shelf life of lipid containing foods such as fish. It will be interesting to study lipid oxidation in fish product processed by thermal methods and perform sensory analysis on the product in order to establish any relationship with deterioration of oxygen barrier of packaging films during storage.